KAPL, Inc.
Knolls Atomic Power Laboratory
Post Office Box 1072 Schenectady, N.Y. 12301-1072
Telephone (518) 395-4000 Facsimile (518) 395-4422

LOCKHEED MARTIN

SPP-67210-0009
B-SE-0161
Page 1

The Manager
Schenectady Naval Reactors Office
United States Department of Energy
Schenectady, New York

Date: January 13, 2005

Subject: Summary of Prometheus Radiation Shielding Nuclear Design Analyses, For Information

References: (a) KAPL Letter FSO-64R00-05-096, "Control Drive Mechanism Streaming Analysis for Space Reactor Shield," DR Reinert, 8/24/2005.

Enclosures:
(1) Computer Code Comparison for Space Reactor Shielding Analyses
(2) Charged Particle Transport Code Selection Summary
(3) Coolant Pipe Penetration Streaming Studies for a Space Reactor Shield
(4) Ground Test Reactor Core Calculated Radiation Levels in M140 for Planning Purposes
(5) Projected Shutdown Radiation Levels Following Zero-Power Critical Testing of a Space Reactor
(6) Space Reactor Pressure Vessel Material Activation Analysis
(7) Initial Ground Test Reactor Shield Sizing Study

Dear Sir:

This letter transmits a summary of radiation shielding nuclear design studies performed to support the Prometheus project. Together, the enclosures and references associated with this document describe NRPCT (KAPL & Bettis) shielding nuclear design analyses done for the project.

DISCUSSION

NRPCT performed a wide variety of analyses relating to the nuclear design of the radiation shielding system for Project Prometheus. These studies included:

Computer Code Comparison for Space Reactor Shielding (Enclosure 1)

The discrete ordinates neutron/photon transport codes PARTISN and ATTILA and the Monte Carlo transport code MCNP were compared using three notional Prometheus reactor/shield configurations. Modeling precision and run time were among the comparison categories. The comparison study was not completed, but the results that had been obtained suggested that PARTISN was not well suited to modeling configurations containing large void regions or non-

rectangular geometry. ATTILA had not quite reached the necessary development stage for extensive use. MCNP required a great deal of computing resources, but appeared to be the most appropriate choice for space craft analyses, so it was used for many of the other shielding analyses performed for the project. Computing resources using MCNP for deep penetration analyses, like the ground test reactor shield, appeared to be prohibitive. Therefore, a discrete ordinates transport code would likely be used for those calculations. NRPCT was also investigating a PARTISN/MCNP splice capability to make use of each code where it is most effective. For example PARTISN could be used in high attenuation regions like the reactor and shadow shield, and MCNP could be used in low attenuation regions like the energy conversion system and void regions.

Charged Particle Transport Code Selection Summary (Enclosure 2)

Radiation transport codes beyond those typically used by the NRPCT will be needed to quantify the effects of the naturally occurring radiation in space. The main sources of ionizing radiation in the space environment are trapped belt radiation, solar energetic particles, and the galactic cosmic ray (GCR) background. This summary discusses six different radiation transport codes, and considers the pros and cons of each. Considering the current capabilities of these six different codes it is suggested that PHITS be used to transport space radiation sources. PHITS is a radiation transport code very similar to MCNP, but it also contains nuclear interaction models that allow it to transport hadrons with energies up to 200 GeV per nucleon and light and heavy ions with energies up to 100 GeV per nucleon. It is important to emphasize that this suggestion is based on capabilities at the time this summary was written.

Also, gamma radiation interactions at the surface of the reactor may eject electrons from the surface of the reactor, reflector, or surrounding micrometeoroid shield. MCNP, MCNPX, or PHITS could be used to evaluate this concern and evaluate solutions, if required.

Coolant Pipe Penetration Streaming (Enclosure 3)

A range of coolant piping penetration configurations was analyzed for a notional reactor shadow shield, with the goal of minimizing the expected increase in radiation levels at the spacecraft payload due to streaming and minimizing shield mass. Straight, curved, and dog-leg penetrations through a Be/B4C/W shield were considered. In each case, the penetration followed the radial edge of the 12°/6° elliptical shield through a specified rotational angle about the axis of the spacecraft. The study showed that using curved coolant pipes traversing at least 90 degrees around the inside edge of the shield resulted in minimal increases in radiation levels at the payload, compared to having no penetrations. Adding the material displaced by the penetrations to the back of the shield further reduced the radiation levels. A benefit of using a thicker shield rather than a cap shield is the reduction of neutron fluence to the control drive motors (CDM), which are located near the shield in a region not protected by cap shields. With a thickened shield, the neutron fluence at the center of the shield would be reduced and the CDM shaft streaming is also reduced. Future studies would have been performed for hydrogenous shields and shields with piping going around the outside of the shield.

Ground Test Reactor Core Calculated Radiation Levels in M140 for Planning Purposes (Enclosure 4)

An estimate of the gamma radiation levels for end-of-life shipment of a representative space reactor prototype core in an M140 type shielding container was performed. The SPAN5 computer code was used to calculate the gamma radiation levels commencing 30 days after shutdown. The fission product gamma yield source data used in the calculations were generated by SPENT3 for a fast reactor with a 1 MeV core average neutron spectrum and 15 EFPY of operation. These preliminary investigations indicated that the conceptual space reactor prototype core would satisfy the 10CFR71 normal shipment dose rate requirements for an M140 shipping container shield within 30 days after shutdown.

Shutdown Radiation Levels Following Zero-Power Testing (Enclosure 5)

The FSTAB option of the SPAN point-kernel code was used to project radiation levels following zero-power criticality testing of the Prometheus reactor. An assumed power history was applied to a homogenized notional reactor model. The analysis showed that radiation levels on the reactor vessel surface following zero-power testing were not trivial. Shipping requirements could be met soon after shutdown, but if the reactor were removed from the shipping container (during final spacecraft assembly, for example), radiation levels might be a concern. Important variables affecting radiation levels include test power level, test operation time, and decay time.

Reactor Pressure Vessel Activation (Enclosure 6)

The activation of several candidate reactor vessel materials was characterized using the NUGACS code. These materials, which could be categorized (from an activation perspective) as tantalum-containing, cobalt-containing, or molybdenum-rhenium alloys, were studied using an assumed power history for a ground test reactor. The results showed that materials containing tantalum would experience the most long-term neutron activation following the one year of operation assumed. Molybdenum-rhenium showed significant activation, but only in the very short term. In this study with a 1 year activation period, cobalt containing alloys had the lowest initial shutdown gamma activity, but the activity was not saturated ($T_{1/2}$=5.27yr). Longer activation periods would increase cobalt alloy activation relative to the non-cobalt alloys. Both tantalum and cobalt-containing materials would have significant disposal concerns. Note that this study was a relative comparison, but activation of any of these materials is expected to cause significant maintenance and servicing difficulties related to their activation from testing activities. Additional studies in this area are required.

Initial Ground Test Reactor Shield Sizing Study (Enclosure 7)

MCNP was used to provide an initial estimate of the shielding needed for the space ground test reactor. A notional Prometheus reactor/shield configuration was modeled inside a notional ground test reactor facility configuration. The required thicknesses of concrete needed to meet three different shield surface dose rates were determined. The thickness required to meet the lowest shield surface dose rate, 125 mrem in one year (2,800hours) with 8 hour/day occupancy, for concrete was between 3 and 3.5 m. The resulting estimates of shield thicknesses serve as an initial worst case estimate. Additional calculations that use more realistic ground test reactor shield designs, which would most likely result in smaller shield thicknesses, are still needed.

Control Drive Mechanism Streaming (Reference (a))

Neutron streaming through CDM penetrations in a Be/B4C/W configuration of a Prometheus reactor shield was analyzed using MCNP. A notional model of the reactor, shield and control drive shafts was constructed and neutron flux values at the spacecraft payload were compared to a case in which there were no CDM penetrations. The results showed that for reasonably sized penetrations, there were very localized increases (~6x nominal) in neutron flux immediately behind the shield and opposite the gap around the shaft, but almost no increase in overall radiation levels at the payload. Gamma streaming effects were small (~20%). Since the streaming peak is very localized, it should be possible to significantly reduce the peak by the time it reaches sensitive components.

CONCURRENCE

This letter and its enclosures have been reviewed by and have the concurrence of the managers of KAPL Space Power Plant Systems (Schwartzman), KAPL FSO-Shielding (Pineau), and Bettis SEA-Shielding (Karnes).

Very truly yours,

J.E. Stephens

JE Stephens, Engineer
Space Reactor Shielding
KAPL FSO-Shielding

Reviewed by:

EC Pheil

EC Pheil, Engineer
Space Reactor Shielding
KAPL FSO-Shielding

Approved by:

MT Collins

MT Collins, Manager
Shield Design Development
KAPL FSO-Shielding

JES:jes

Computer Code Comparison for Space Reactor Shielding Analyses

Jonathan E. Stephens, Engineer
Space Reactor Shielding
Fleet Support Operation
KAPL, Inc.

Thomas M. Miller, Senior Engineer
Shielding Design and Development
Ship Engineering Activity
Bechtel Bettis, Inc.

Gary B. Zeigler, Engineer
Shielding Technology
Fleet Support Operation
KAPL, Inc.

Vernon Simmons, Senior Scientist
Shielding Design and Development
Ship Engineering Activity
Bechtel Bettis, Inc.

INTRODUCTION

Space shielding nuclear design presents computational analysis challenges not normally encountered in terrestrial shielding nuclear design. Modeling issues include unusual geometric configurations and large void spatial regions. Computer code preferences relating to standard shielding problems may not be appropriate for space shielding work. This enclosure documents the results of code testing done up to the point of project termination; however, additional work would have been required to choose the preferred code(s).

Several candidate computer codes were being tested with models representative of space shielding configurations, to determine which code(s) would be most appropriate for further design work. These codes were: PARTISN, a LANL discrete ordinates transport code utilizing a standard rectilinear spatial mesh; Attila, a discrete ordinates transport code using an arbitrary tetrahedral spatial mesh; and MCNP, a LANL Monte Carlo code. The intent was to test each code with 3 space shielding models: a spacecraft configuration with hydrogenous material in the shield, a spacecraft configuration with only non-hydrogenous material in the shield, and a configuration representing a ground test reactor (GTR) facility.

DISCUSSION

Code Descriptions

The candidate computer codes for space shielding were PARTISN (version 2.92), Attila (version 4.1), and MCNP (version 5). Other transport codes including the RACER and MC21 Monte Carlo codes were not considered because of their inability to handle photon transport. For MCNP, version 5 was selected because it is the first version to support mesh tallies (i.e. the flux solution over all elements of a spatial mesh). Relevant characteristics of each code are described below. Summary comparisons of the codes are displayed in Tables 1 and 2.

PARTISN (Cognizant tester: JE Stephens)

PARTISN, a finite difference discrete ordinates code, is well-established as a shielding design code in the NR program. It is simple to construct, visualize, and mesh a 3D model using the Sabrina and CoGeDif utilities. There are clear difficulties in using PARTISN for space shielding, however. The use of angular quadratures results in "ray effects" in large void regions, such as the space between the shield near the reactor and the electronics (a.k.a. "dose plane") at the payload (aft) end of the Prometheus spaceship. Also, since the mesh lines must be rectilinear and progress the full length of the model, a conical geometry such as the spacecraft is modeled within a much larger rectangular space; in other words, a large fraction of the mesh boxes are wasted in locations of zero importance. In addition, non-rectangular shapes such as the elliptical-conical Prometheus shield and spiral pipes are poorly represented using rectangular mesh regions, unless the mesh is extremely fine. Fine mesh can significantly increase problem run time or make the problem too large to run with available resources.

There are some advantages to using PARTISN. Results are obtained at all mesh boxes in the model and are accurate to the extent that the meshed geometry represents the actual design. In addition, PARTISN utilizes massively parallel computing machines very efficiently. Computer

jobs could use at least as many processors that could be made available at KAPL and Bettis without any appreciable degradation in per-processor performance. However, due to the large number of cells needed to mesh the problem and the detailed quadratures necessary to minimize ray effects, the memory requirements are very large (often greater than 100 GB). This requires calculations to reserve large numbers of processors just to secure the memory needed. A PARTISN calculation is expected to complete quickly (i.e. less than a day) since NR Program experience with PARTISN has shown that the code utilizes large numbers of processors efficiently. PARTISN also has the capability of producing contributon flux plots to help characterize how radiation gets from a source to a dose plane, which could be useful for improving shield effectiveness and reducing shield mass.

Table 1: Summary Comparison of Computer Codes

	PARTISN (Stephens)	Attila (Zeigler, Simmons)	MCNP (Miller)
Geometry	Simple to construct using Sabrina/CoGeDif; Rectilinear continuous meshing poorly suited to space geometries	Generated from CAD model, e.g. Solidworks; Tetrahedral mesh allows for efficient spatial representation	Constructed/checked using Sabrina/MCNP; Nearly exact representation of model
Cross Sections: Energy/ Angular Treatment	Collapsed to few groups; P7 scattering order; Large void regions result in "ray effects", even using highly biased quadratures	Collapsed to few groups; P7 scattering order; Large void regions result in "ray effects", even using highly biased quadratures	Continuous energy treatment; No angular approximations
Results	Results obtained everywhere; accurate to the extent of the modeled geometry, quadrature, and cross section/energy group structure.	Results obtained everywhere; accurate to the extent of the modeled geometry, quadrature, and cross section/energy group structure	Results obtained only where specified; subject to statistical variations; New mesh tallies available
Additional Comments	Extensive NR program experience with code	Little NR program experience with code	Experimentation needed to characterize statistics

color key: positive attribute, neutral attribute, negative attribute

ATTILA (Cognizant testers: GB Zeigler, V Simmons)

Attila is a finite element discrete ordinates transport code that utilizes a tetrahedral spatial mesh. Attila is not subject to some of the problems associated with a PARTISN-like mesh. The conical Prometheus model may be represented with many fewer mesh cells in Attila as compared to PARTISN, because it is not necessary to mesh unimportant locations outside the spacecraft. Also, curved/slanted surfaces are much easier to model with tetrahedrons than with rectangular prisms. Attila reads in a solid CAD model (from Pro-Engineer or Solidworks, for example) and

applies the mesh, making model generation simple. Since the geometry more accurately represents the design compared to PARTISN, the results are correspondingly expected to be more accurate.

Otherwise, Attila suffers from some of the same drawbacks as PARTISN, including the presence of ray effects due to using angular quadratures in large void regions. The NR program has much less experience using Attila than PARTISN, such that Attila is not verified on any KAPL or Bettis computer or qualified for any application. While computer memory requirements are much lower than in PARTISN because of the more efficient spatial mesh, Attila currently does not parallelize well on the supercomputers (this will likely change in the future), so the run time is expected to be longer.

Table 2: Code Performance Comparison on the Supercomputers

	PARTISN	Attila	MCNP
Processor Use	No limit to parallelization; Min. processor limit needed to reserve sufficient memory	Diminishing returns observed above 4 CPUs	No limit to parallelization
Memory Use	> 100 GB for space models; problematic on machines with low memory per CPU	High, but efficiency of meshing reduces requirements compared to PARTISN	Memory requirements not limiting, assuming mesh tallies are not used excessively
Speed	~ 1 day for space models	Expected to be slower than PARTISN due to limited parallelization with the current version	Several days or more, depending upon configuration and statistical criteria
Verification	Verified on BSC, but not for coupled neutron-gamma or space models K05 verification in progress	Not verified on any machine	Verification test suite run on Bettis '04 & '05 machines, but not yet documented
Additional Comments	Currently having problems with intermittent crashes on KAPL '04 & '05 machines	Would like Pro-Engineer capability to convert models to Attila geom	Significant (~2x) speed increases noted on KAPL '05 machine (K05)

color key: positive attribute, neutral attribute, negative attribute

MCNP (Cognizant tester: TM Miller)

Monte Carlo particle transport codes have several advantages when compared to discrete ordinates codes. The geometry can be modeled nearly exactly (the Prometheus shield is a truncated elliptical cone—this cannot be modeled exactly in any Monte Carlo code, but it can be approximated very closely) and Monte Carlo codes use continuous energy cross sections and no angular approximations. NR program Monte Carlo codes do not currently handle photon transport, leaving MCNP as the obvious Monte Carlo choice for space reactor shielding analyses.

Monte Carlo codes have 2 major drawbacks that prevent them from being the obvious platforms for nuclear calculations. First, the solutions are obtained only where specified, making it difficult to produce large-scale contour plots as can be done with the discrete ordinates codes. Version 5 of MCNP, however, permits the use of mesh tallies, where the solution is obtained over all regions of a user-supplied mesh (Reference (a)). The other significant drawback of Monte Carlo is the run time, which can be days or weeks (or longer) depending upon the statistical criteria, configurations, and the total amount of radiation attenuation required. Some time must be spent to experiment with variance reduction techniques and numbers of histories to optimize a problem for the required statistics.

Code Selection Models

Three code selection models were generated to test the three candidate codes in a variety of space shielding configurations. The first model was a spacecraft configuration with a shadow shield containing hydrogenous material, referred to as the "H Model" and pictured in Figure 1.

The reactor regions were homogenized, which was sufficient for space shielding code selection since the focus was on the shield and locations behind the shield. For simplicity, the shadow shield was modeled as a circular cone rather than an elliptical cone; again, this was considered adequate for the purposes of code selection. Even though these simplifications resulted in a geometry that could be modeled as a 2D r-z plane, calculations were performed in three dimensions since future design models would not be expected to demonstrate such symmetry.

For consistency, all codes assumed the same source (1 MWt uniformly distributed over the "core" region shown in Figure 1), room temperature cross sections, and equivalent material compositions. For the H model, flux results were analyzed on the aft surface of the shadow shield and at the payload dose plane, which was 50 meters aft of the aft end of the fuel region.

The second code selection model, referred to as the "non-H model" because the shadow shield did not contain hydrogenous material, is shown in Figure 2. This model was similar to the H model, except that the shadow shield materials were changed to layers of Be and B_4C (resulting in a reduced shield thickness but higher mass). In addition, a single control device mechanism and an associated shield penetration were added to the model to investigate how each computer code handled neutron streaming through void gaps. As in the H model, results were analyzed on the aft surface of the shadow shield, and at the payload dose plane.

Figure 1: Schematic of H Model

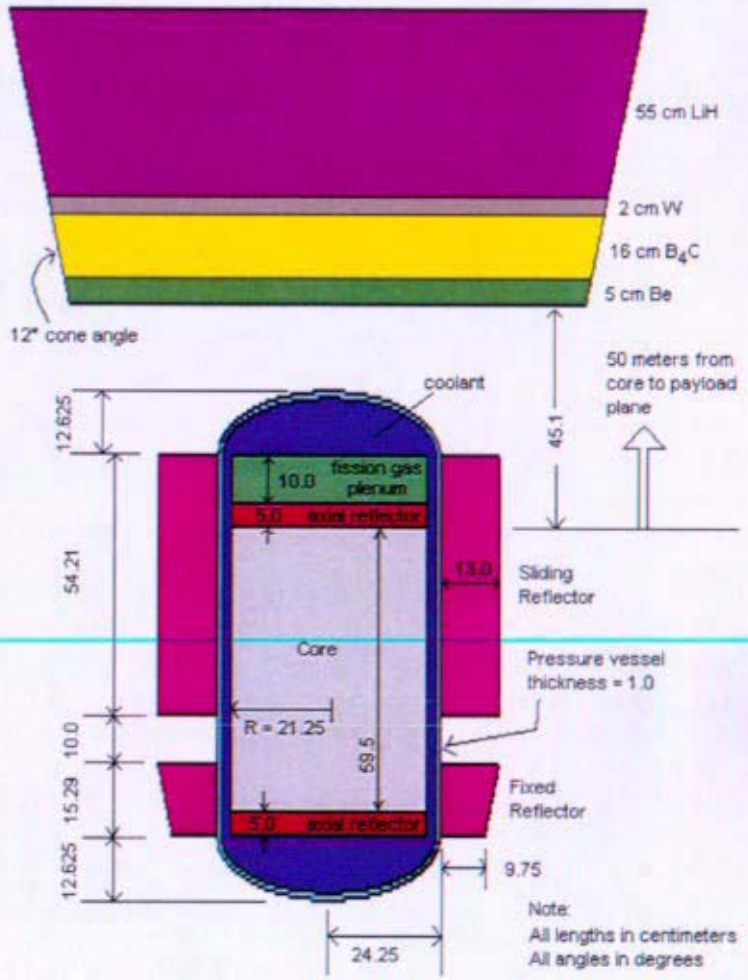

Figure 2: Schematic of Non-H Model

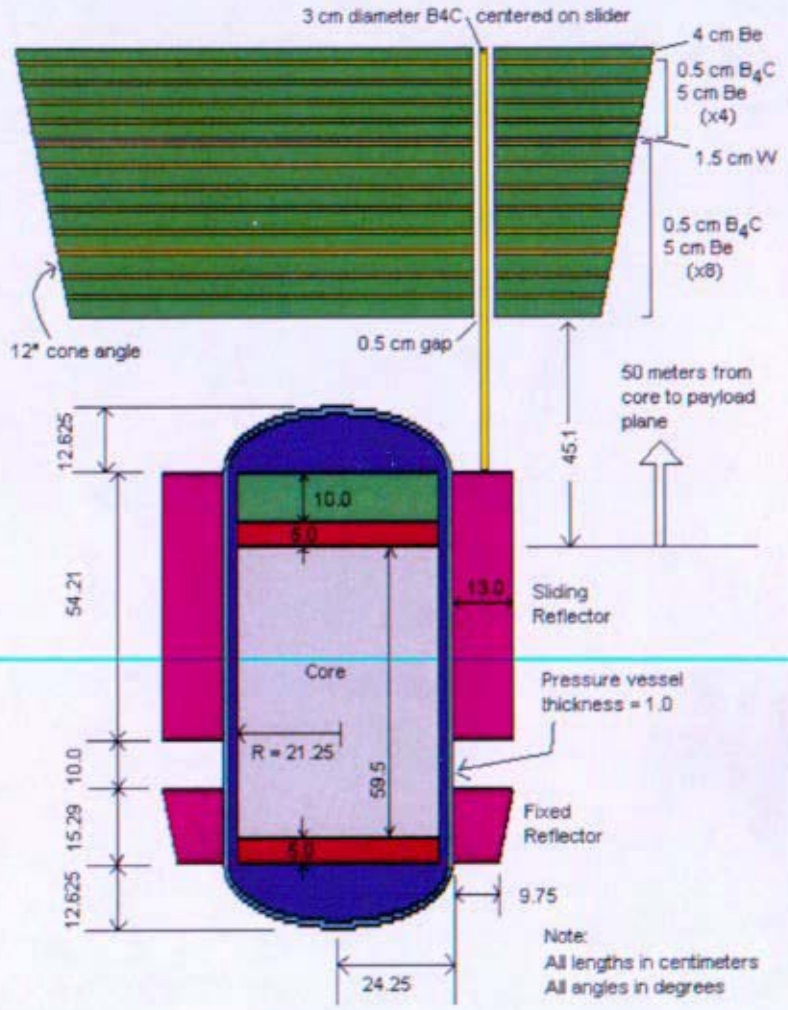

The third code selection model consisted of the non-H model inserted into a notional ground test reactor facility. This model was referred to as the "GTR model" and is pictured in Figure 3. Results for this model were to be analyzed at the radial outer surfaces of the water tank and concrete room.

Figure 3: Schematic of GTR Model

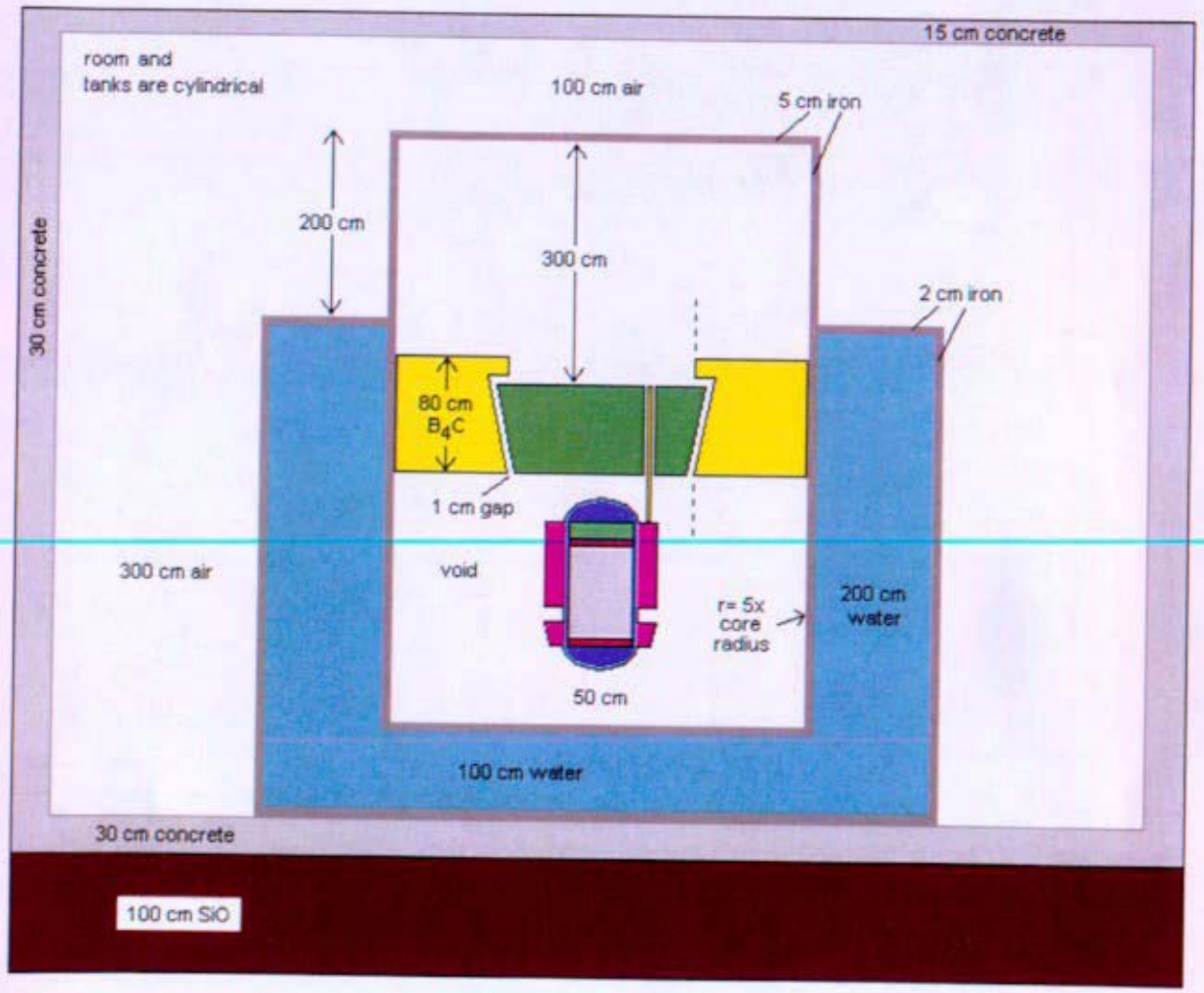

Results

PARTISN

Initially, the H model was run in two dimensions (r-z) with several different biased quadratures to determine which quadrature minimized ray effects aft of the shadow shield. The results of this study are displayed in Figure 4. In each image, the reactor and shield can be seen at the bottom left, and the upper edge of the plot is the payload dose plane. Despite using the most biased quadratures readily available (i.e. greatest density of angles aimed in the axial direction), all quadratures result in ray effects at the dose plane. Since the most important part of the dose plane is directly behind the reactor and shield, and regions of the plots that are radially outside the primary cone angle are not important, it can be inferred from the plots that the SG40 quadrature showed the best performance.

Figure 4: PARTISN Results for 2D H Model for Various Biased Quadratures
(each contour line represents an order of magnitude of total neutron flux)

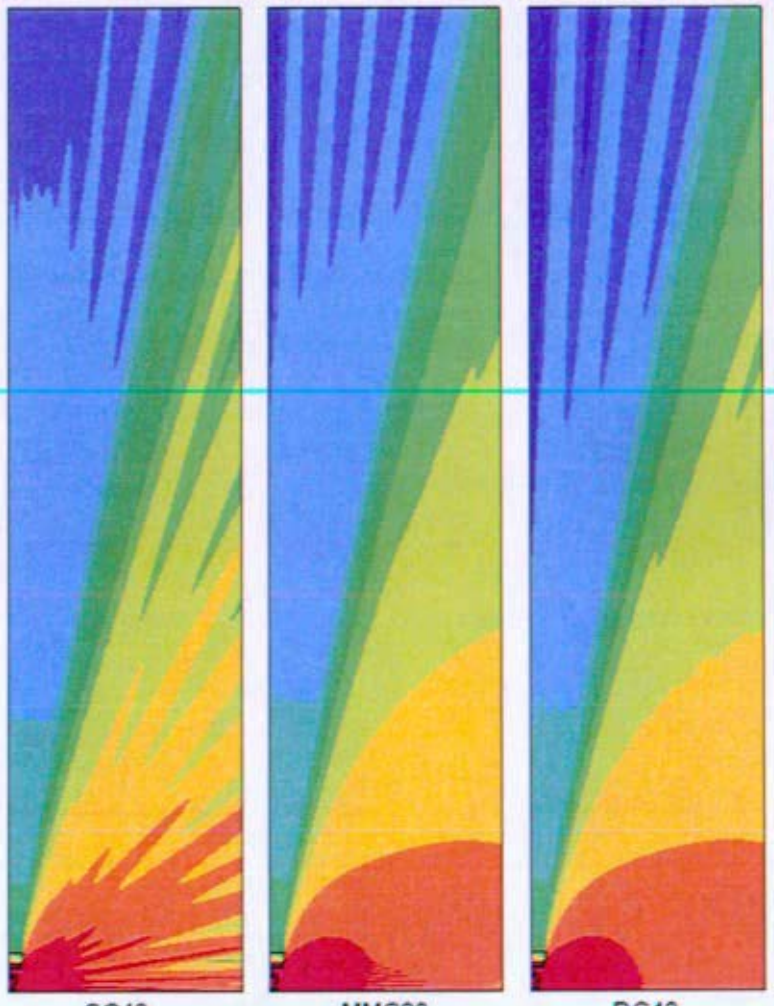

SG40	MMG20	DG40
40 Single Gauss cones, 200 angles/octant	20 modified-midpoint Gauss cones, 124 angles/octant	40 Double Gauss cones, 250 angles/octant

Regardless of which quadrature is used, a method would need to be developed to correct for the ray effects at the dose plane. Based on the results above, 3D PARTISN models utilized the SG40 quadrature because it minimized ray effects at the payload dose plane. Investigation of quadrature effects on piping penetration analyses would need to be included in future studies with this biased SG40 quadrature. With 200 angles per octant, the memory requirements for PARTISN computer jobs were very large.

At the time the study was terminated, only the H Model had been run using PARTISN. Because of the memory-intensive SG40 quadrature and the large model geometry (going from the reactor to the dose plane 50 meters away), the radial dimensions of the model had to be truncated and the mesh was coarse. The mesh size was 2 cm at the reactor and shield and 20 cm radially outside and aft of these regions. The radial extents, which should have been roughly +/- 12 meters at the dose plane, were modeled only to +/- 2 meters, reducing the number of mesh cells needed by a factor of four.

Neutron results for the 3D H Model in PARTISN are shown in Figure 5. The disadvantage of using the PARTISN mesh is demonstrated by the vertical mesh lines, which must progress the full distance to the dose plane (which is well beyond the upper edge of the plot) even though the 2-cm mesh is only intended to be in the reactor and shield. The plot shows 1-MeV equivalent Silicon-damage neutron fluence, obtained by applying a response function to calculated group fluxes. For comparison to the other codes, the peak total neutron flux on the aft surface of the shield was 2.77×10^5 n/cm^2-sec. Small ray effects are already visible at about 2 meters beyond the back of the shield.

Gamma results for the same case are shown in Figure 6. The plot shows gamma dose in rads-Silicon, obtained by applying a response function to the calculated gamma group fluxes. For comparison to the other codes, the peak total gamma flux on the aft surface of the shield was 1.36×10^9 gammas/cm^2-sec.

Figure 7 shows the same results as Figures 5 and 6, but for a larger part of the model and without the mesh displayed. The upper extent of the plot is about half the distance to the dose plane. Significant ray effects are observable in both plots. Also, for the neutron fluence plot, some of the contour lines immediately aft of the shadow shield appear to progress directly aft rather than following the 12-degree cone angle as would be expected. These lines are coincident with the transition between the 2-cm and 20-cm meshes and suggest that such mesh size transitions in void areas introduce additional numerical errors into the problem.

The PARTISN job was run on the KAPL '04 Linux cluster, using 64 processors. For 15 neutron groups, 19 gamma groups and a group relative convergence criterion of 0.025, the job ran in 31.7 hours. As suggested earlier and from NR program experience, running on twice as many processors would cut the run time in half. Also, evidence from other work suggests that running on the '05 Linux cluster would reduce run time by up to 50%. It should be noted that a discontinuous mesh capability has recently been added to a newer version of PARTISN, which was not available to the NR program at the time of the study. This option would greatly reduce the number of mesh cells in a problem by eliminating the requirement that mesh lines progress to the full extents of a model.

Figure 5: 1-MeV Equivalent Silicon-Damage Neutron Fluence for H Model in PARTISN

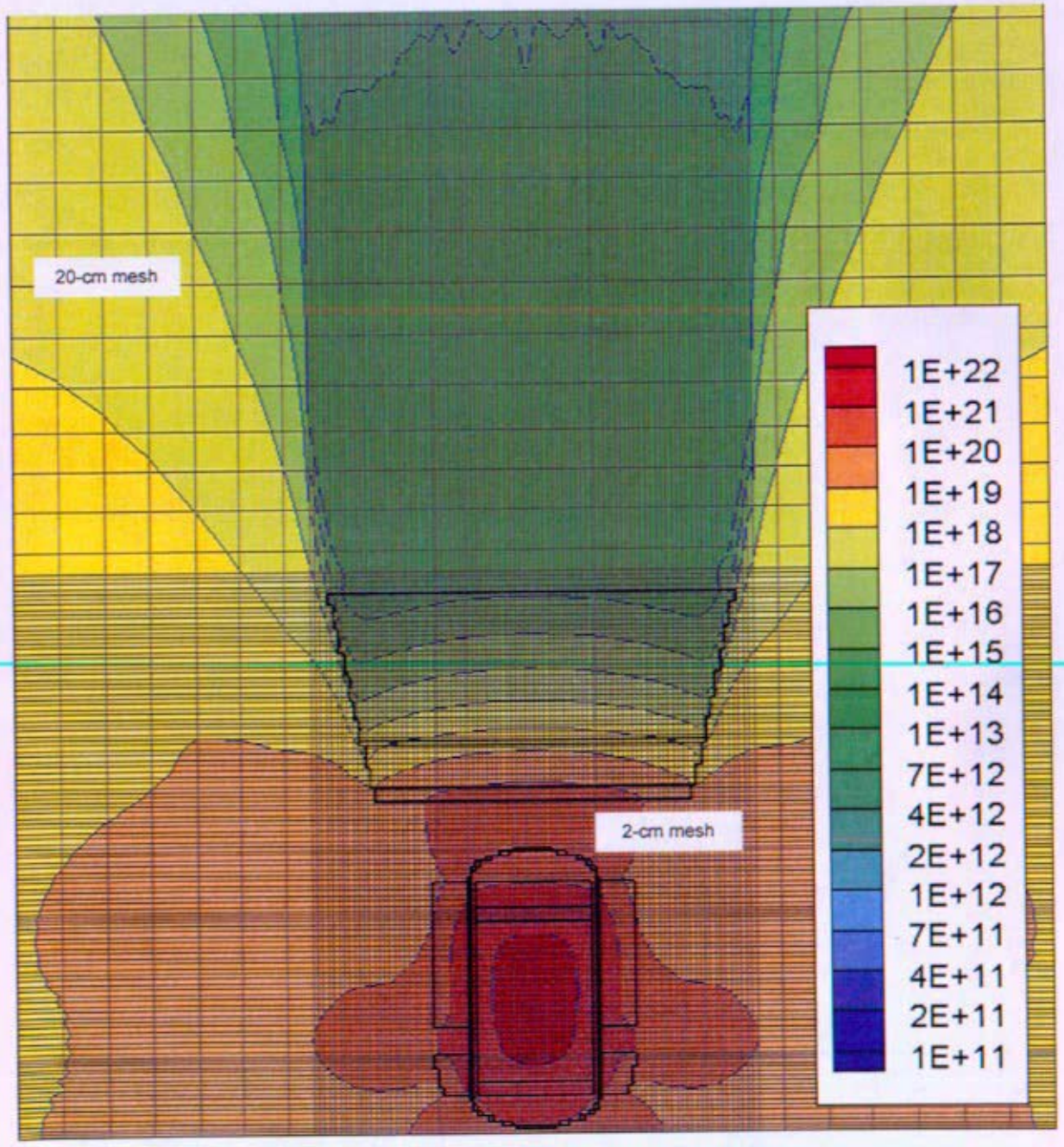

Figure 6: Gamma Dose (rads-Silicon) for H Model in PARTISN

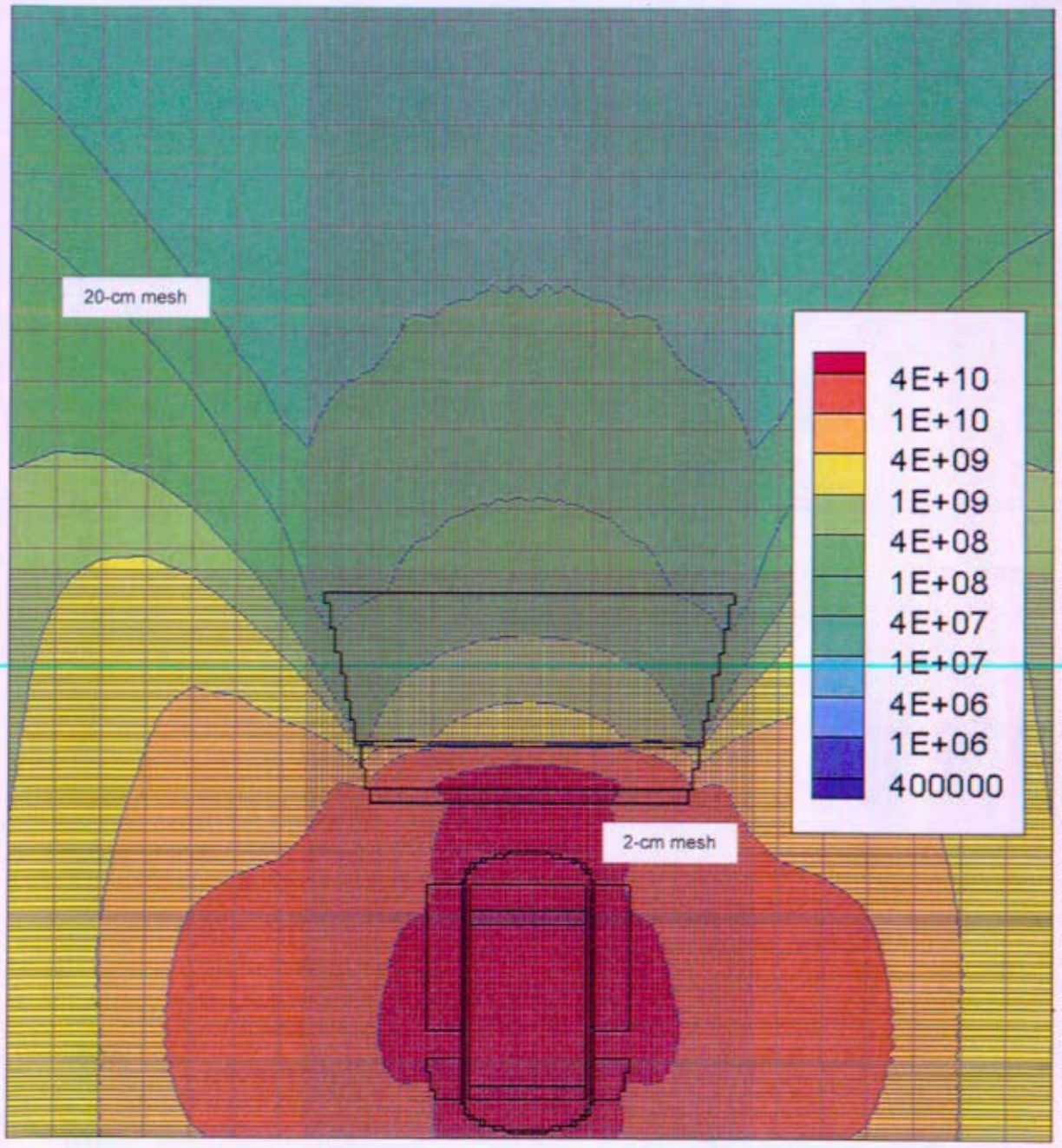

Figure 7: 1-MeV Equivalent Si-Damage Neutron Fluence (left) and rads-Si Gamma Dose (right)
Results for H Model in PARTISN (same scales as Figures 5 & 6)
model width = 4 meters, model length = 18 meters

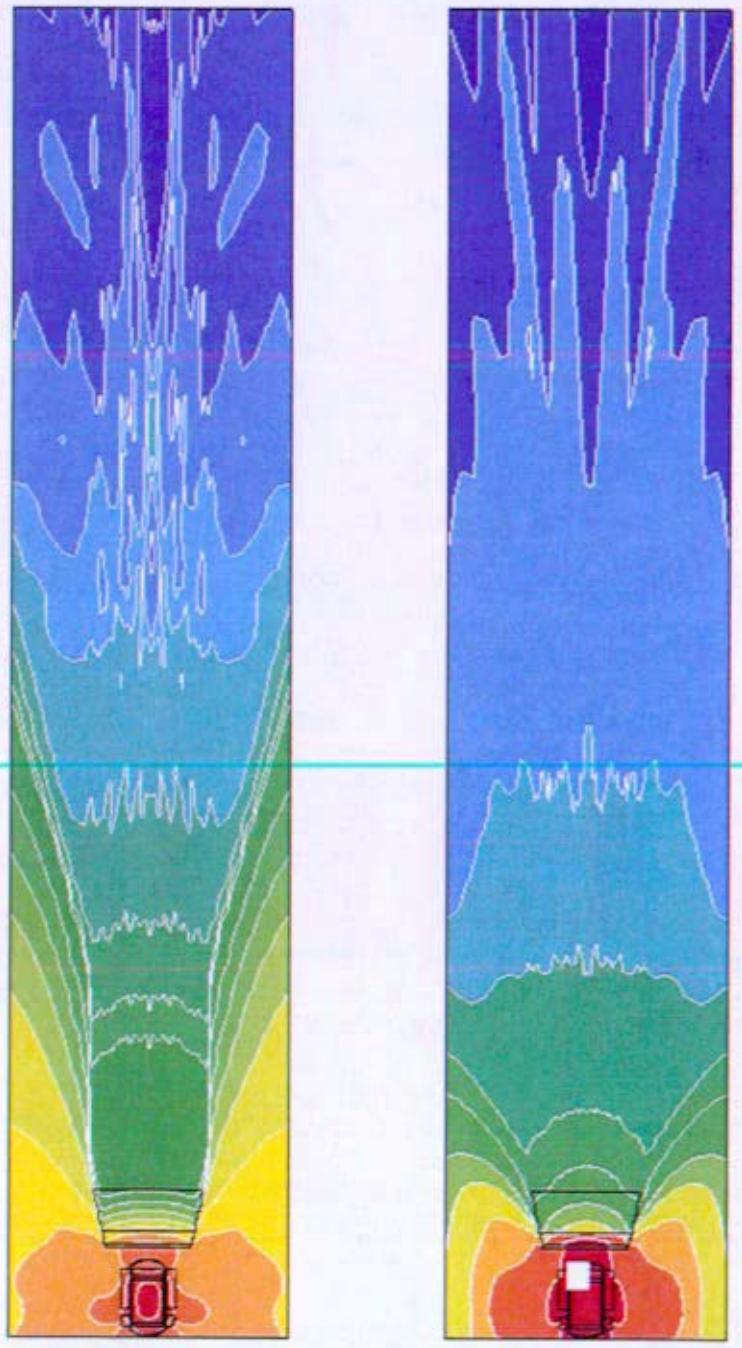

ATTILA

Initial attempts at creating the first two test models were made using the Pro-Engineer Wildfire software. However, several bugs were uncovered in these initial attempts that prevent Pro-E Wildfire from generating a sound Parasolid geometry file. Therefore, final model development was performed with the solid geometry modeling tool, SolidWorks. 3D Parasolid geometries for all three hypothetical models were created using this tool. Due to the symmetry of the models (or near symmetry in the GTR model), only ½ of the total geometry was modeled for the H and non-H space models, and ¼ of the total geometry was modeled for the GTR model.

The Parasolid geometries were all read into Aetius, the Attila input set-up GUI, and tetrahedral meshes were generated for each. All other job input parameters, including cross section data, source specification, and edit specification were also entered into Aetius, which then generated Attila input decks for each job.

The first two jobs created used the 1st and 2nd hypothetical geometries (H Model and non-H Model), respectively, and were run as basic proof-of-principle jobs on a PC. Both meshes were relatively coarse with maximum lengths of 5 to 10 cm for any given tetrahedron side in the reactor and shield components, and a maximum of 1 meter in the space region. Using these mesh specifications, the H Model used 75943 mesh cells, and the non-H model used 197852 mesh cells. Both jobs used the same 34 group (neutron + gamma) structure used in PARTISN jobs, and a 1% convergence criterion.

The first job used very coarse parameters for quadrature (a level symmetric S4 quadrature) and P2 scattering cross sections with the Galerkin scattering treatment (equivalent to P3 scattering cross sections). The second job, however, used a more refined quadrature (an S16 Triangle Chebyshev Double Legendre quadrature) and P6 scattering cross sections with the Galerkin treatment (equivalent to P7 scattering cross sections). The first job took approximately 2 hours to run. TECPLOT contour plots were generated by Attila of the total neutron and total gamma fluxes, which are shown in Figure 8. The second job took approximately 135 hours to run. TECPOT contour plots were again generated by Attila of total neutron and gamma fluxes, which are shown in Figure 9. As seen in both Figures 8 and 9 for both neutrons and gammas, parameter refinement would be necessary due to the large regions in which negative fluxes were generated in the shield region. Negative neutron and gamma fluxes were predominant throughout the space region (not shown) for both jobs, which made all comparisons to PARTISN and MCNP at the dose-plane irrelevant for these jobs.

Finally, several preliminary attempts were also made at generating results for the GTR model, which with 1/4th of the geometry modeled was comprised of 400,482 mesh cells. As with the space models, this mesh was generated using very coarse mesh parameters, though some of the advanced meshing features available in the Aetius GUI were used in order to better control the axial and azimuthal meshing segments in a preferred direction. Initial attempts to run the GTR problem were made on the Wildfire supercomputer platform. However, even a coarse, truncated problem proved very memory intensive. Since the parallel capability of the current version of Attila reaches peak performance at 4 processors, this made the initial, large jobs virtually impossible to run on the Wildfire, either due to computer memory or time constraints. A final calculation was performed with the GTR model with the mesh described above on the Bettis FY05 Linux Cluster, and as with the space models, also used a coarse quadrature

(Square Chebyshev Legendre quadrature with Sn order set to 4), and only P1 scattering cross sections. This final Attila job took approximately 7 hours to run. Despite the coarseness of the parameters used for this final model, the results, seen in Figure 10, seem (qualitatively) reasonable. This final case indicates that with some additional parameter refinement, Attila would most likely be able to produce an accurate solution comparable to either MCNP or PARTISN. However, in order to perform such refinement, better parallel capability (i.e. an MPI version of Attila being developed) would be necessary.

Figure 8. Attila Generated Total Neutron (left) and Gamma (right) Fluxes (per cm^2) in Reactor and Shield Regions for H Model. Note the large areas of dark purple at back of shield: these regions are dominated by negative fluxes and indicate the need for mesh and parameter refinement.

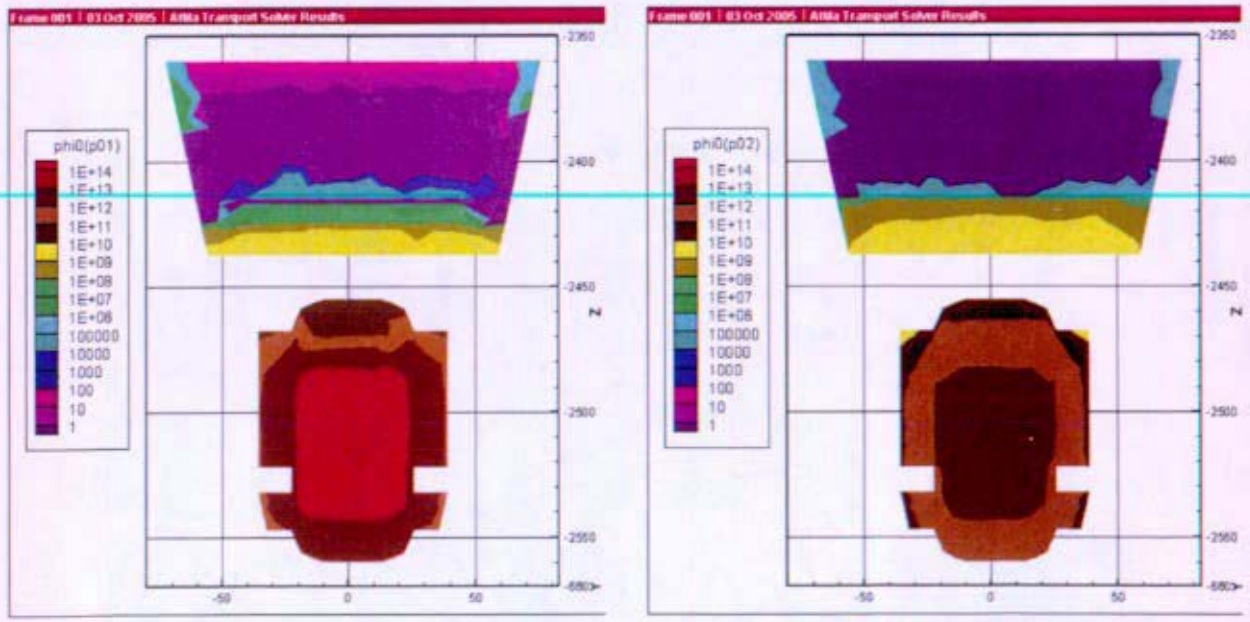

Figure 9. Attila Generated Total Neutron (left) and Gamma (right) Fluxes (per cm^2) in Reactor and Shield Regions for non-H Model. Note that there are still large areas of dark purple (negative fluxes) for both neutron and gammas with refined quadrature and cross section expansion. This indicates the need for mesh refinement in these components.

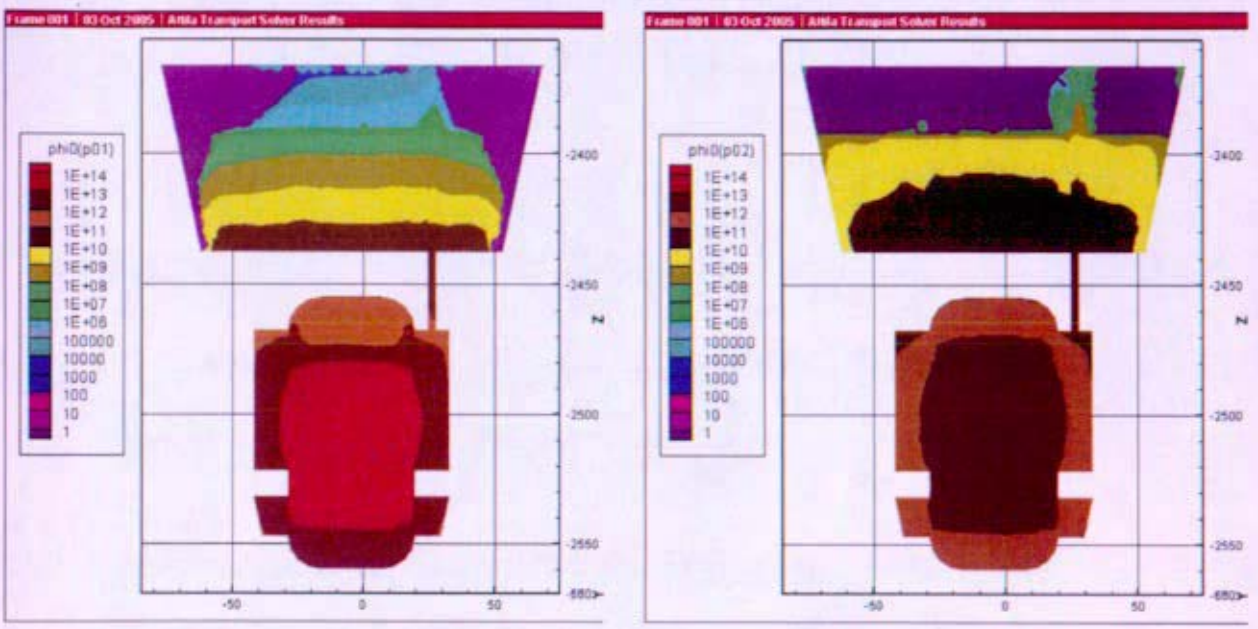

Figure 10. Attila Generated Total Neutron (left) and Gamma (right) Fluxes (per cm^2) in Reactor and Shield Regions for the ¼ GTR Model in the XZ Plane.

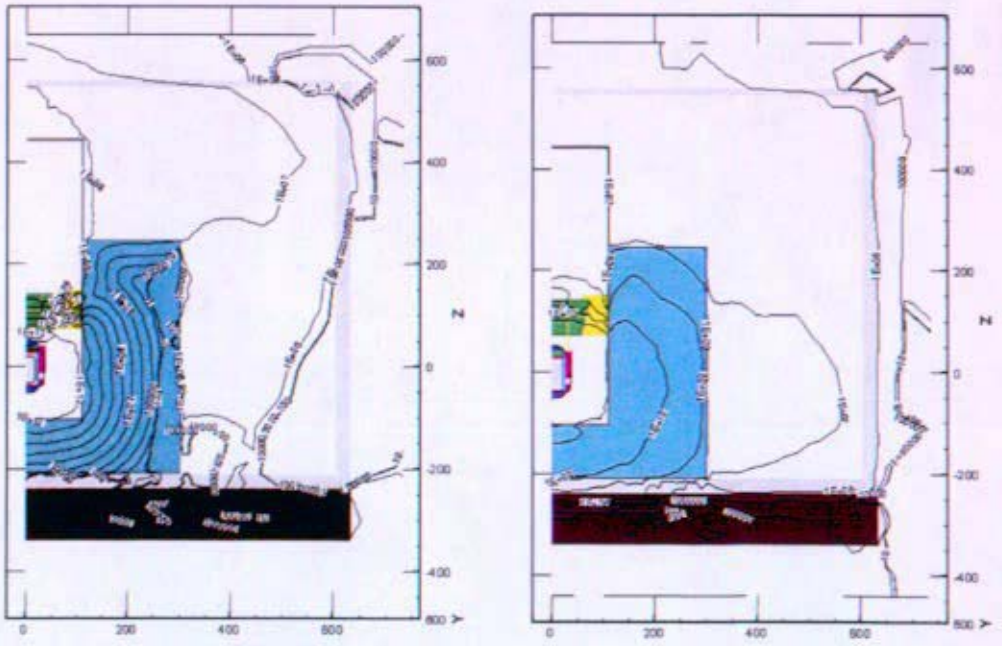

MCNP

At the point at which the code selection study was terminated, only the H Model had been run in MCNP, and the statistics were inadequate at the dose plane to make any conclusions other than ones related to run time. The relative uncertainties (1 standard deviation) for the tallies at the dose plane were about 10%.

The statistics on the aft surface of the shadow shield were very good, however. The total neutron and gamma fluxes were obtained for a 2-cm square mesh covering the back of the shield. The average relative uncertainties (1 standard deviation) were less than 0.5% for the mesh tallies. The neutron flux is displayed in Figure 11. A zero importance region was used radially outside of the shadow shield resulting in zero flux in the four corners of the figure.

Figure 11: Total Neutron Flux (n/cm^2) on the Aft Surface of the Shield for H Model in MCNP5 (dimensions in cm)

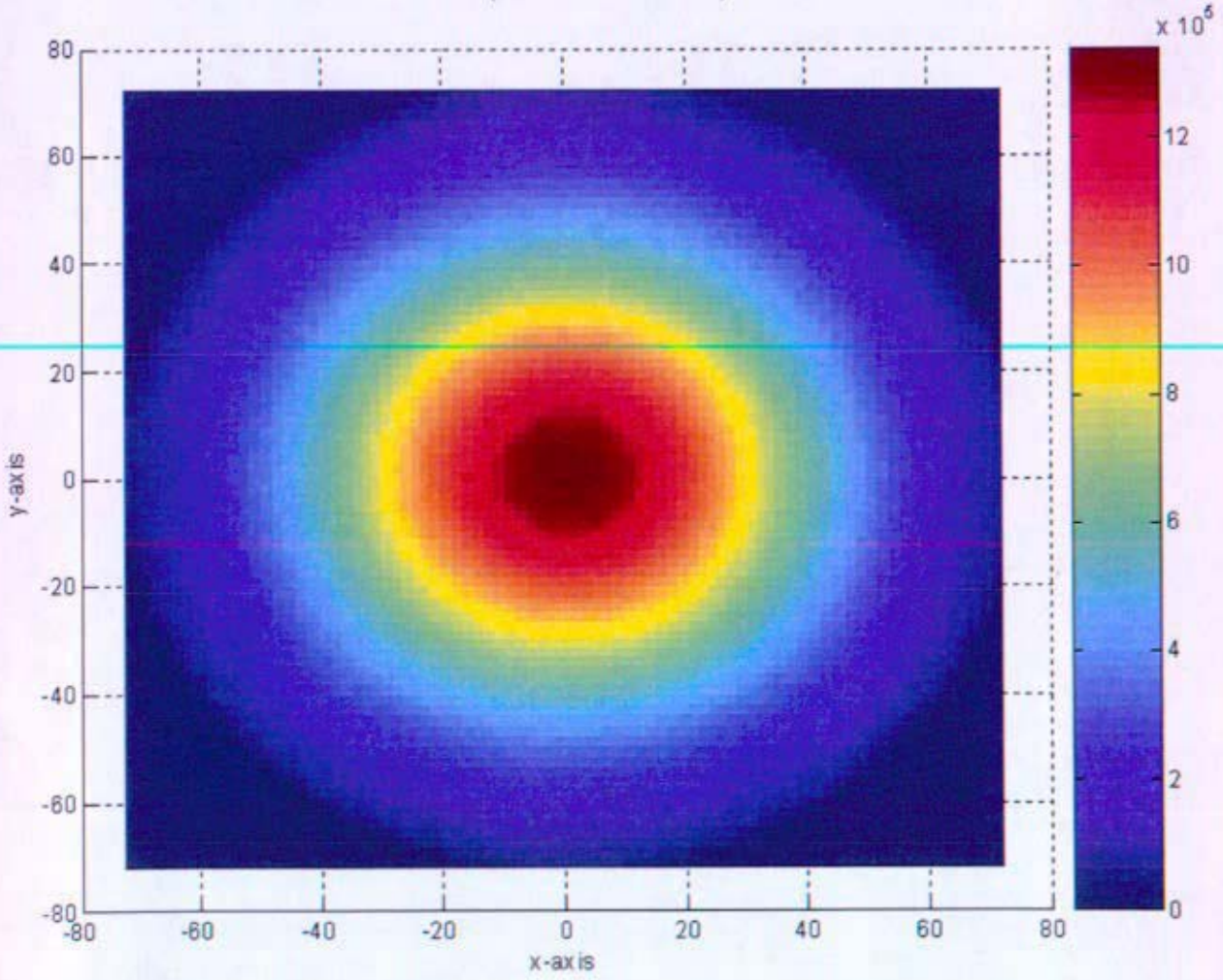

The peak neutron flux on the aft surface of the shield for the MCNP H Model was 1.34×10^6 n/cm^2-sec. This value was a factor of 4.8 higher than the neutron flux calculated by PARTISN at the same location. The peak gamma flux calculated by MCNP was 2.37×10^9 gammas/cm^2-sec, which was a factor of 1.7 higher than the PARTISN value. The differences between the PARTISN and MCNP results would have been investigated further had time permitted, by comparing more detailed data such as flux by energy group. The differences could be caused by the modeling approximations in the PARTISN case, energy group collapsing, scattering order, cross-section differences, etc.

The MCNP computer job was run on the Bettis '05 Linux cluster using 128 processors. Seven billion histories were run in only 22 hours, but as mentioned earlier the resulting statistics at the payload dose plane were inadequate, despite having used extensive variance reduction techniques.

CONCLUSIONS

Much of the code testing was not completed, so a final decision on which code should be used for space reactor shielding work was not made. However, much was learned from the testing that was completed.

PARTISN alone did not appear to be well-suited to large space system configurations with significant void space. Ray effects were problematic, regardless of quadrature selection. Many mesh cells were wasted in zero-importance locations due to the continuous rectilinear meshing requirements of PARTISN. Also, it may be possible to use PARTISN, which performed well in the immediate vicinity of the reactor and shield, in conjunction with MCNP. This is referred to as a PARTISN/MCNP Splice and was not investigated in this study, but was being investigated. The objective of a PARTISN/MCNP Splice would be to use PARTISN in the reactor and shield where it is more efficient than MCNP and use MCNP in largely void regions where discrete ordinates programs, like PARTISN, produce ray effects.

Attila utilized a much coarser spatial mesh than PARTISN and coarse options for quadrature and cross section scattering order to meet the memory constraints of the platforms used, and to run jobs in a reasonable amount of time. In doing so, results for the two space models were plagued by negative fluxes within the shield, making results at the dose plane unreliable. The GTR cases were also run with coarse parameters, though the final GTR mesh was created with the advanced meshing tools available in the Attila GUI, Aetius. The results for the GTR model with a slightly refined mesh suffered less from the negative fluxes seen in the space models, which indicates that with some additional parameter refinement, Attila solutions would be much more accurate. The limited parallelization of Attila on the supercomputers restricts the amount of parameter refinement achievable, though, and results in unreasonably long run times when problems with finer parameters can be run. This code would likely be a much stronger competitor in the future, as the NR program gains more expertise in Attila and the code is updated to utilize massively parallel computers more efficiently.

MCNP provides the most accurate results, provided enough histories are run to achieve acceptable statistics. As computing power increases with time, Monte Carlo methods are

increasingly likely to be the best choice for space reactor shield transport calculations. All Prometheus shielding sensitivity studies were performed using MCNP and seemed to be the leading candidate for space craft evaluations. However, PARTISN or Attila might be required for GTR shields because MCNP has difficulty getting acceptable statistics in a reasonable amount of time for deep penetration problems like the GTR. A discrete ordinates/MCNP splice could be used for either the spacecraft or GTR model

The final code selection would also have been dependent upon the particular mission undertaken. For example, PARTISN may have performed better relative to MCNP for a ground-based configuration than for the conical Prometheus geometry.

QUALIFICATION OF METHOD

All results presented herein were pre-decisional and intended for planning and discussion purposes only. No method uncertainty or design assurance factors were applied to any of the results.

The codes used in this analysis (PARTISN 2.92, Attila 4.1, MCNP5) were in various pre-production states on the supercomputer platforms. None of these codes were verified for space work or coupled neutron-gamma calculations, though efforts to verify PARTISN and MCNP on the Linux clusters are in progress. DATATRAN modules used to post-process PARTISN results were production level. Tecplot version 10.0 was used to visualize results.

This enclosure is a summary of work documented in KAPL SWR-00073, Reference (b).

REFERENCES

(a) LANL document LA-UR-03-1987, "MCNP – A General Monte Carlo N-Particle Transport Code, Version 5," X-5 Monte Carlo Team, April 24, 2003.

(b) KAPL Shielding Work Record: SWR-00073, "SPP Space Shielding Analyses," J.E. Stephens, July 2005.

This page intentionally left blank.

Charged Particle Transport Code Selection Summary

Thomas M. Miller, Senior Engineer
Shielding Design and Development
Ship Engineering Activity
Bechtel Bettis, Inc.

INTRODUCTION

This is a discussion of the charged particle radiation transport code selection. Radiation transport codes beyond those typically used by the NRPCT will be needed to quantify the effects of the naturally occurring background radiation in space and possible charged particle radiation leaving the surface of the reactor.

The main sources of natural ionizing radiation in the space environment are trapped belt radiation (such as the Van Allen belts), consisting mainly of protons and electrons, solar energetic particles, produced by events such as coronal mass ejections and associated phenomena on the Sun, and the galactic cosmic ray (GCR) background, composed of all naturally occurring elements.

Any planet or moon in our solar system that is a magnetic dipole will be surrounded by trapped belt radiation, consisting mainly of protons and electrons. The strength of that magnetic field and its relative location to the Sun will determine the spatial and energy distribution of the trapped belt radiation. Jupiter and its moons are all surrounded by tapped belt radiation.

An example of trapped belt radiation in our solar system is the Earth's own Van Allen belts. The Earth is protected from much of the radiation in space by its own magnetic field. However, this magnetic field can capture charged particles and keep them trapped in belts surrounding the Earth (Van Allen belts). Therefore, the belts' spatial distribution is determined by the magnetic field of the Earth, which also means that the belts are subject to deformation by solar activity. In general, particles in the belts are located at higher altitudes at the equator and lower altitudes at the poles; one exception is the South Atlantic Anomaly. The protons in the Van Allen belts likely come from fragmentation events with the GCR and Earth's atmosphere and from the Sun. The electrons in the trapped belts can come from the Sun and from stripping reactions of GCR, which are not fully ionized, as they enter the Earth's atmosphere. Figure 1 gives an idea of these particles energies and distances from the Earth.

The Sun is a major source of radiation in the space radiation environment. This radiation consists of energetic particles that are emitted from solar flares and coronal mass ejections, which are collectively known as solar particle events (SPEs). The species of these particles include electrons, protons, alpha particles, and other heavy ions, and their energies extend over a broad range. A SPE can occur at any time, but typically more occur during the maximum of the approximately 11-year solar cycle. The duration of a SPE can be from a few hours to several days. Usually, the energies and/or fluxes of an SPE are too low to be a major concern, or the particles emitted by the event may not travel in a direction that is a concern. Figure 2 shows the integral proton fluence of four large SPEs.

The particle species present in the GCR background include all naturally occurring isotopes from hydrogen to uranium, and also include beta particles. The energies of the GCRs have a very broad range and cover several orders of magnitude with a peak around 1 GeV per nucleon. The intensity of GCRs seen on Earth or in low Earth orbit is affected by the solar cycle because solar activity affects the Earth's magnetic field. The GCR spectrum is at a minimum during solar maximum and at a maximum during solar minimum. The GCR intensity below 1 GeV per nucleon can fall about an order of magnitude between solar minimum and solar maximum.

Figure 3 shows the fluence of GCR ions at 2 GeV per nucleon relative to the fluence of silicon at 2 GeV per nucleon.

In addition to the natural radiation occurring in space, the reactor could also emit electron radiation from the outer surface of the reactor, reflector, or micrometeoroid shielding. The space reactor is not surrounded by large amounts of equipment and shielding and is not grounded like land based reactors. Gamma radiation levels at the outer surface of the reactor are very high. Gamma radiation is attenuated by interactions and transference of energy to the electrons in materials. Within materials the electrons lose energy and can be recaptured. However, at the surface of the reactor, reflector, or surrounding micrometeoroid shield the electrons could leave the surface of the reactor. An equilibrium would be established depending on the voltage of the spacecraft. The gamma flux at the exposed surface of the reactor is fairly high, so there is the potential for the electron radiation leaving the surface of the reactor to become important to spacecraft charging. Also, because the electrons are charged, they could go around the shield and be pulled back into the spacecraft. Therefore, a code is required to determine the production rate and transport of these electrons to evaluate whether this is a concern, and, if so, to evaluate solutions.

DISCUSSION

Codes that are typically used by the NRPCT transport neutral particles with energies that are seen in reactor applications using measured cross-sections. These codes may be adequate to use when designing shielding for the gamma and neutron radiation that would be produced in a space reactor. However, these codes can not handle charged particles or neutral particles at the necessary energies in space: eV to several GeV per nucleon. Looking at the body of radiation transport codes, several stand out as a possibility to fill this need. These codes are MCNPX (Reference (a)), PHITS (Reference (b)), FLUKA (Reference (c)), HZETRN (Reference (d)), HETC-HEDS (Reference (e)), and GEANT4 (Reference (f)). All of these codes use Monte Carlo techniques except for HZETRN which is a deterministic code. The codes FLUKA, HETC-HEDS, and HZETRN are part of NASA's radiation transport code development consortium. Each of these six codes has their own pros and cons, which will be discussed next.

Of these codes, the one about which the least is known is GEANT4. GEANT4 was developed by people all around the world, but is maintained by a group at the CERN laboratory on the border of Switzerland and France. Essentially, GEANT4 is a collection of hundreds of nuclear models that have been brought together into one place. The user chooses which nuclear models are applicable to their problem, and only those are used during the transport calculation. What is not clear about GEANT4 is whether or not the nuclear models work together. For example, if one nuclear model is used to create a distribution of neutrons produced in a reaction and another model is used to create a distribution of protons produced in that same reaction it is not clear when sampling those distributions if charge and mass will be conserved. This is pointed out because the developers say that any combination of models can be chosen. It would seem then that coding independent of these nuclear models would be necessary for conservation of charge and mass in our previous example, and that coding may need to change with different combinations of nuclear models.

MCNPX was developed at the Los Alamos National Laboratory, and is a high energy multi-particle extension of MCNP (Reference (g)). Particles of interest that MCNPX can transport that

MCNP can not are protons, deuterons, tritons, and alphas. The nuclear models used to describe the interactions of these light ions along with neutrons, photons, and leptons allows for the reliable transport of particles with energies up to about 5 GeV per nucleon and 1 GeV for photons and leptons. Above 5 GeV per nucleon, some of the nuclear models begin to break down. For particles that are heavier than an alpha, MCNPX is not applicable. Users often try to use MCNPX to transport ions heavier than the alpha by disassociating the individual neutrons and protons that make up the heavy ions and transporting them individually. This will provide the user with an answer, but it is problem dependent as to whether that answer is valid, totally invalid, or a bounding solution. To illustrate this point, consider a 1 GeV ^{56}Fe ion entering a shield. Since the ^{56}Fe ion has a net charge it will undergo continuous slowing down effects. When the neutrons of the ^{56}Fe ion are separated from the protons, the neutrons no longer undergo continuous slowing down effects. These neutrons would also scatter as an individual neutron would instead of how they would scatter as part of the ^{56}Fe ion.

The code HETC-HEDS was developed at the University of Tennessee, and is a multi-particle extension of the already high energy code HETC. HETC alone transports neutrons and protons over the same energy range as MCNPX, but HETC has a cutoff energy at 20 MeV. To transport neutrons and protons less than 20 MeV or any photons and electrons HETC-HEDS must be coupled to another code like MCNPX, MCNP, or MORSE/EGS. Ions up to Fe can be transported over an energy range of 25 MeV per nucleon to 22.5 GeV per nucleon, but the target nucleus must not be heavier than Pb. The fragmentation model in HETC-HEDS is a semi empirical model. Therefore, it is probably the fastest but also the least detailed of the ion fragmentation models in these six codes. Finally, as part of the NASA radiation transport code development consortium, it is very much still under development.

HZETRN has been under development for several years by NASA at their Langley Research Center. As stated previously, it is the only code discussed here which does not use Monte Carlo methods. In its original state, HZETRN was a 1-D analytic code that generated its cross sections using the same nuclear models that are now used in HETC-HEDS. Therefore, the energy range and species of ions transported were the same as HETC-HEDS. To calculate the flux of particles at a point, the flux would be calculated along several distinct rays (usually between 500 and 1000) that passed through the desired position. This methodology is very simple and very fast, but is not very useful for complex geometries. As part of NASA's radiation transport code development consortium, HZETRN is being extended to 3-D, and improved nuclear models are being developed for cross section generation. The improvements to HZETRN do not include photon or electron transport.

The code FLUKA, which is the most sophisticated code discussed thus far, was developed by a joint venture between the CERN laboratory and the INFN laboratory in Italy. FLUKA will transport hadrons, light ions, and heavy ions over an energy range of ~0 eV per nucleon up to 10000 TeV per nucleon and photons and leptons up to 1 GeV. Below 5 GeV per nucleon, a relativistic quantum molecular dynamics model is used for nucleus-nucleus interactions, while above 5 GeV per nucleon a dual parton model is used. Four shortcomings of FLUKA are: (1) It only runs sequentially (however the developers provide software to combine the results of many single processor calculations). (2) Below 100 MeV per nucleon nucleus-nucleus interactions are not modeled (ions below 100 MeV per nucleon only undergo continuous slowing down effects). (3) Below 20 MeV neutrons use multi-group cross sections instead of continuous energy cross sections. (4) Currently, the developers will not release the FLUKA source code. As part of the

NASA radiation transport code development consortium, the nucleus-nucleus interaction model below 5 GeV per nucleon is being improved by a group of developers at the University of Houston.

Finally, the most sophisticated code that will be described here is PHITS, which is developed at RIST in Japan. Like FLUKA, PHITS will transport photons, leptons, hadrons, light ions, and heavy ions. However, the energy range is from ~0 eV to 200 GeV per nucleon for hadrons and ~0 eV to 100 GeV per nucleon for ions, but these energy ranges are broad enough for our purposes. The nucleus-nucleus interaction model is a quantum molecular dynamics model. The four shortcomings listed for FLUKA serve as strengths for PHITS. PHITS can run in parallel via the message passing software MPI, nucleus-nucleus interactions are modeled down to 10 MeV per nucleon, below 20 MeV neutrons, photons, and electrons use continuous energy cross sections (this is very similar to MCNP), and the developers will distribute the source code. Another useful fact about PHITS is that its geometry package is compatible with MCNP. Therefore, the combination of MCNP and PHITS would allow for the same geometry to be used in reactor design calculations and shielding design calculations for neutral and charged particles.

MCNP has the capability of performing electron transport calculations. Therefore, either MCNP, MCNPX, or PHITS could be used to evaluate transport of electrons from the surface of the reactor. Since MCNP is already being used for neutron and gamma transport from the reactor, it may be more convenient to use MCNP for electron transport from the reactor.

CONCLUSIONS

Considering the previous discussion, it was decided to look more closely at FLUKA and PHITS. MCNPX was not considered because in its current state it does not transport heavy ions. HETC-HEDS, HZETRN (the 3-D version), and GEANT4 were not considered because they are still in the early states of development. FLUKA and PHITS were chosen because they cover the needed range of energies and particles species and are the most mature in terms of development.

The FLUKA developers will only release object files, which are to be linked to create an executable using the GNU FORTRAN compiler on a Linux machine. Two different versions of FLUKA (2003.1b and 2005.6) object files were used to try and create an executable on the Bettis FY05 Linux cluster (AMD Opteron). Using the GNU FORTRAN compiler as suggested by the developers, neither attempt was successful. The 2003.1b version was attempted on the Bettis FY04 Linux cluster (Intel Itanium), but that was not successful because both versions of all the FLUKA object files were built on a computer with x86 architecture. The FLUKA developers claim that they will release their source code around the beginning of the 2006 calendar year.

Version 1.97 of PHITS was compiled successfully on the Bettis FY05 Linux cluster using the GNU FORTRAN compiler. A few simple sample problems, provided by the developers, were successfully run using the MCNP5 continuous energy cross sections and JENDL 3.3 continuous energy cross sections below 20 MeV. These tests all used a single CPU. It was never attempted to build a parallel executable. Just recently, the developers have released PHITS version 1.98.

In closing, it appears that PHITS is going to be the best choice of code to use for charged particle transport, although MCNP could be used for electron transport from the reactor for convenience. However, the preference for PHITS could change as further developments are made to all the codes considered here. Of the six codes considered, all used Monte Carlo methods except HZETRN. The development of HZETRN should be followed closely because it would be better to have two tools available that solved the same problem using different methodologies.

REFERENCES

(a) McKinney, G., "MCNPX 2.5.0 – New Features Demonstrated," *Proceeding of the Monte Carlo 2005 Topical Meeting* (CD-ROM), Chattanooga, Tennessee, April 2005.

(b) Nitta, K., "Particle and Heavy Ion Transport Code System: PHITS," *Proceeding of the Monte Carlo 2005 Topical Meeting* (CD-ROM), Chattanooga, Tennessee, April 2005.

(c) Fasso, A., "The FLUKA Code: Physics and Applications," *Proceeding of the Monte Carlo 2005 Topical Meeting* (CD-ROM), Chattanooga, Tennessee, April 2005.

(d) Wilson, J., et. al., "HZETRN: Description of a Free-Space Ion and Nucleon Transport and Shielding Computer Program," NASA Technical Paper 3495, May 1995.

(e) Miller, T., "HETC-HEDS Radiation Transport Code Development and Benchmarking for Cosmic Ray Shielding Applications in Space," *Proceeding of the Monte Carlo 2005 Topical Meeting* (CD-ROM), Chattanooga, Tennessee, April 2005.

(f) Wellisch, J., "GEANT4," *Proceeding of the Monte Carlo 2005 Topical Meeting* (CD-ROM), Chattanooga, Tennessee, April 2005.

(g) X-5 Monte Carlo Team, "MCNP – A General Monte Carlo N-Particle Transport Code, Version 5," Los Alamos National Laboratory, LA-CP-03-0245, June 2004.

(h) Parker, J. F., Jr. and V. R. West, editors, "Bioastronautics Data Book," NASA SP-3006, 1973.

(i) Townsend, L. W., J. E. Nealy, and J. W. Wilson, "Preliminary Estimates of Radiation Exposures for Manned Interplanetary Mission from Anomalously Large Solar Flare Events," NASA TM-100620, 1988.

(j) Sauer, H. H., R. D. Swickl, and M. J. Ness, "1990: Summary Data for the Solar Energetic Particle Events of August Through December 1989," Space Environment Laboratory, National Oceanic and Atmospheric Administration, February 21, 1990.

(k) Mewaldt, R. A. "The Abundances of Isotopes in Cosmic Radiations," *Proceeding of the Cosmic Abundances of Matter Meeting*, Minneapolis, Minnesota, April 1988, p. 124.

Figure 1: Van Allen Belts (Reference (h))

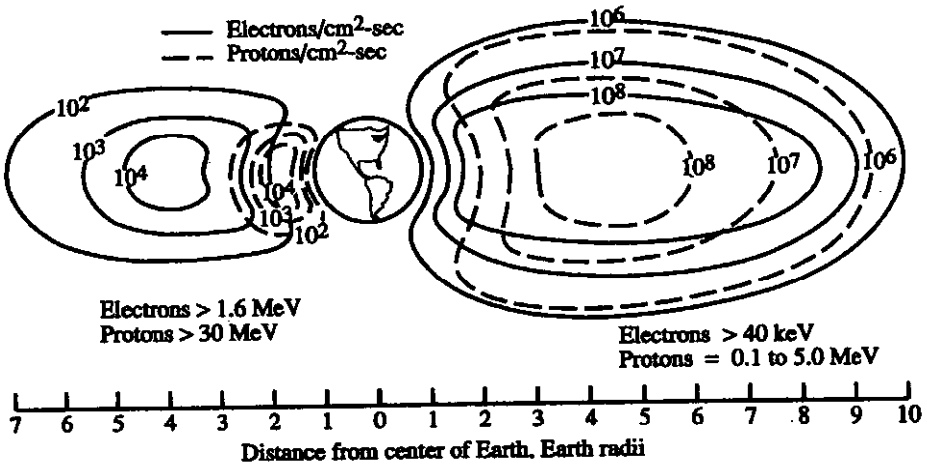

Figure 2: Integral Proton Fluence of Four Large SPEs (References (i) and (j))

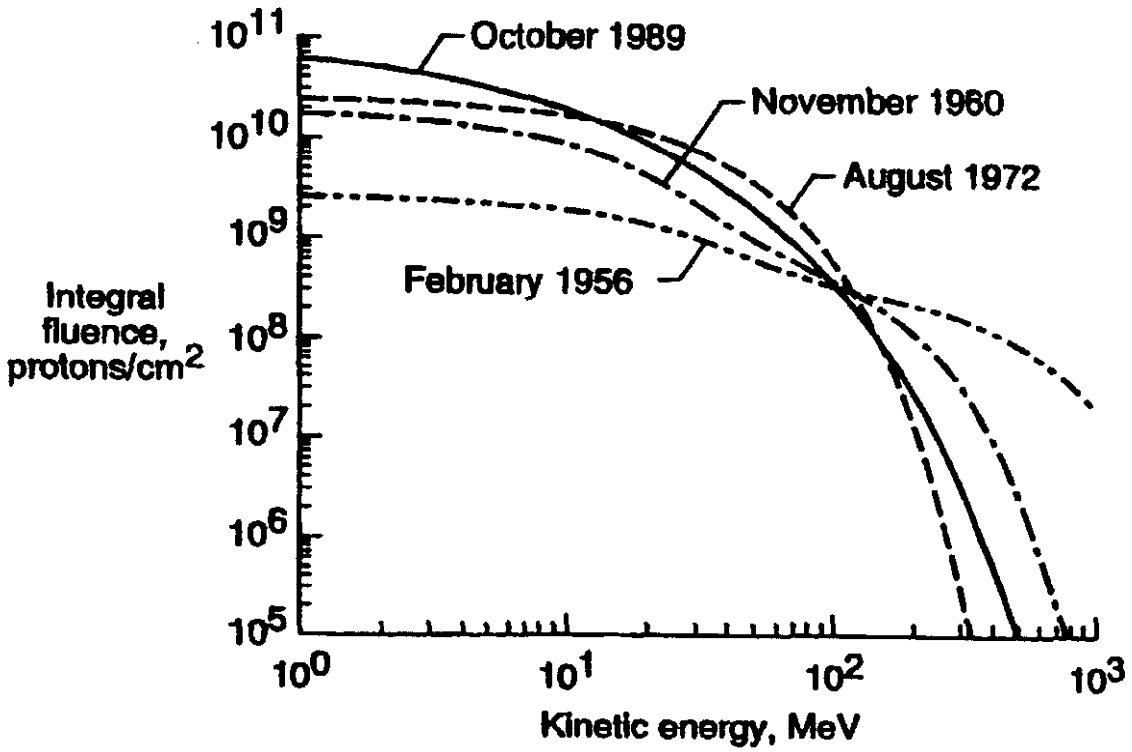

Figure 3: GCR Fluence at 2 GeV per Nucleon (Reference (k))

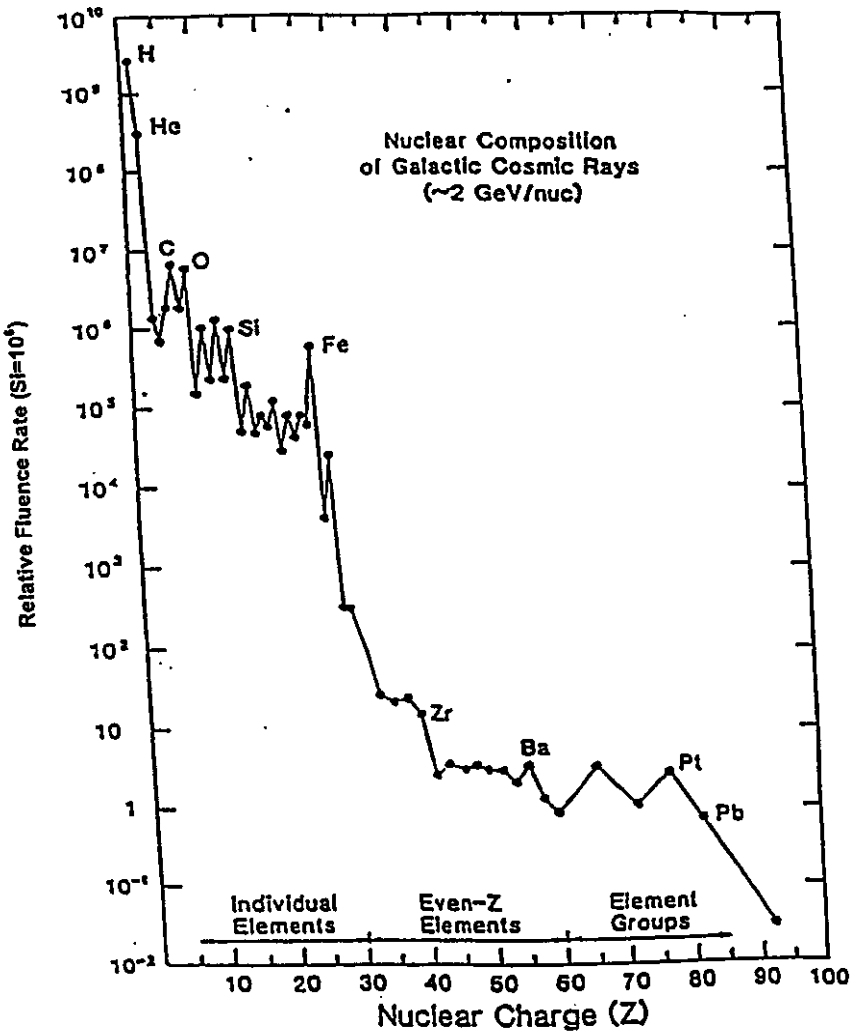

Intentionally Left Blank

Coolant Pipe Penetration Streaming Studies for a Space Reactor Shield

Jane M. Derboven, Engineer
Space Reactor Shielding
Fleet Support Operation
KAPL, Inc.

INTRODUCTION

This enclosure describes an analysis of radiation streaming through coolant pipe penetrations in a space reactor shield. Calculations were performed using MCNP version 5 to examine radiation streaming and overall shielding effectiveness for selected geometric configurations of a space reactor shield with coolant pipe penetrations.

DISCUSSION

Coolant pipe penetrations present significant streaming paths through any bulk shielding, in addition to displacing a large amount of shielding material. This is especially true of shielding penetrations in gas reactor systems, in which the coolant pipe contents have a very low density and the pipe diameters are large. Calculations performed at ORNL predicted as much as a factor of 10,000 increase in neutron flux levels at parts of the spacecraft payload due to straight piping penetrations, as stated in Reference (a), section 2.8.4.2. A geometric solution to maximize bulk shield effectiveness with minimal mass increase was desired. Sensitivity calculations were performed to determine the relative effects of coolant pipe geometry on the total flux emerging from the back of the shield and on the radiation damage to the payload. The geometric variables, penetration curvature and angle traversed around the shield edge, will be discussed in further detail below. The study focused primarily on neutron effects because the gamma dose is significantly less sensitive to penetration geometry than the neutron dose.

This analysis was performed specifically for a spacecraft shadow shield, but is extensible to other gas reactor shielding penetration problems. Analyses of pipes going around the outside of the shadow shield, although started, were not completed because such analyses would not have been extensible to lunar missions and because of the subsequent program closeout.

Reactor Model

The 1 MW reactor model source DSO470X based on reactor parameters given in Reference (b) was used throughout the analysis. This model is shown in Figure 1. The shield material stack-up used in this study was not optimized for this reactor, and so the absolute radiation levels should not be used for estimating component doses. The primary focus of this study was the relative fluxes/fluences as a function of penetration geometry.

Shield Model

The shield model used in this analysis was 74.5 cm thick and comprised alternating layers of beryllium (5 cm per layer) and boron carbide (0.5 cm per layer), with a single layer of tungsten (1 cm) for additional gamma attenuation and front and back layers of Haynes Alloy 230 to simulate support structure (1.5 cm and 2 cm, respectively). The shield was shaped as a truncated elliptical cone, opening from the circle of the forward-most core reflector edge at a 12° half-angle on the semi-major axis to accommodate JIMO's radiator array, and a 6° half-angle on the semi-minor axis. This model is detailed in Figure 2. No energy conversion or other equipment was modeled between the shield and the payload for this pipe routing evaluation.

Figure 1: Reactor and Shield Model Cutaway.

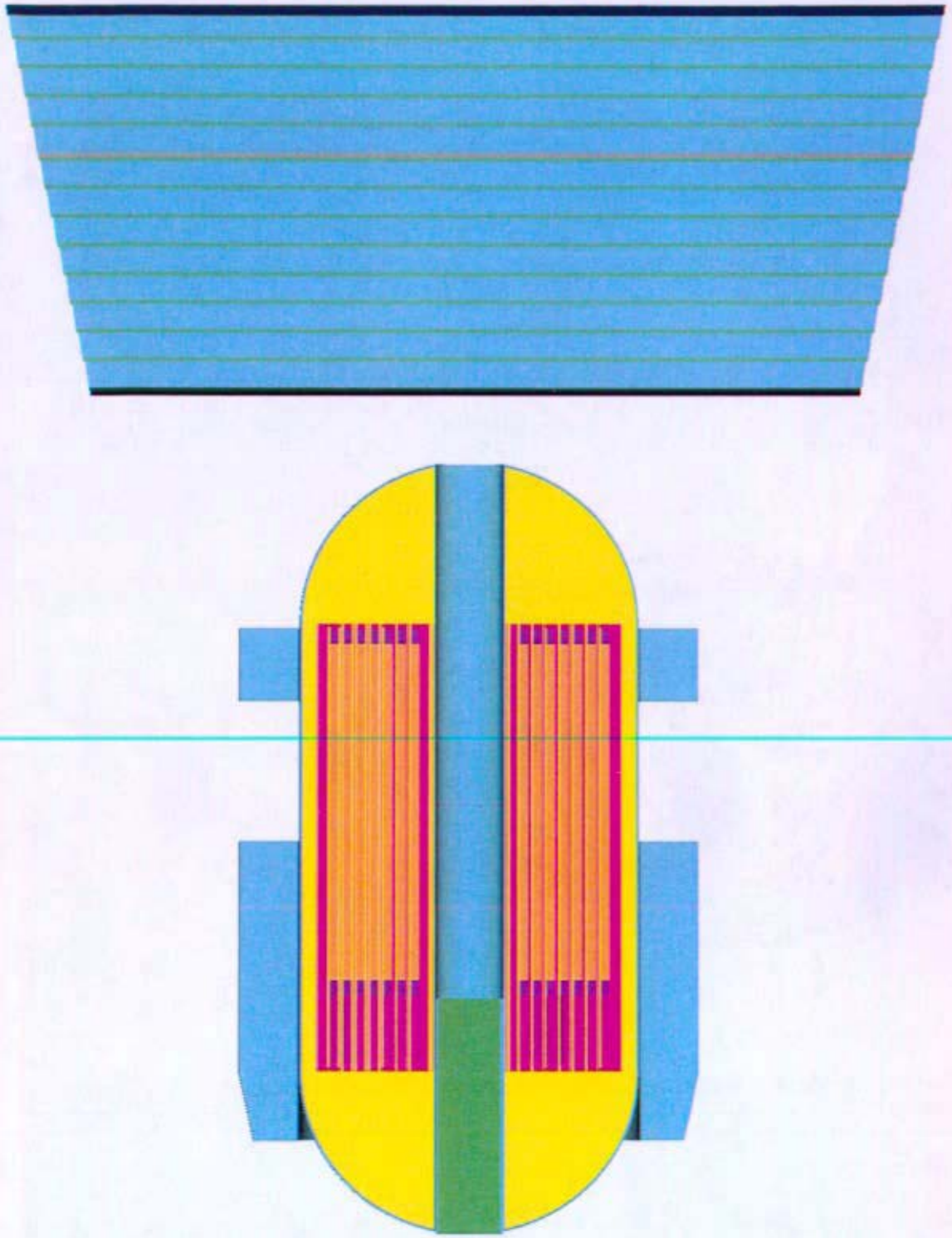

Figure 2: Space Shield Base Case

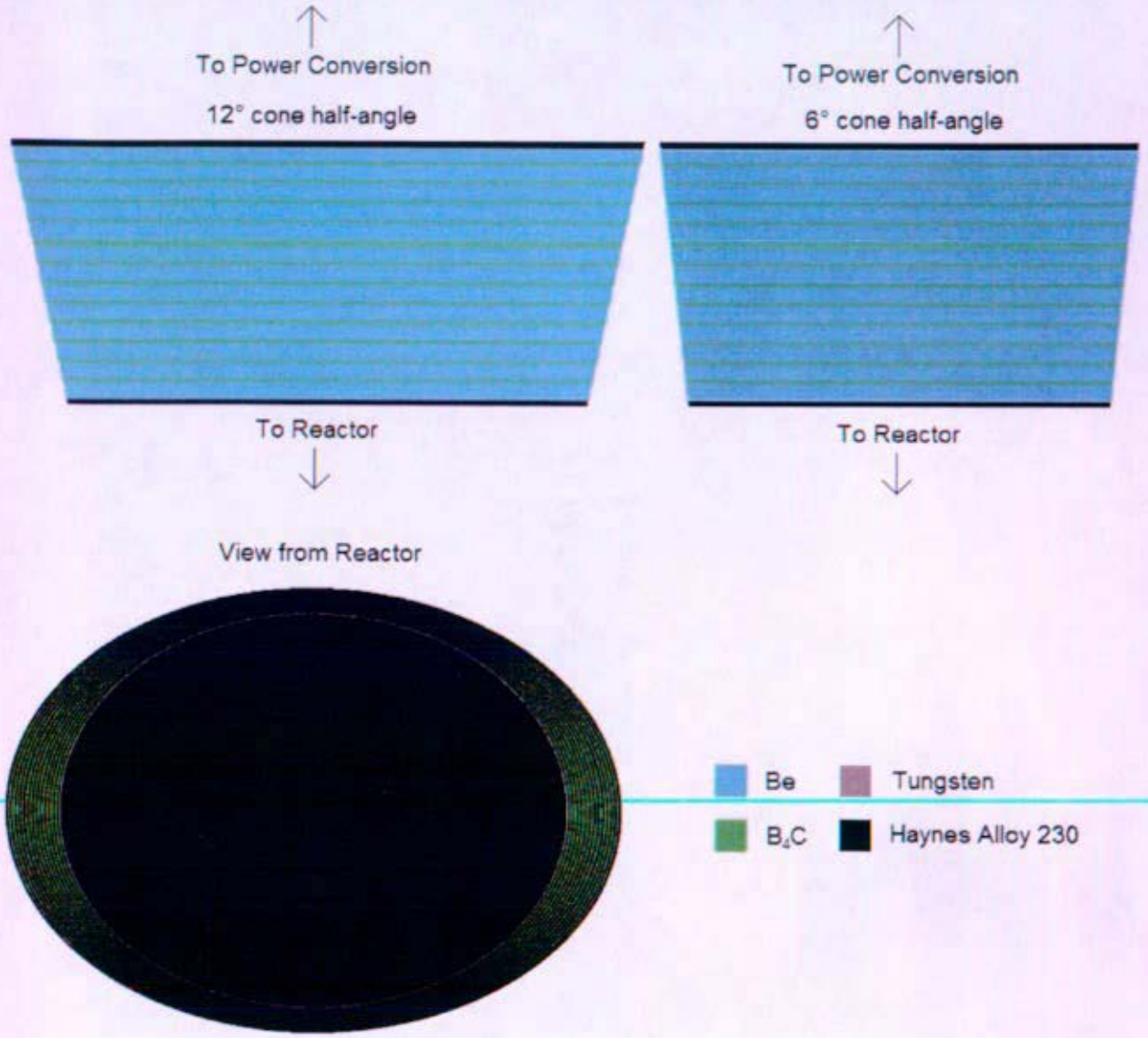

Selected Penetration Geometries

The coolant pipes used in this study were made of Inconel 617 and had a 16 cm outer diameter, with 0.8 cm wall thickness. An annular clearance gap of 0.5 cm was modeled around the pipes, for a total penetration diameter of 17 cm. Geometries with 2 pipes were analyzed: one hot pipe and one cold pipe. Annular clearance and pipe interiors were modeled as void. No insulation was modeled: insulation within or around the pipes would only improve radiation attenuation unless it resulted in a larger shield penetration diameter.

Three assumptions were made during the selection of possible penetration geometries to help limit the scope of the evaluation. First, it was assumed that the penetrations should enter the shield from the reactor side on the shield's major axis to minimize initial streaming into the penetrations and to leave room for the core reflector control drive shafts. Second, it was assumed that the penetrations should follow the shield edge as closely as possible to avoid displacing mass near the spacecraft axis, where the radiation flux is highest. Third, it was assumed that a limit should be set on the number of bends in the piping to facilitate manufacturing and minimize coolant pressure drop.

Two variables emerged from this simplification. The first was the penetration curvature, which was narrowed to three options: straight penetrations, helical penetrations, and dog-leg penetrations. An example of each of these is given in Figure 3.

Figure 3: From left to right: straight penetrations, spiral penetrations, and dog-leg penetrations

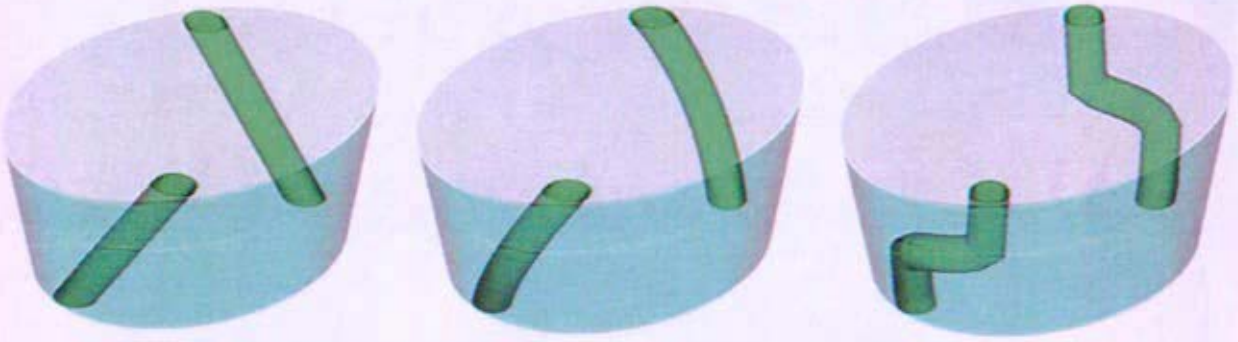

The second variable was the azimuthal angle relative to the spacecraft axis, ϕ, traversed by the penetrations around the shield edge, as demonstrated in Figure 4. The three curvature selections above were analyzed for $\phi = 0°$, 45°, 90°, 135°, and 180°. Additionally, one geometry was analyzed with coolant pipes coming straight into the shield from the reactor head and branching out to exit near the shield edge, with the intent of directing all radiation streaming at an angle to exit the shielded cone before reaching the payload. The base case with no penetrations was also analyzed for comparative purposes. The shield thickness and constituent materials were kept constant for initial comparisons. The complete set of calculated geometries is displayed in Figure 5.

Figure 4: Angle traversed by the penetrations around the shield edge, from reactor-side entrance to payload-side exit, as measured relative to the spacecraft axis.

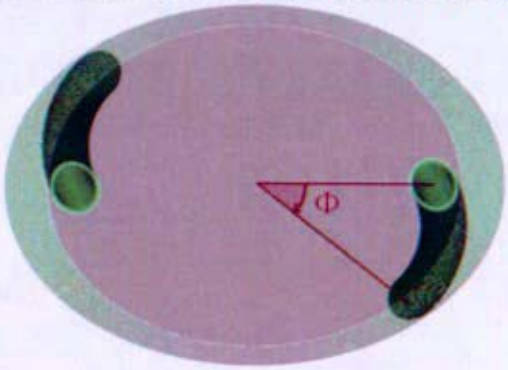

Figure 5: Penetration Geometries Analyzed

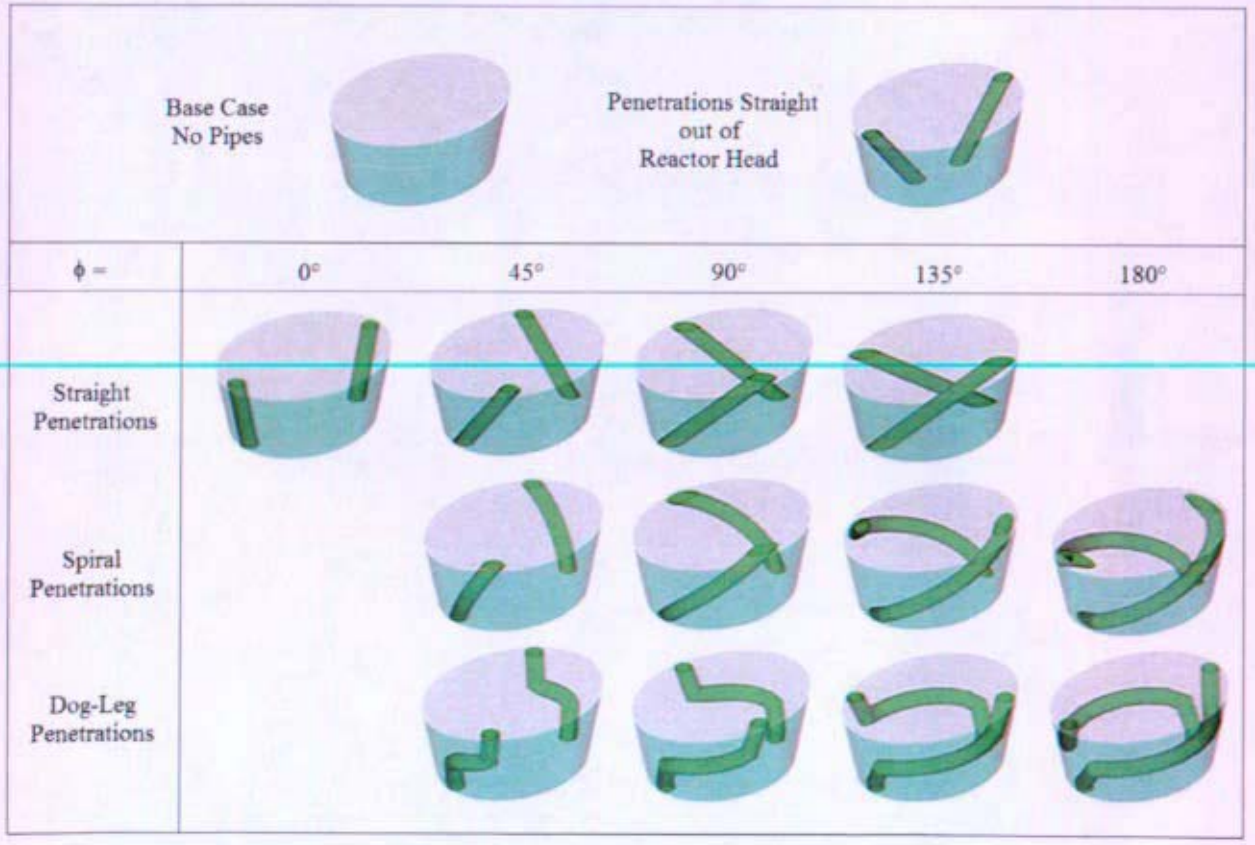

RESULTS

Gamma and neutron radiation results for the geometries shown in Figure 5 are summarized in Figures 6 and 7, respectively. Results are given in total dose at the science payload over the assumed 15-year life span of JIMO. Error bars indicate one standard deviation. Gamma results show little dependence on penetration geometry, with worst case results giving less than a factor of 2 increase over the base case with no penetrations. These small gamma result differences would be investigated in a more detailed design study because of the strong influence of gamma shielding (tungsten) on total shield mass. Opportunities to reduce this mass by decreasing the gamma shielding radius may be possible based on results shown in Figures 15 through 19.

Neutron results show a strong dependence on geometry. The lowest doses were given by spiral penetrations for $\phi \geq 90°$. The 90° spiral was selected for further analysis, since larger ϕ would increase pressure drop and manufacturing difficulty. Note that payload dose is used as a guide, but does not necessarily imply the lowest shield mass because the piping also displaces shield mass. For example: if two cases have the same radiation dose, then the case with the larger azimuthal traverse would have the lower shield mass because the pipe displaces more of the shield. Contrarily, the larger angle would also increase piping length and hence piping and pipe insulation mass. Future studies would need to investigate these mass tradeoffs.

Detailed flux contours are included at the end of this enclosure.

Figure 6: Gamma Dose at the Payload

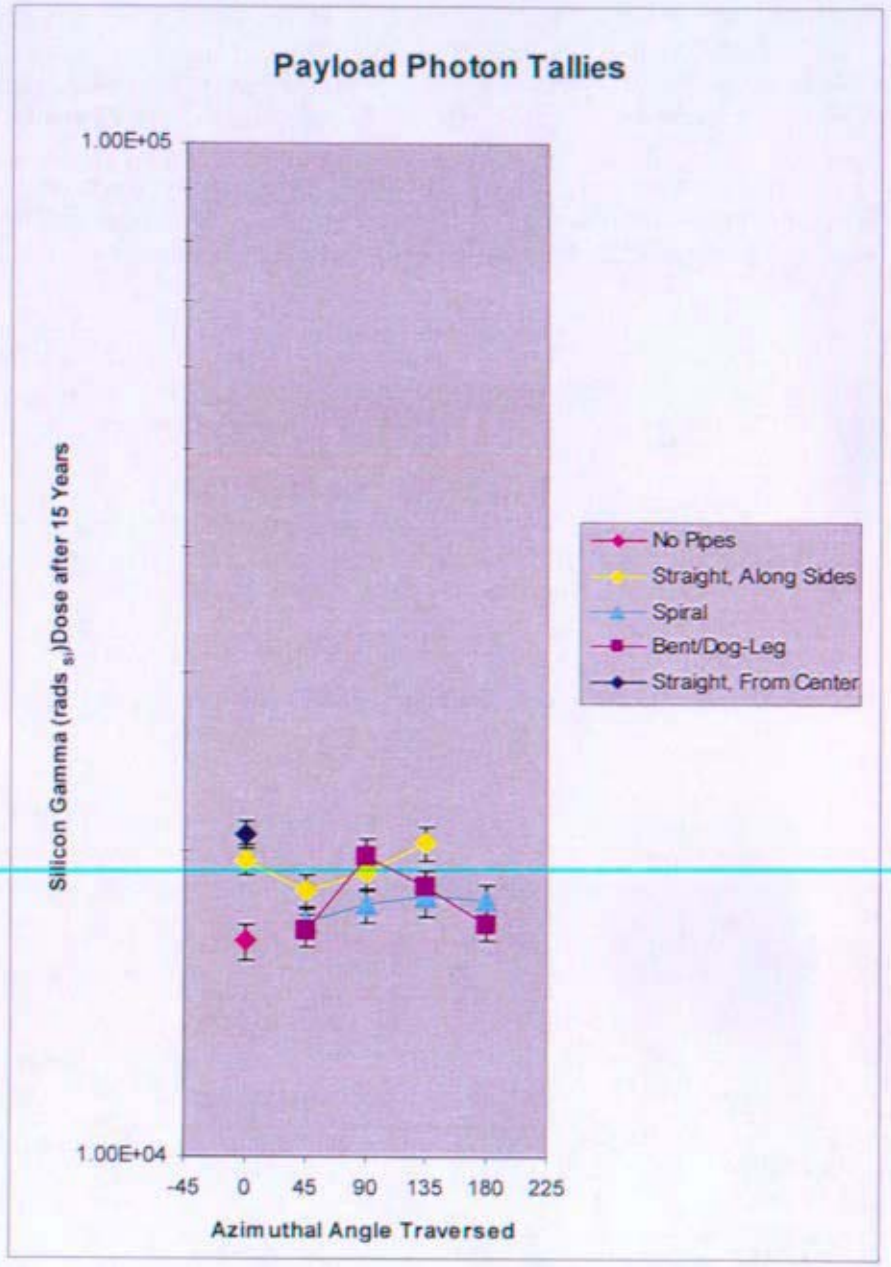

Figure 7: Neutron Damage at the Payload

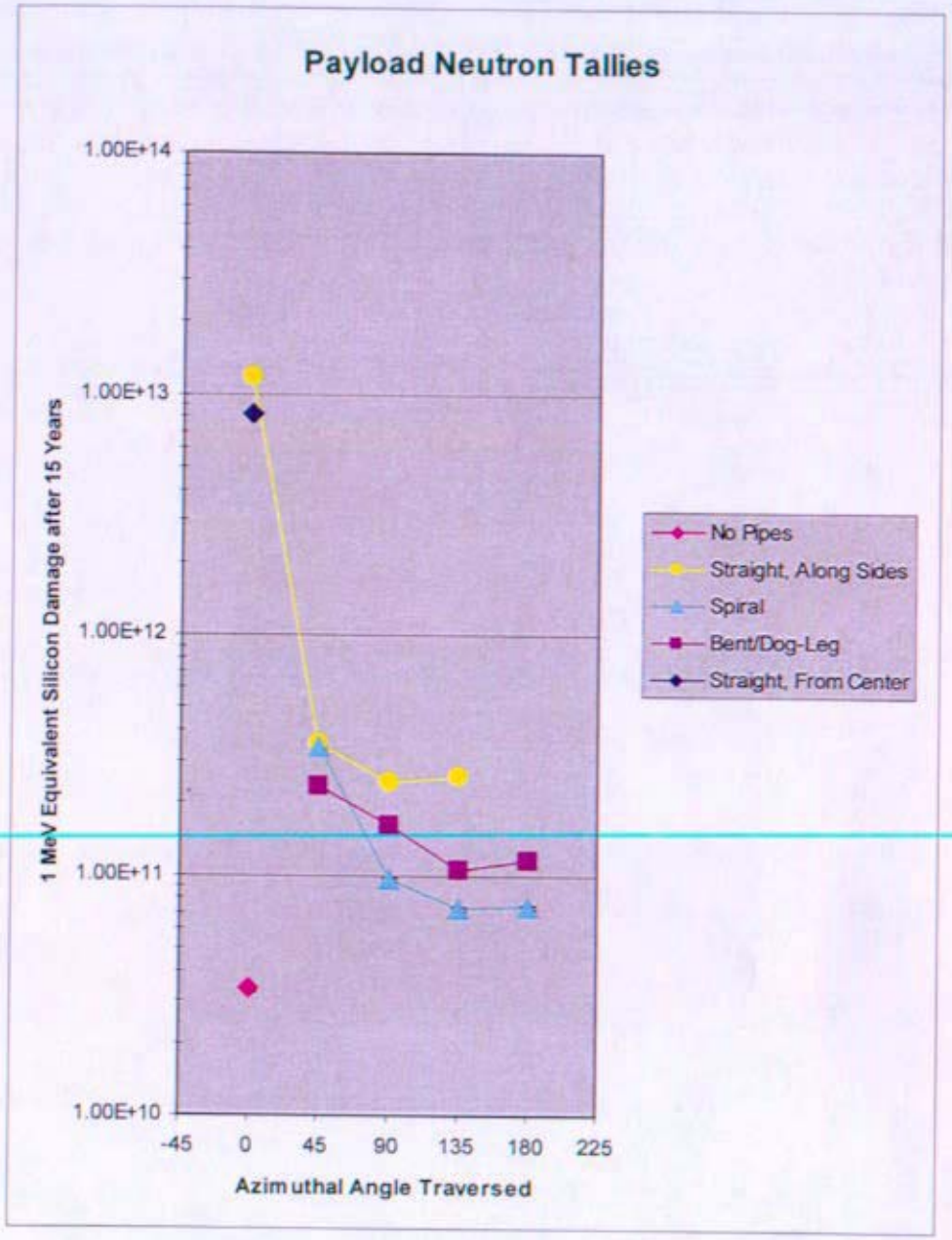

The amount of neutron streaming along the penetrations was analyzed using the four geometries shown in Figure 8. The neutron payload dose from the base case with no penetrations (8a) was compared to the dose from the selected penetration case (8b). These results were then compared to cases analyzed with artificially capped regions at the penetration inlets and outlets, shown in red (8c and 8d): all particles entering these regions were immediately terminated. Results indicate that neutrons do not all stream along the entire length of the penetrations, but instead enter and/or leave the penetrations partway through the shield. From these results, cap shields are predicted to have limited effectiveness. Calculations with hydrogenous cap shields were consistent with this prediction, and gave similar results to those obtained from the model shown in Figure 8d. Error values shown in the figure represent one standard deviation.

Figure 8: Streaming analysis comparisons. Particle termination regions are shown in red. Units are 1-MeV Equivalent Silicon-Damage Neutron Fluence over 15 years at the payload.

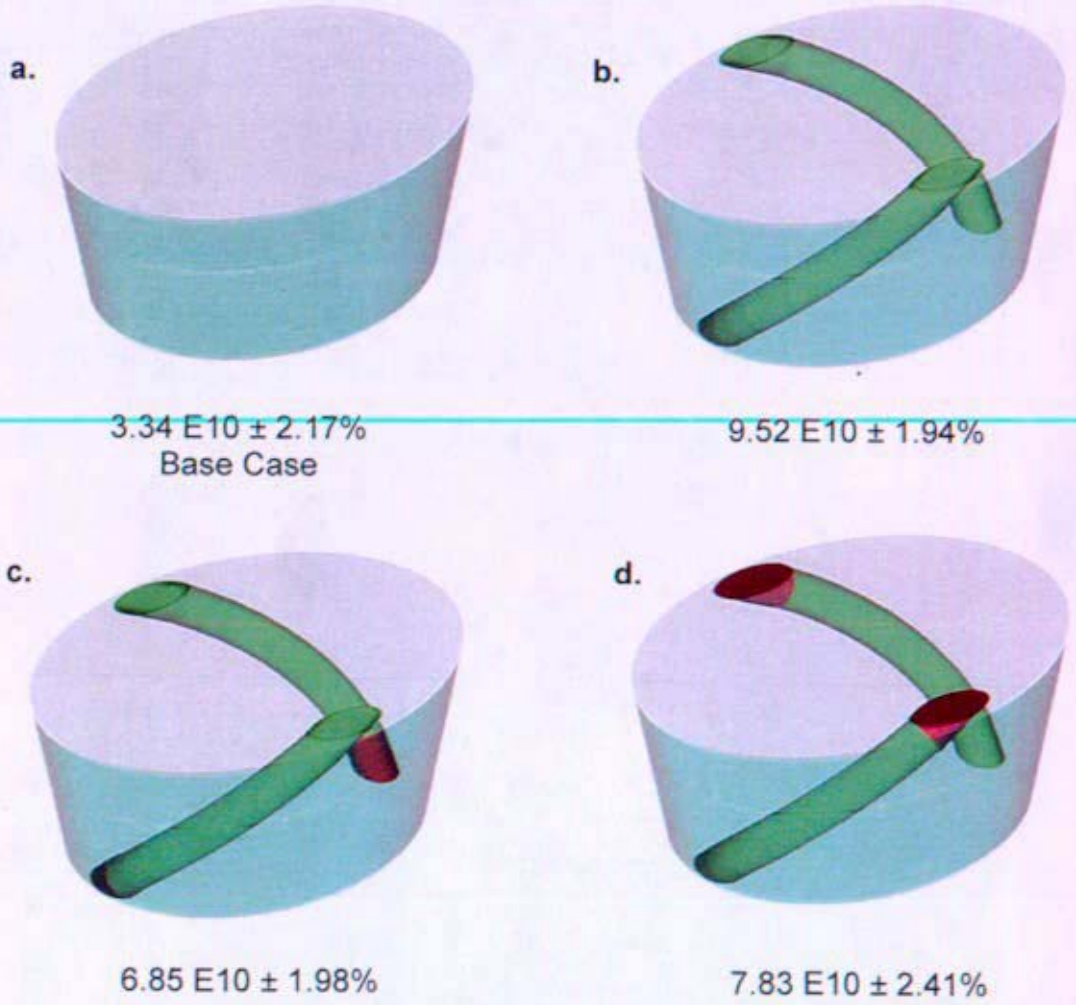

To reduce the payload dose to base case levels, additional layers of shielding material were added to the back of the shield to compensate for neutron radiation level increases from the addition of the penetrations. As an initial estimate, the mass displaced by the penetrations was added to the back of the shield as additional thickness. Mass displaced by the 90° spiral model was calculated at 140kg. This allowed the addition of 3.5 cm of beryllium and 0.5 cm of boron carbide. The resulting model is shown in Figure 9. Silicon-damage neutron fluence at the dose plane for this geometry was calculated at 6.28E10 ± 2.02%, still roughly twice the dose of the shield with no penetrations, but better than the case with penetrations and the small cap shields.

Figure 9: 90° spiral with additional bulk shield layers to replace mass displaced by penetrations

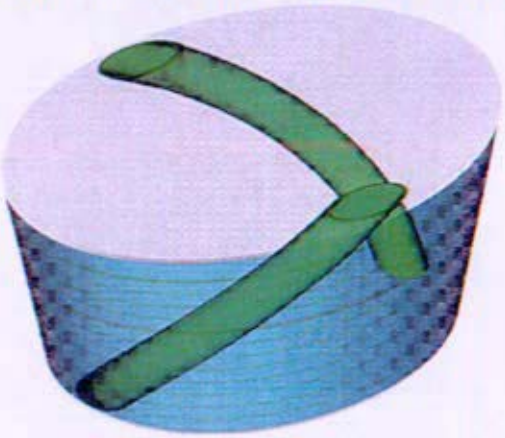

Neither simple cap shields nor a thicker bulk shield provided satisfactory neutron attenuation when applied to the 90° spiral case, as they were insufficient to restore base case radiation levels. Two solutions to this problem were analyzed.

The first solution entailed hydrogenous cap shields which covered the entire penetration length, as shown in Figure 10. This stopped any neutrons which short-circuited the shield via the penetrations as well as those streaming directly through the penetration ends. The mass of the cap shields is approximately 20 kg greater than the mass displaced by the penetrations. This does not account for structure or canning required for hydrogenous material. Silicon-damage neutron fluence at the dose plane for this geometry was calculated at 3.656E10 ± 3.68%, roughly equivalent to the base case accumulated damage.

The second possible solution was to increase ϕ to 180°, again with additional layers appended to the shield to compensate for displaced mass, as shown in Figure 11. This effectively removed all direct streaming, eliminating the need for any cap shields. Silicon-damage neutron fluence at the dose plane for this geometry was calculated at 2.48E10 ± 1.96%, slightly better than base case accumulated damage. This dose improvement is likely due to the fact that the increased layering was distributed evenly over the back of the shield, including the shield center where neutron flux is highest. This suggests a possible opportunity for mass savings when utilizing this geometry. This solution also eliminates two pipe bends behind the shield that were needed for the pipes to circumvent the cap shields. Therefore, the coolant pressure drop, piping length, and piping mass would be reduced for the configuration with the 180° spiral and

no cap shields. This second solution also reduces the neutron dose to the CDMs because it places additional shielding between the core and the CDMs, relative to the cap shield option.

Figure 10: 90° spiral with cap shields completely covering penetrations

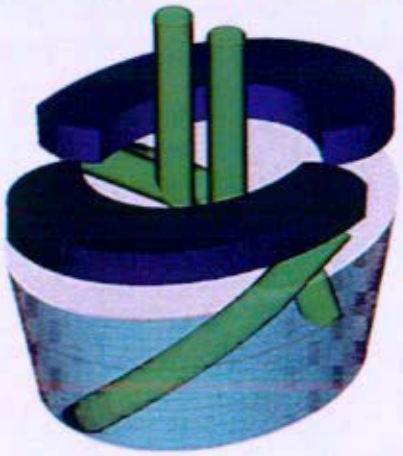

Figure 11: 180° spiral with additional 6 cm of Be and 0.5 cm of B_4C

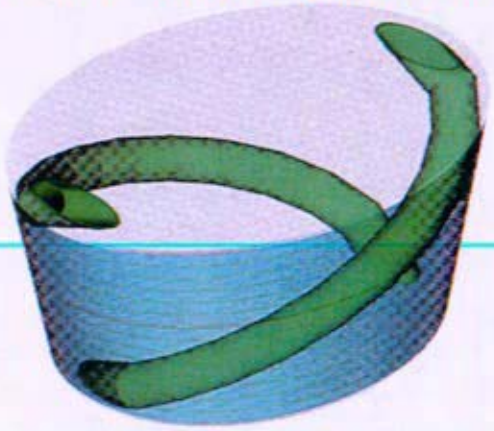

CONCLUSIONS

Inclusion of coolant pipe penetrations without significant payload dose increase or shield mass increase is feasible. As previously stated in Reference (a), straight penetrations through the shield provide too direct a path for neutron streaming towards the payload and/or allow neutron scatter in the direction of the payload near the back of the shield. Geometric accommodations (addition of dog-leg segments and donut cap shields) made in Reference (a) to adjust for streaming were predicted to net an increase in shield mass by 200 kg for four pipes. Removal of one hot/cold piping pair and addition of spiral penetration geometries in this analysis has eliminated this predicted mass increase.

It is recommended that any continuation of this project resume with the assumption of 180° spiral coolant pipe penetrations, with shield thickness adjustments made to offset neutron radiation increases. Approximations to the spiral using two or three straight segments should be analyzed, as these would greatly facilitate shield manufacture. Small perturbations (< 45°) in penetration endpoints should be analyzed, to further resolve azimuthal traverse angle dependence. Removal of shield mass between the penetrations and the shield edge to form u-shaped channels, as shown in Figure 12, is expected to allow outboard scatter and facilitate manufacture and should also be analyzed. Additional shielding material stack-ups and their interactions with this design should be analyzed. Detailed input regarding manufacturing capabilities, coolant flow, and thermodynamic issues should be considered during any further model refinement.

Figure 12: Suggested U-shaped Cavity in Shield Side

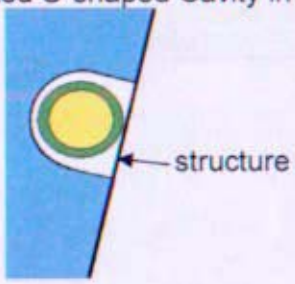

QUALIFICATION OF METHOD

Radiation levels were calculated using MCNP 5. This is a pre-production level computer code. The results are based on nominal geometry and do not include method uncertainty, design assurance, or design contingency factors. Perl scripting was used for geometry calculations and to generate MCNP input. This enclosure has been reviewed by and has the concurrence of the manager of KAPL FSO-Shielding. This enclosure is a summary of work documented in KAPL SWR-00072.

REFERENCES

(a) Jet Propulsion Laboratory Document 982-00007, "JIMO Shield Trade Study: Reactor and Natural Space Radiation," E. Blakeman (ORNL), J. Johnson (ORNL), I. Jun (JPL, Lead), W. McAlpine (JPL), I. Remec (ORNL), J. Yugo (ORNL), April 2004.

(b) Bettis Document B-SE(RE)NE-0010, "Reply to Request for Information Regarding Prometheus Reactor Designs with UO2 Fuel for Shielding Design Study," Robert Schmitt, July 19, 2005.

ADDITIONAL FIGURES

The following figures represent half the shielded cone, assuming reflective symmetry. Calculations were performed over rectangular meshes: the cone boundary is sketched in to aid visualization. Error values represent one standard deviation. Note that some of the result variability appears to be due to variations in the relative errors. The results near the edges of the payload plane, shield back, and piping show edge effects on the following figures due to finite mesh resolution. The mesh tally sizes were selected as a reasonable compromise between result detail and computer time.

Figure 13: 90° spiral payload gamma mesh tally in $rads_{Si}$ after 15 years, with corresponding mesh cell relative error percentages. All other payload gamma tallies showed very little variation from this example. Axis units are in centimeters.

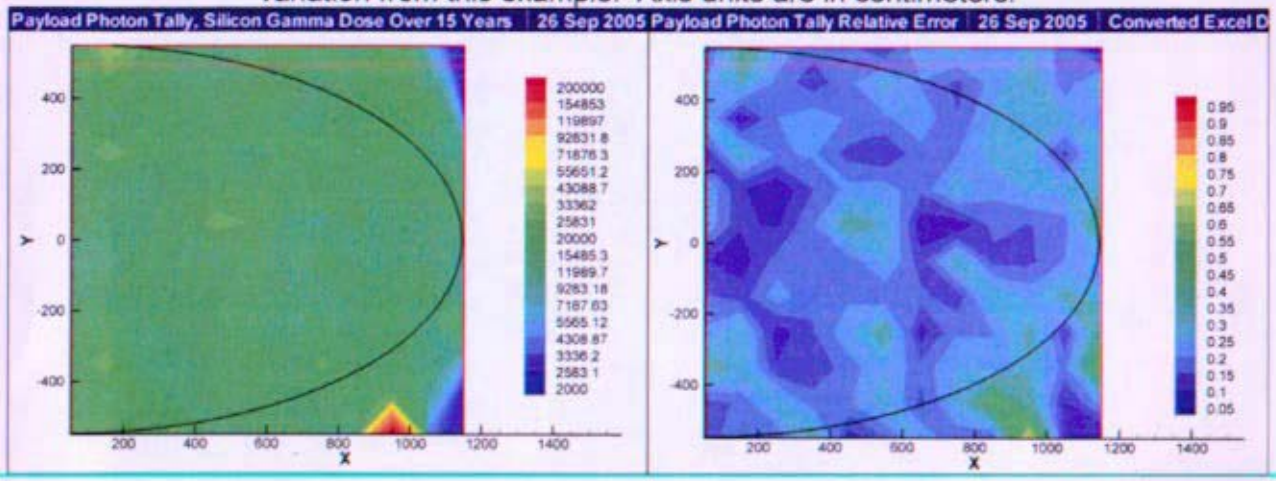

Figure 14: 90° spiral payload neutron mesh tally in 1-MeV equivalent neutron fluence after 15 years, with corresponding mesh cell relative error percentages. All payload neutron tallies were similarly flat within statistical limits. Axis units are in centimeters.

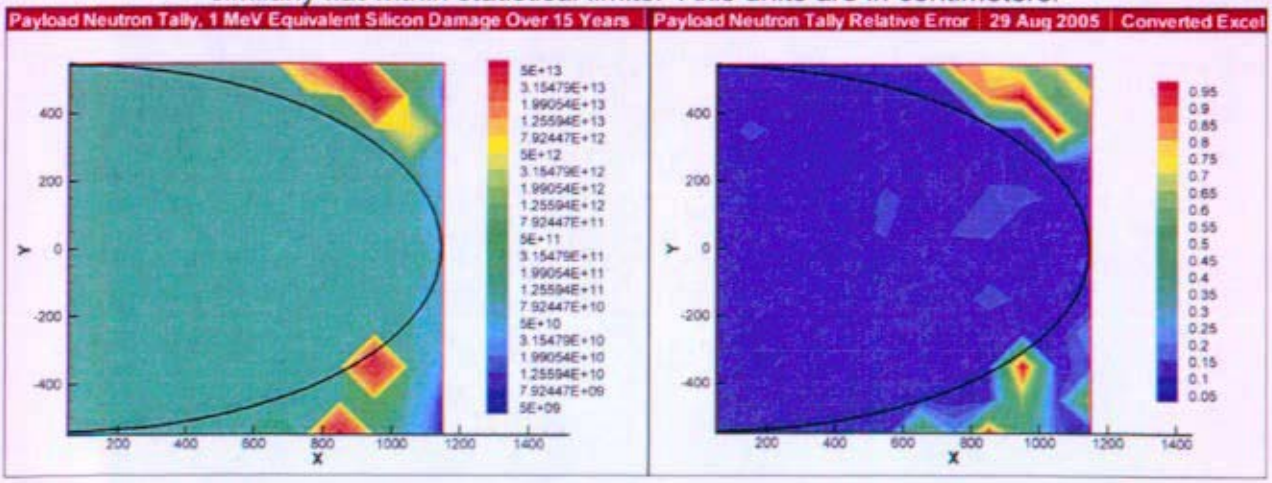

Figure 15: 0° straight pipe gamma flux mesh tally behind the shield.
Axis units are in centimeters.

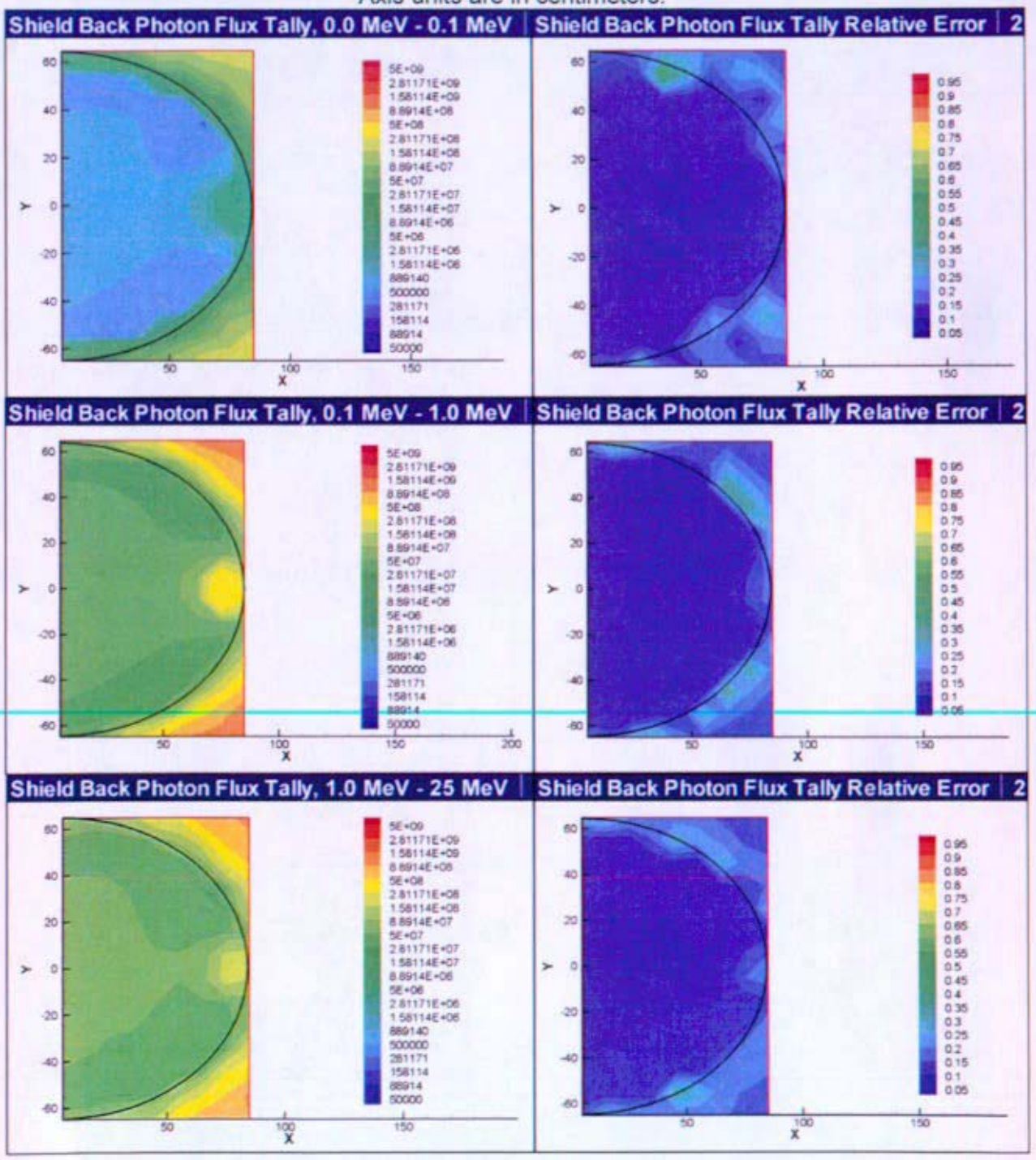

Figure 16: 90° straight pipe gamma flux mesh tally behind the shield.

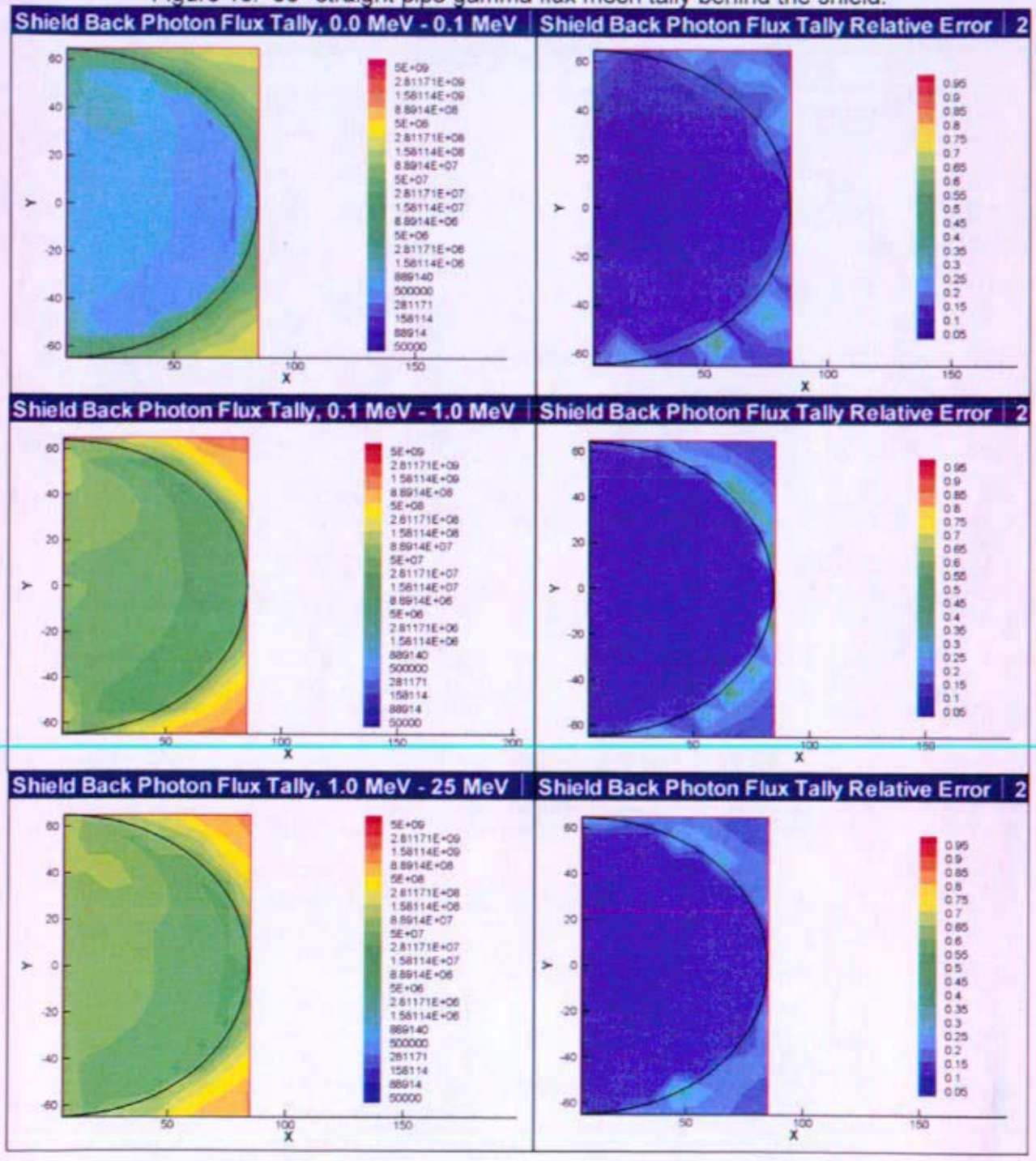

Figure 17: 90° spiral gamma flux mesh tally behind the shield.

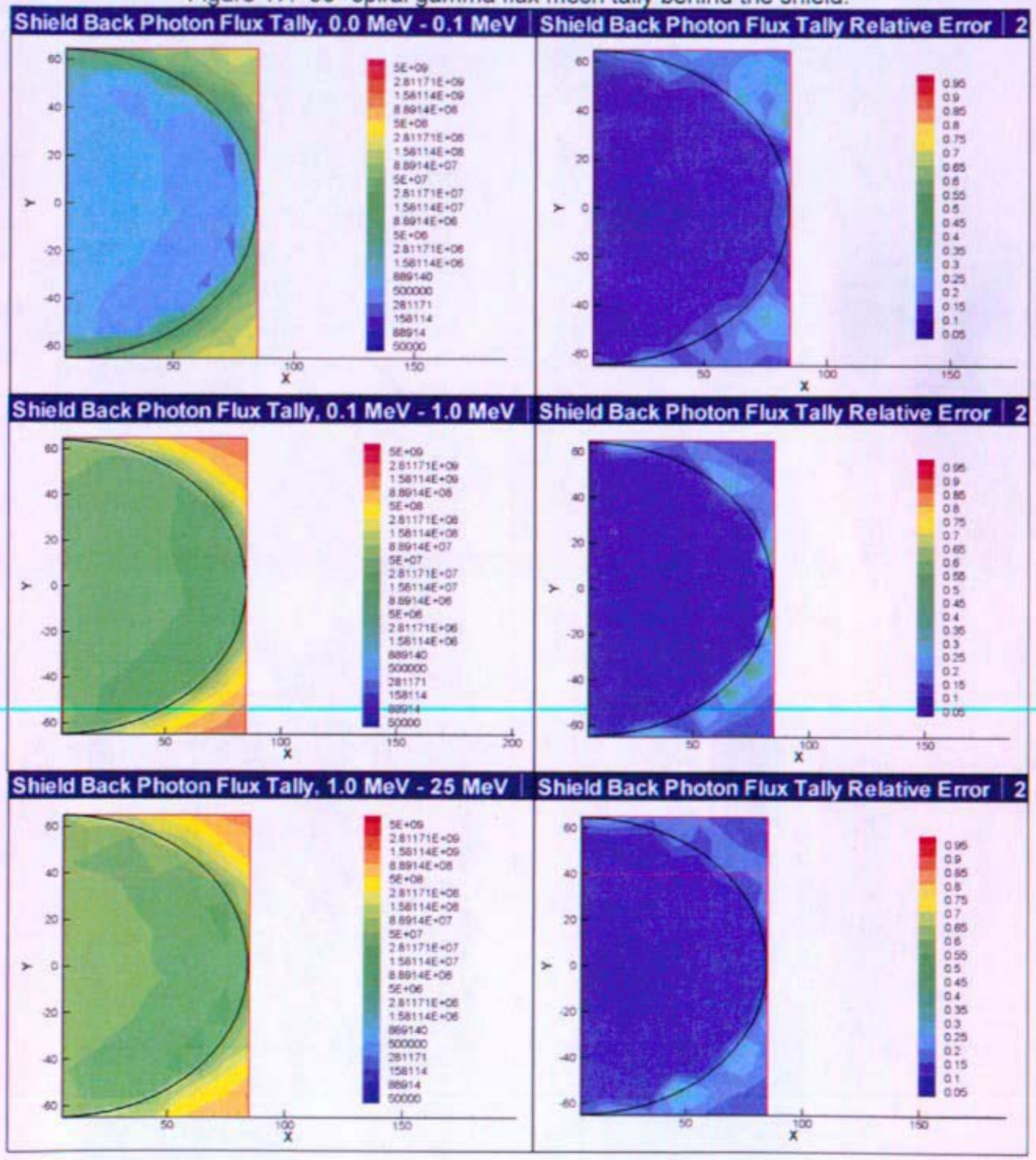

Figure 18: 180° spiral gamma flux mesh tally behind the shield.

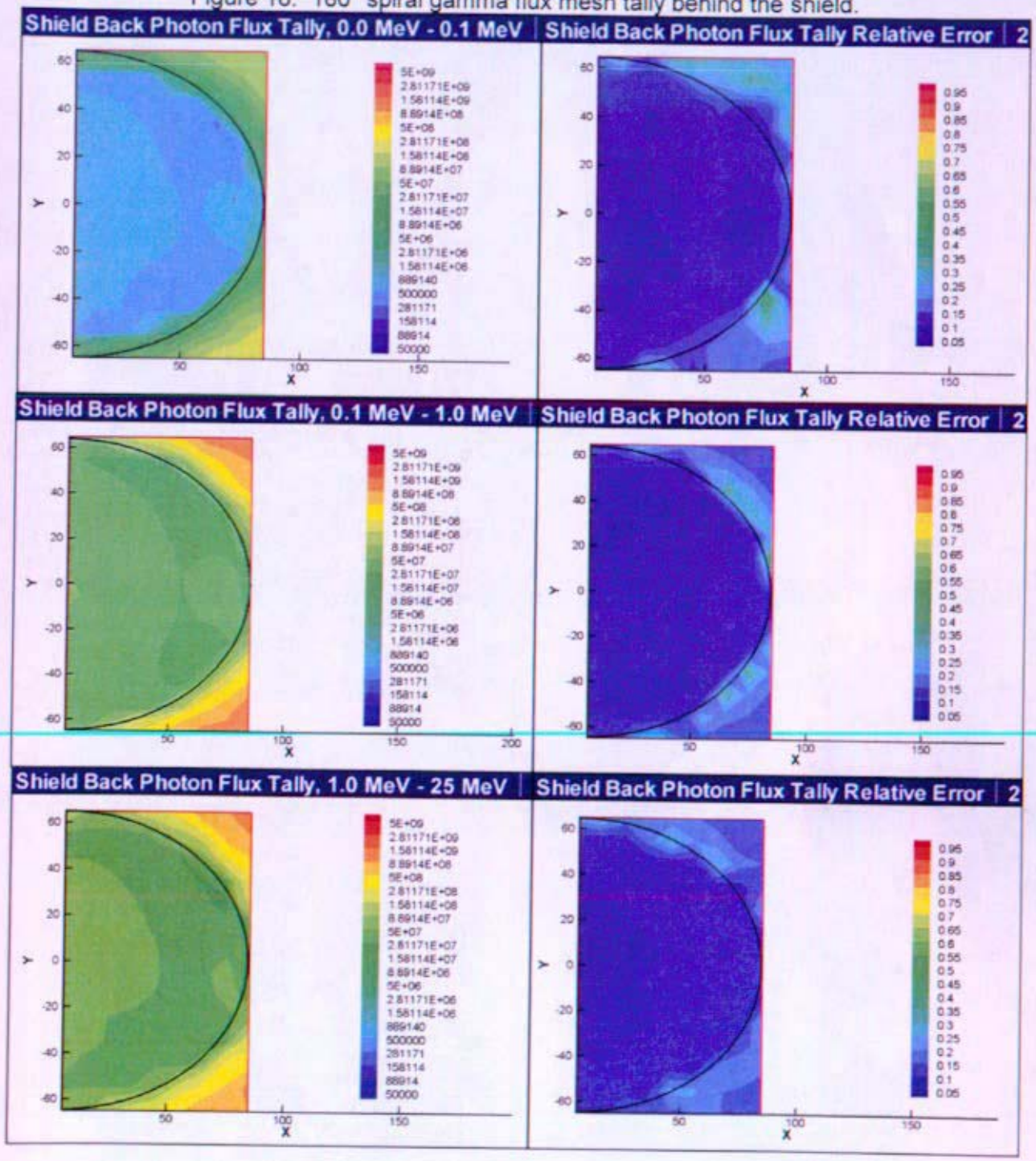

Figure 19: 180° dog-leg gamma flux mesh tally behind the shield.

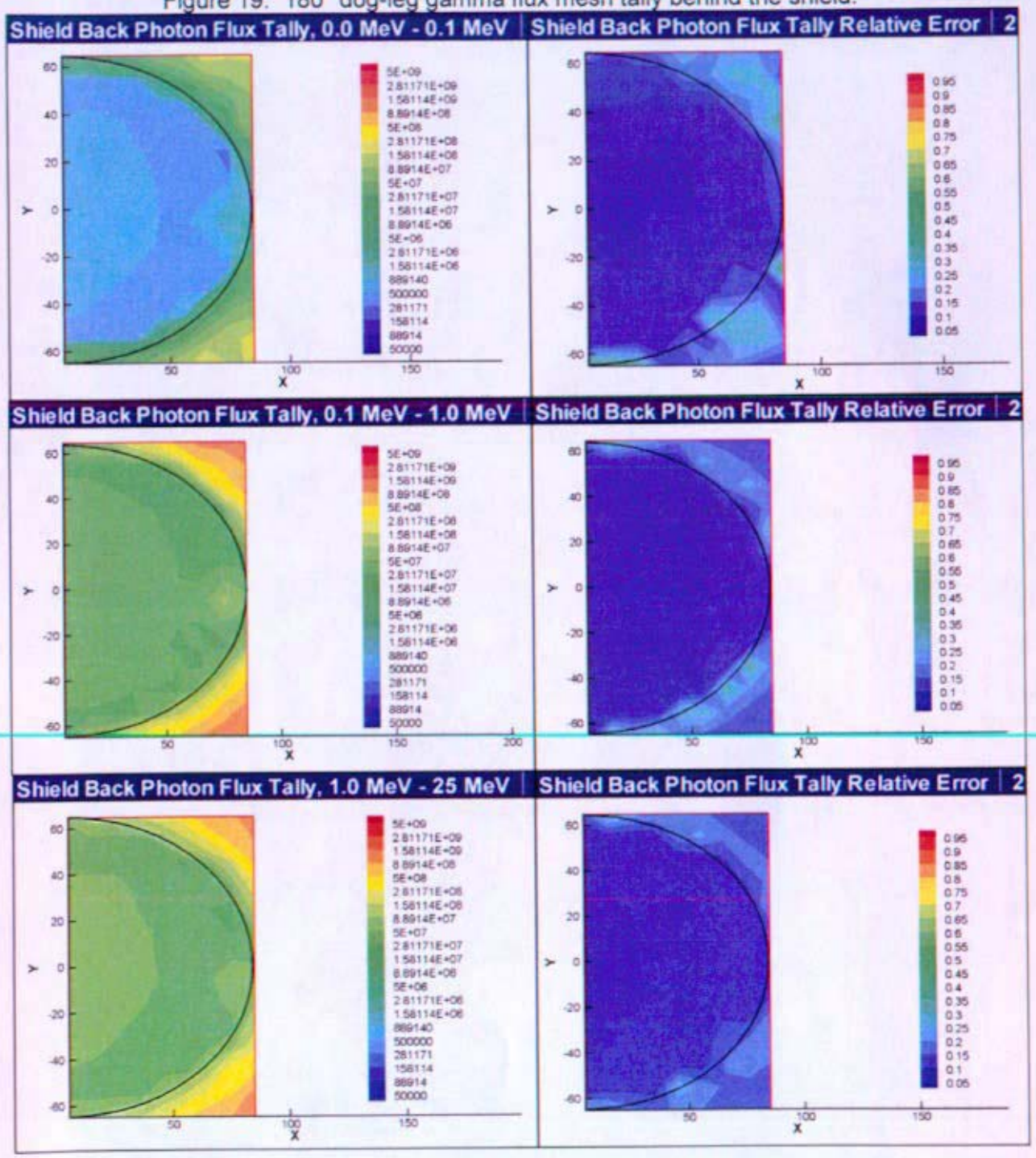

Figure 20: Base case neutron flux tally behind the shield. All neutron fluxes are given in neutrons/cm^3/second.

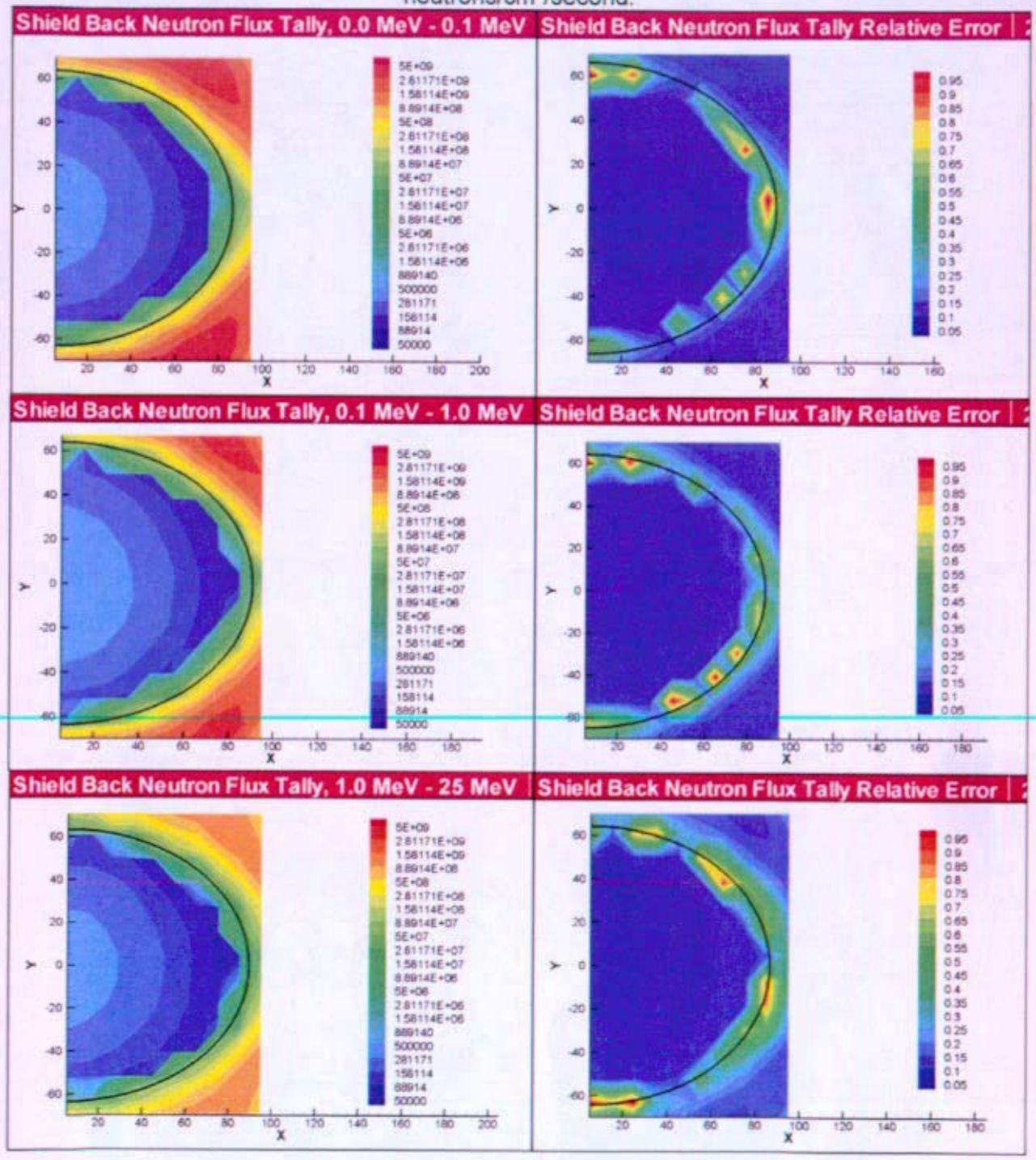

Figure 21: 0° straight pipe neutron flux tally behind the shield.

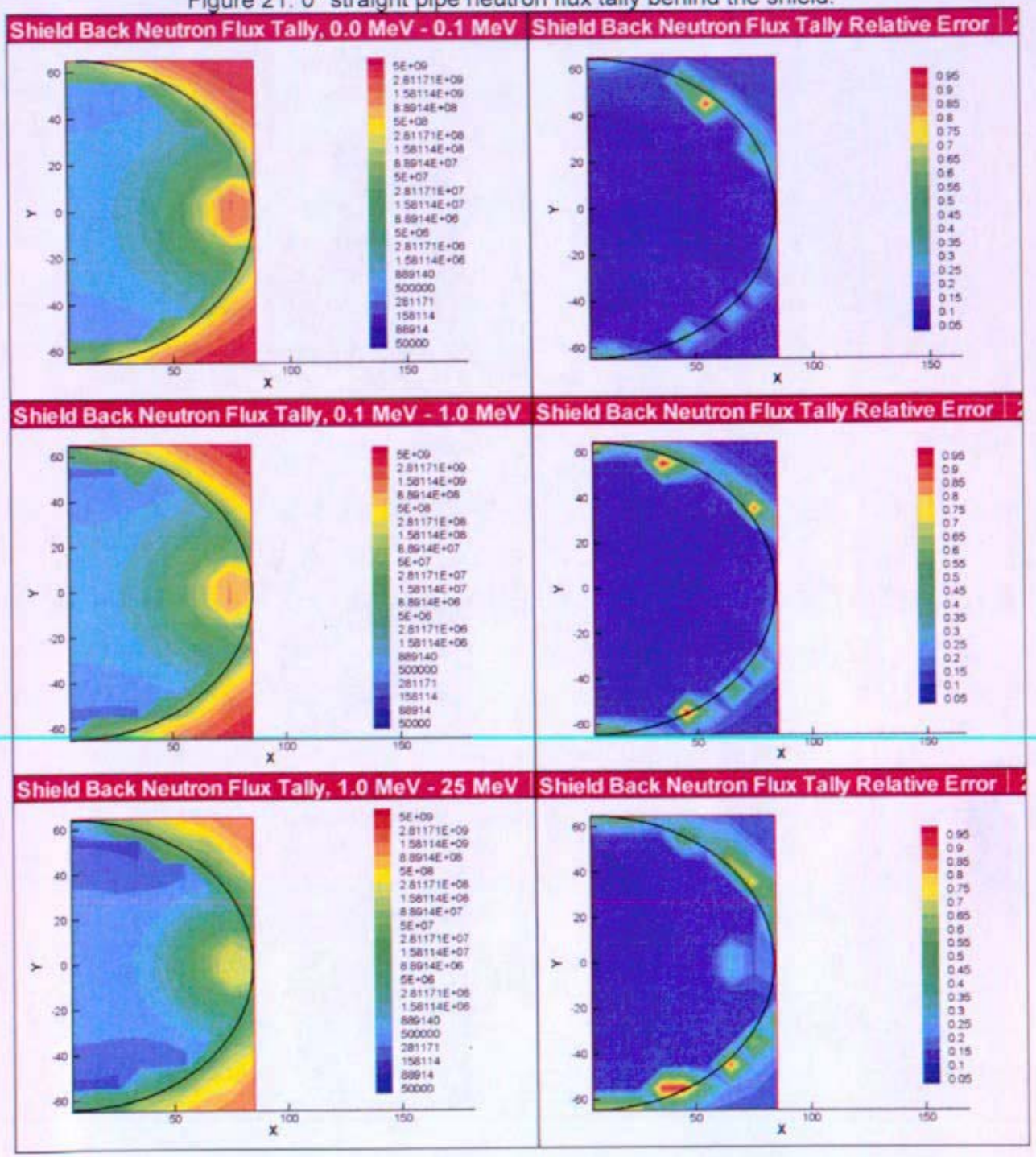

Figure 22: 45° straight pipe neutron flux tally behind the shield.

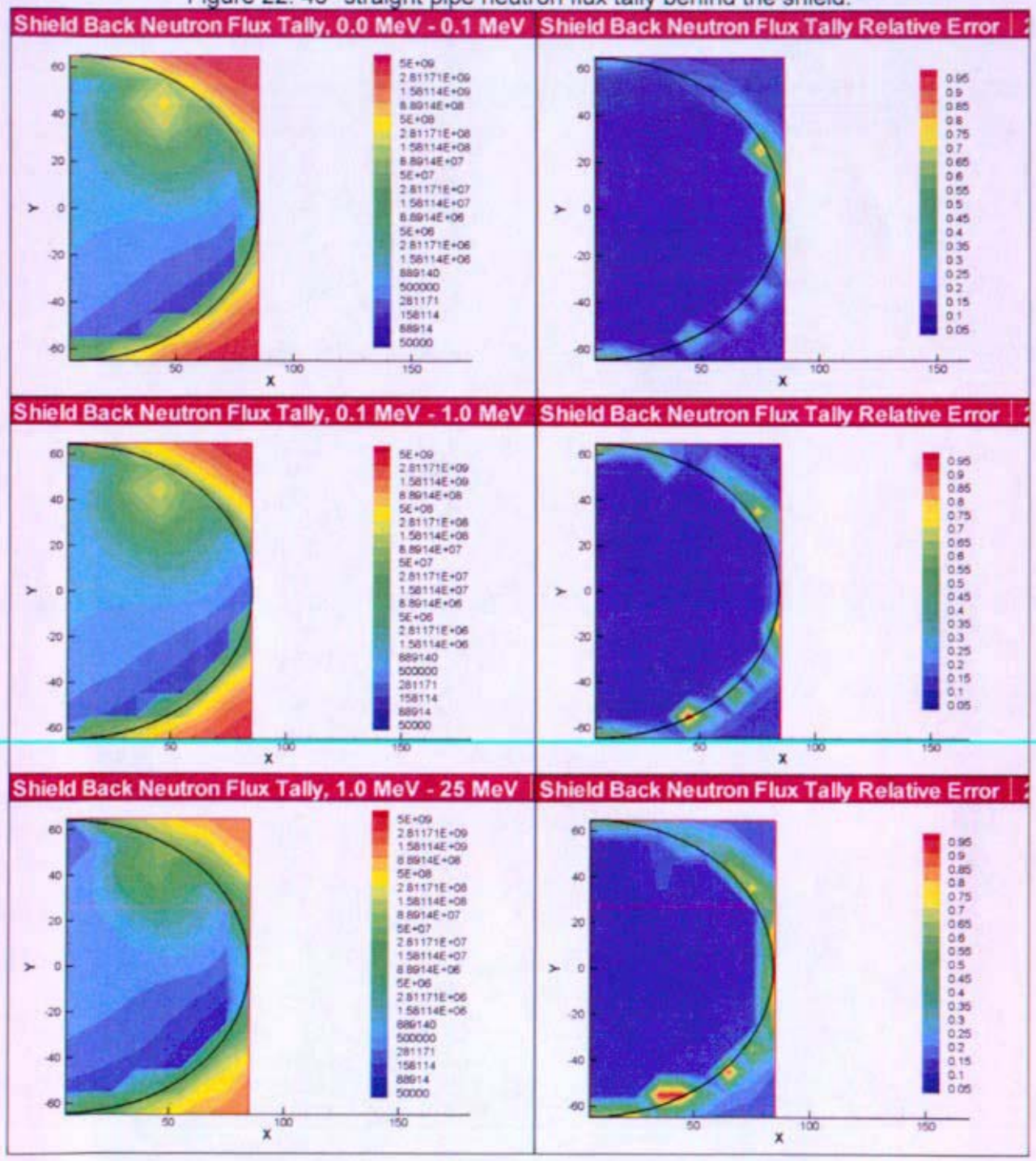

Figure 23: 45° spiral pipe neutron flux tally behind the shield.

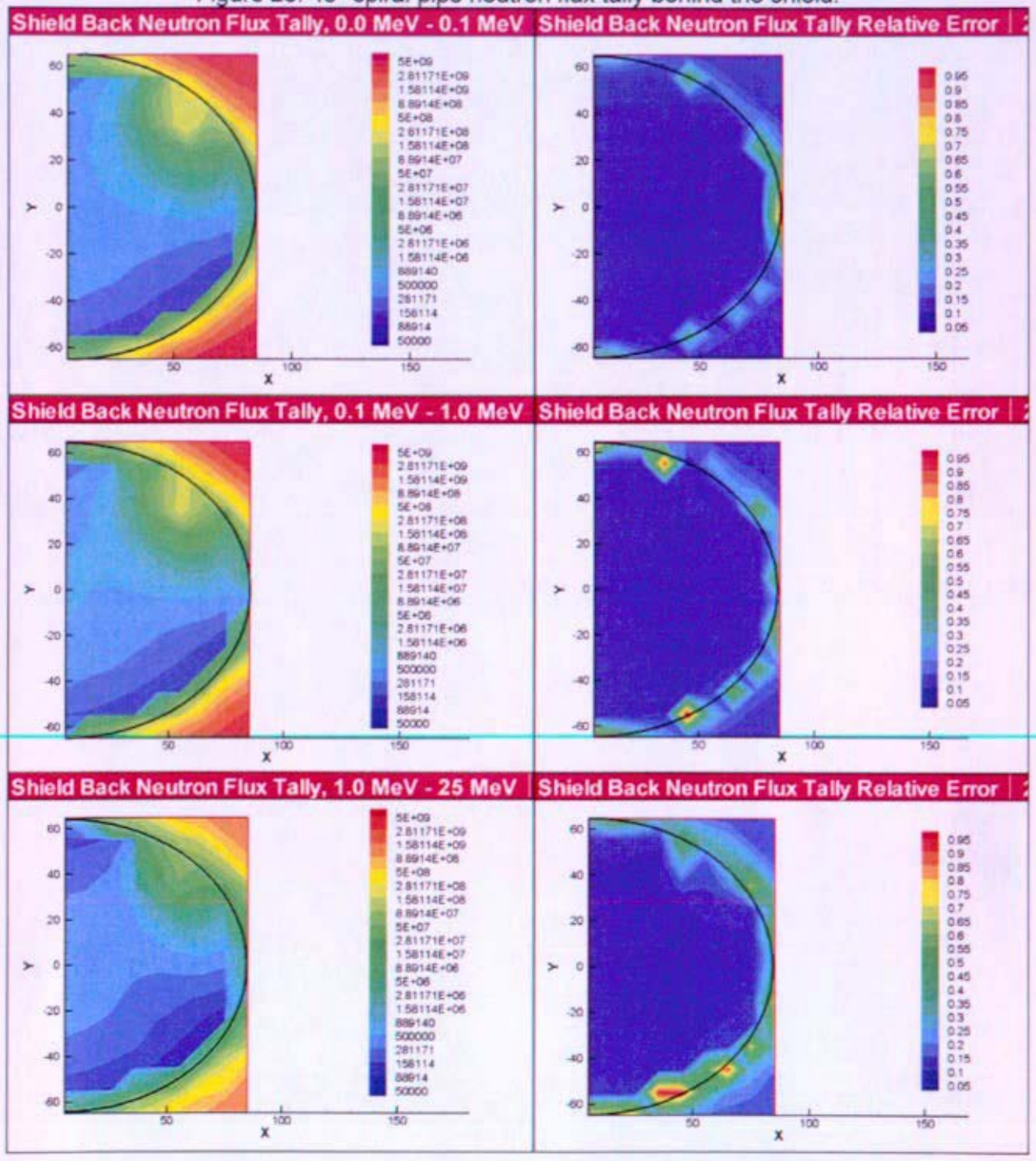

Figure 24: 45° dog-leg pipe neutron flux tally behind the shield.

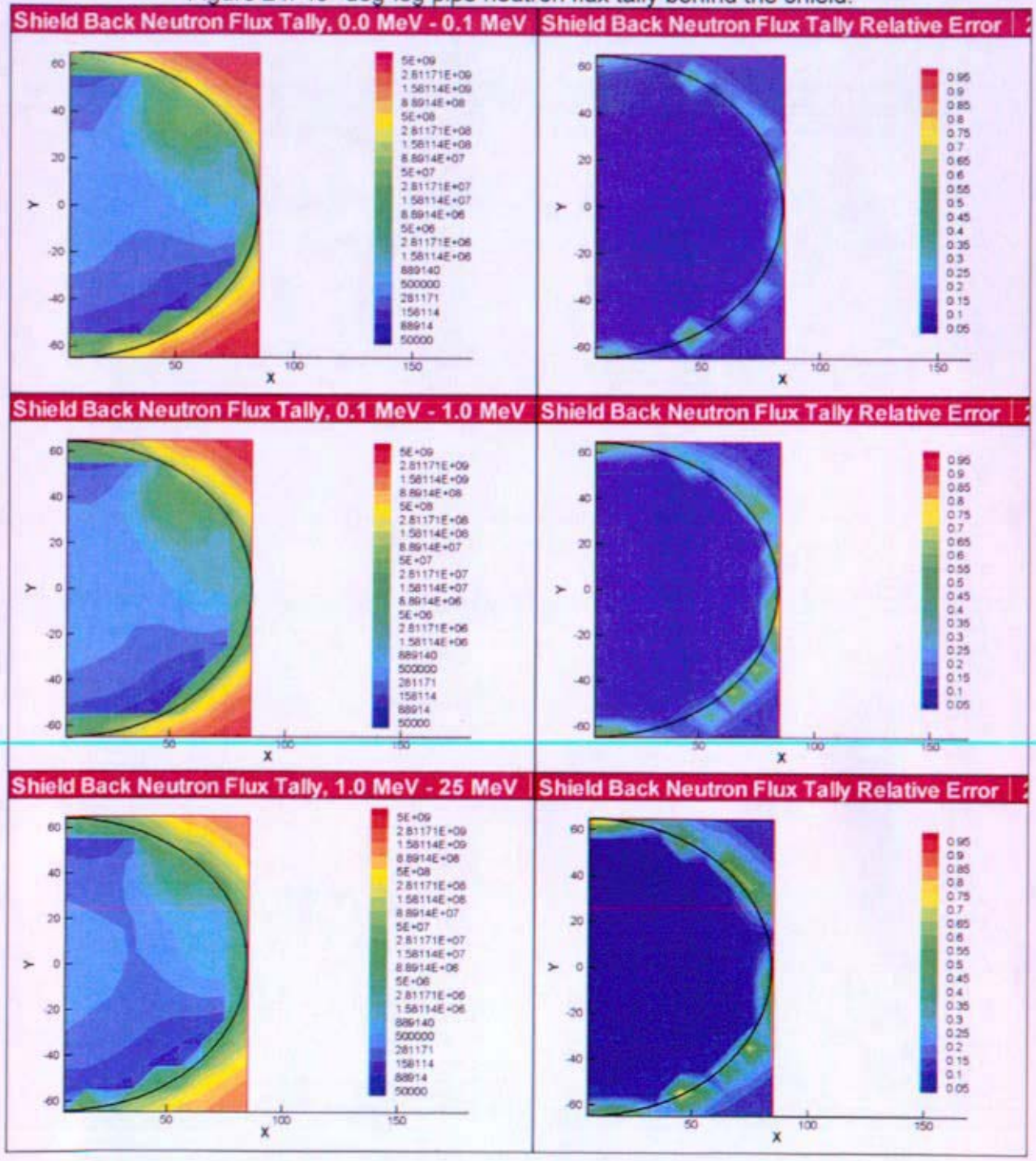

Figure 25: 90° straight pipe neutron flux tally behind the shield.

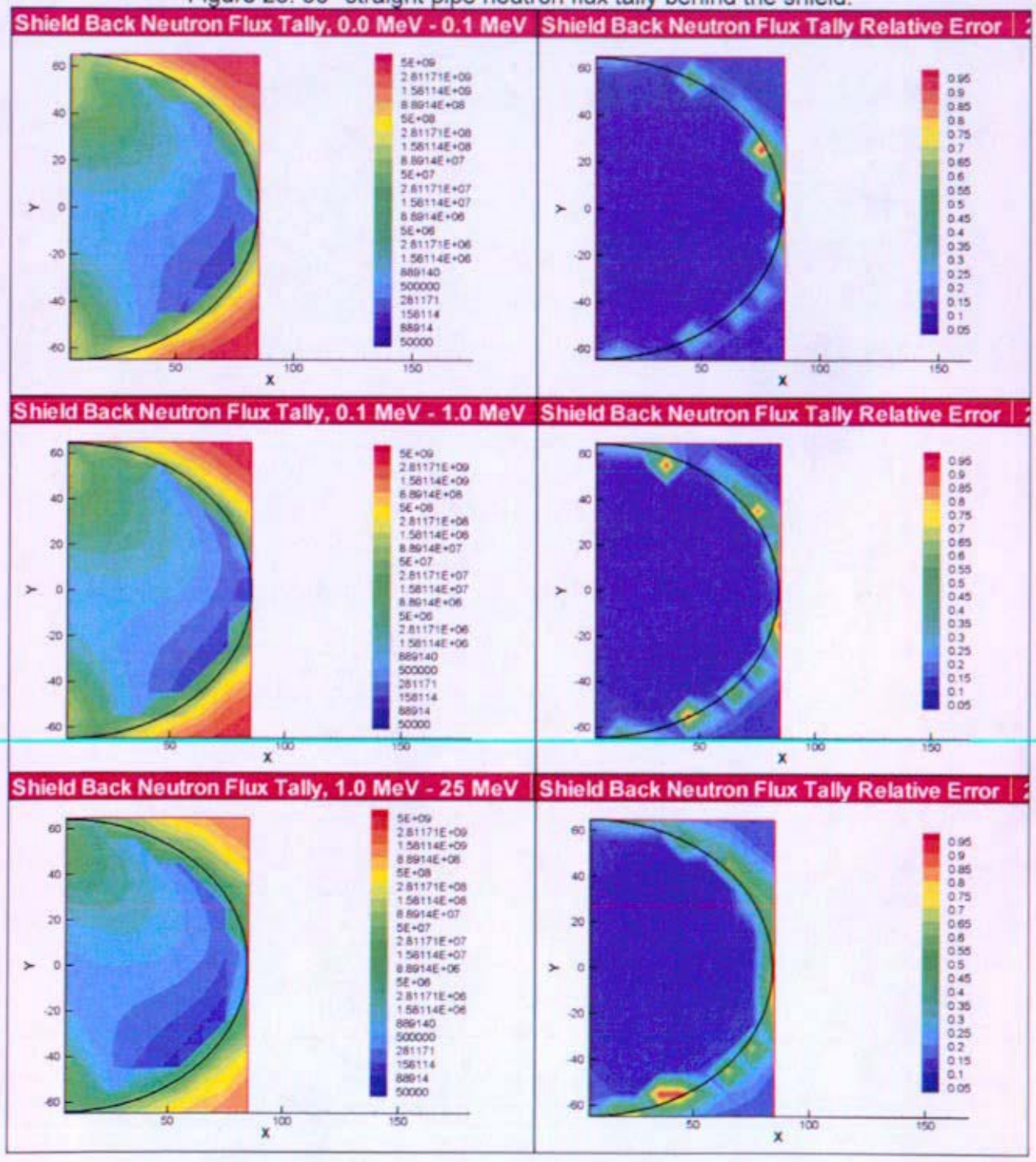

Figure 26: 90° spiral pipe neutron flux tally behind the shield.

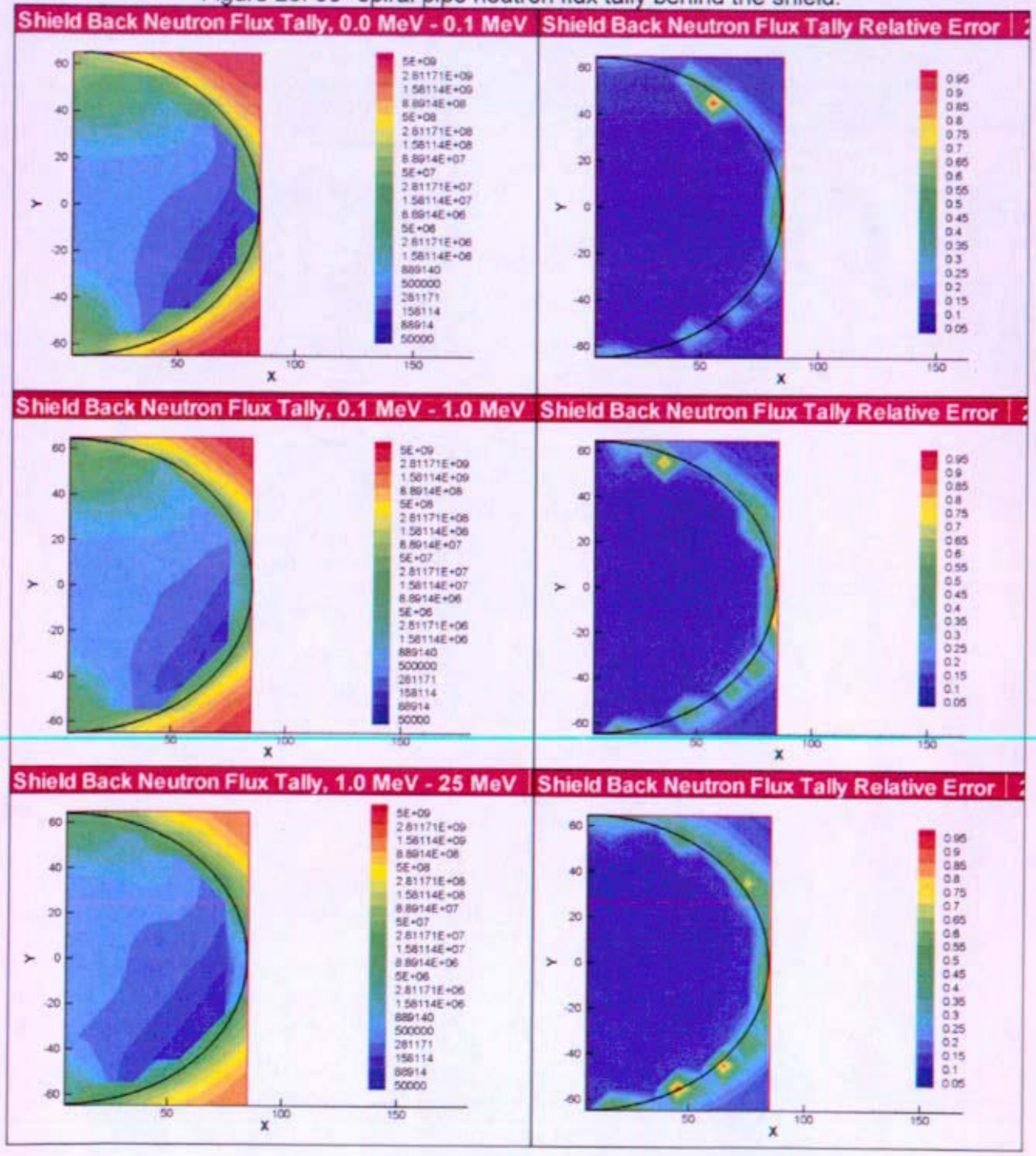

Figure 27: 90° dog-leg pipe neutron flux tally behind the shield.

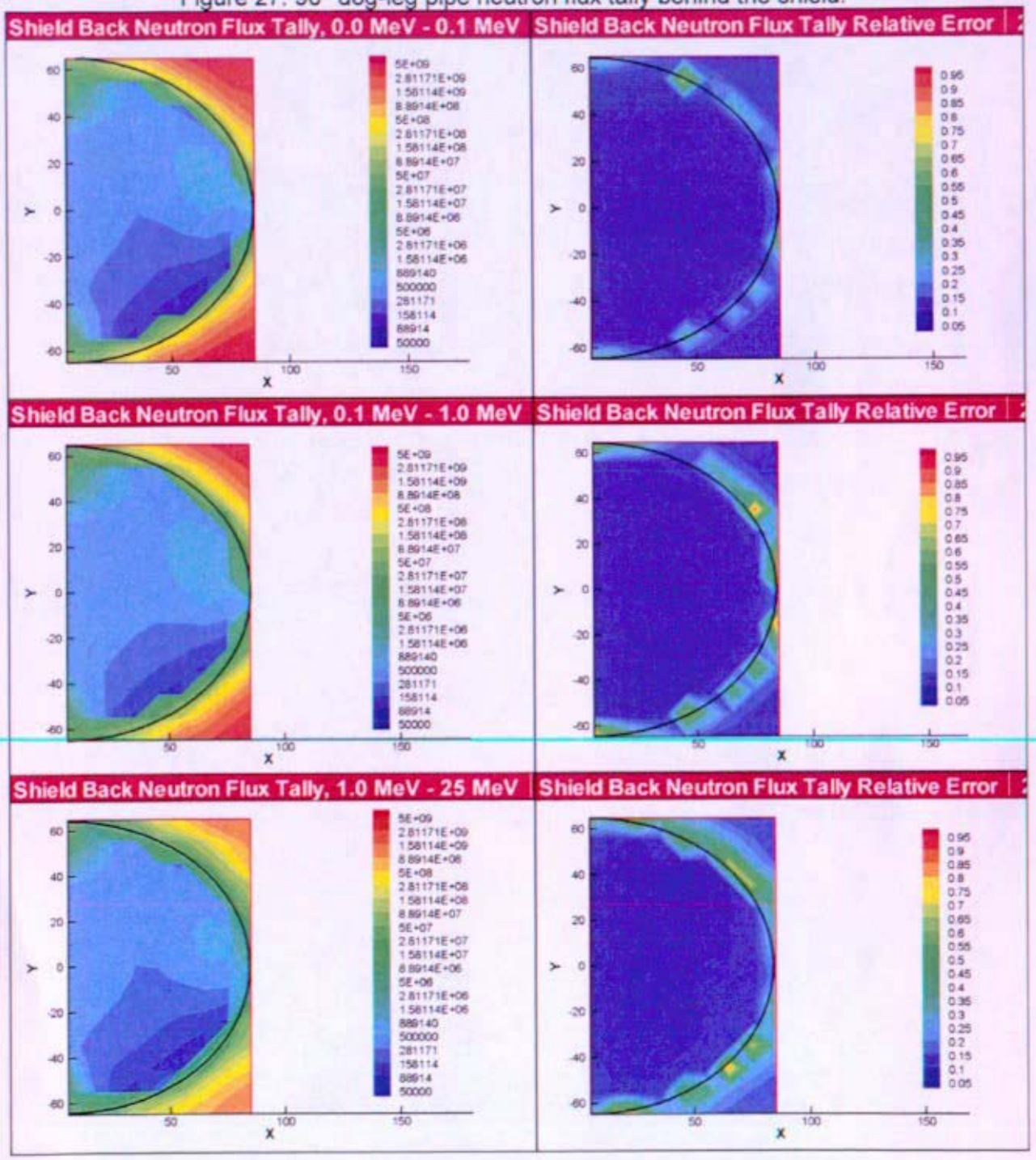

Figure 28: 135° straight pipe neutron flux tally behind the shield.

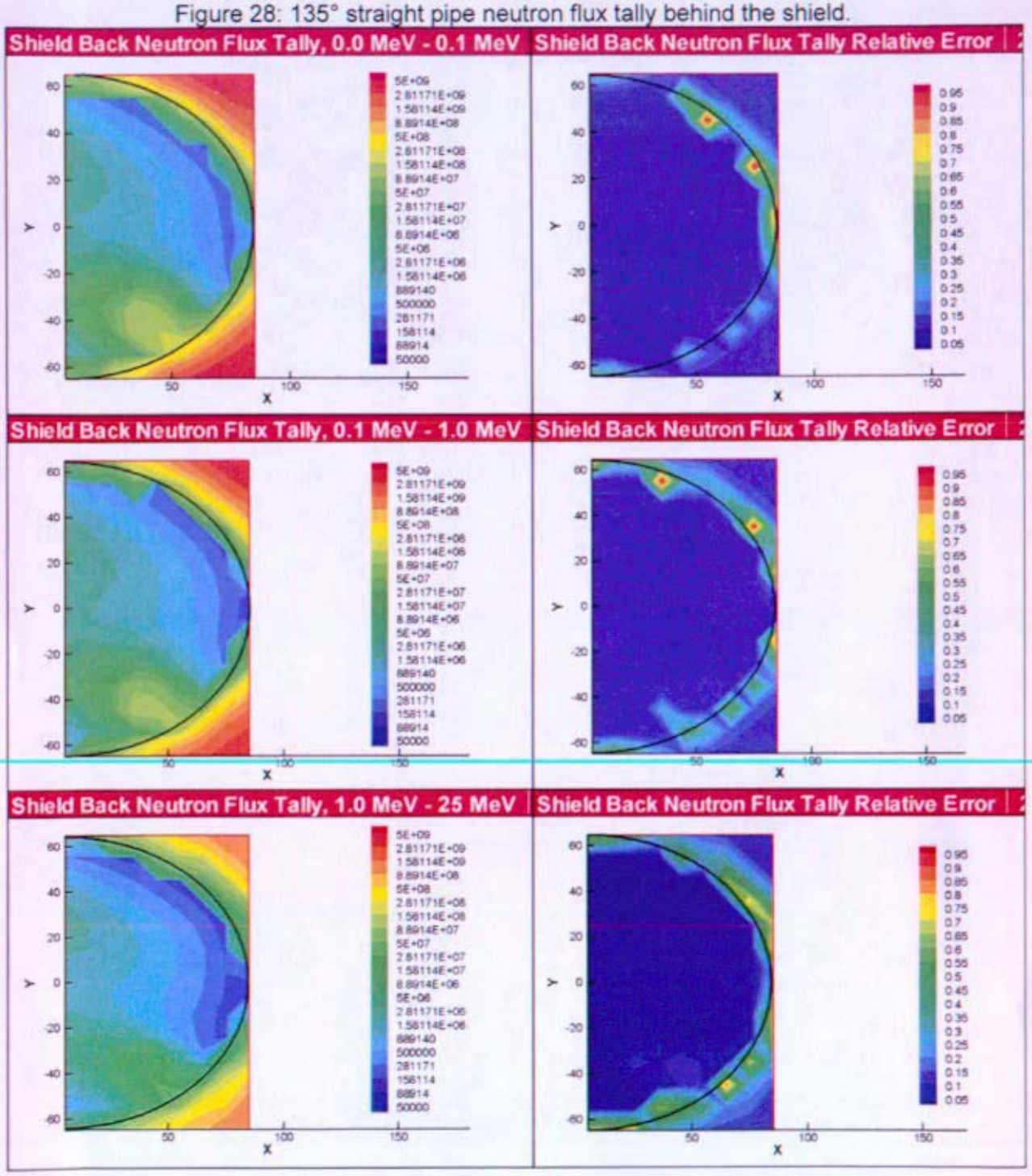

Figure 29: 135° spiral pipe neutron flux tally behind the shield.

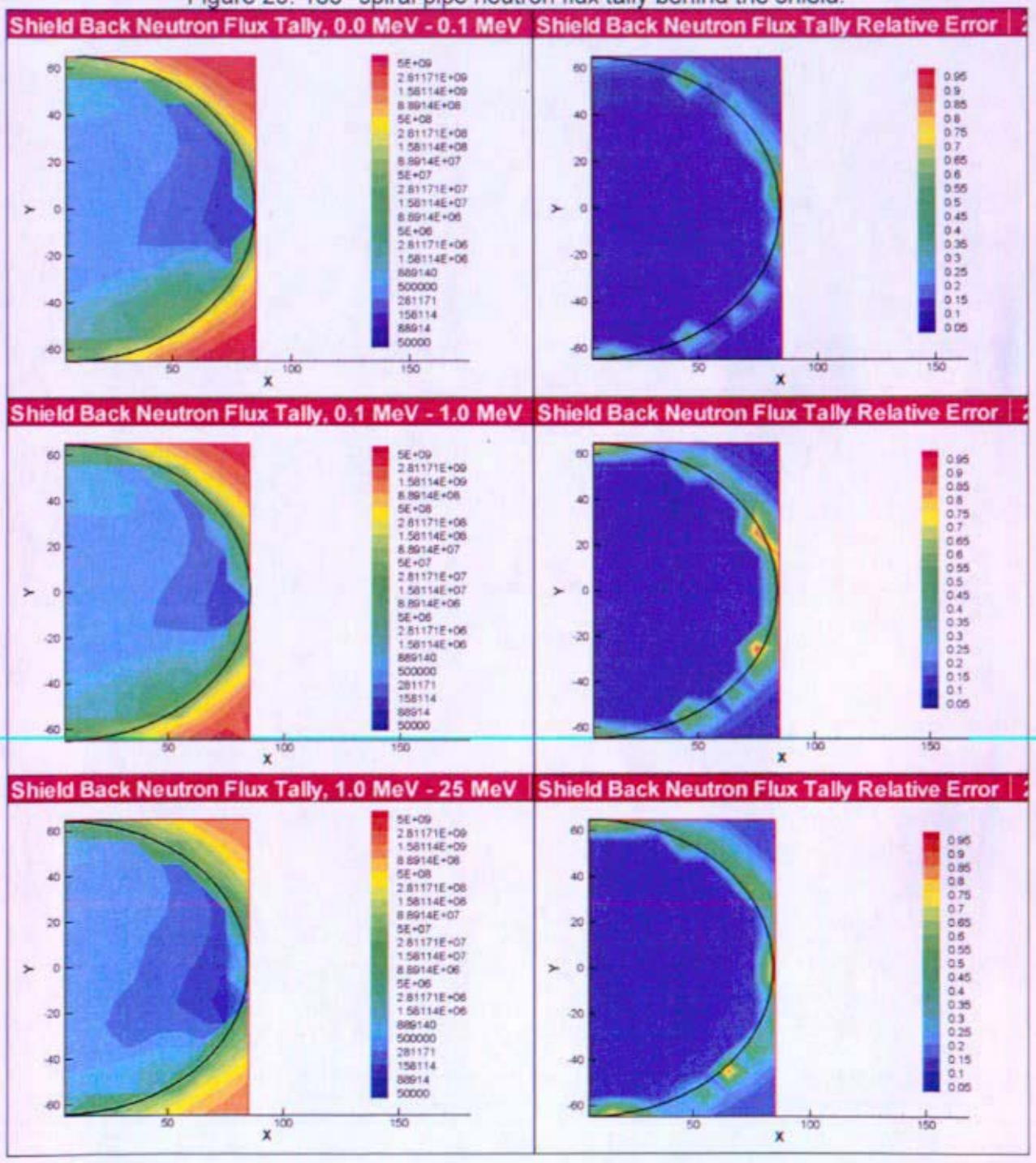

Figure 30: 135° dog-leg pipe neutron flux tally behind the shield.

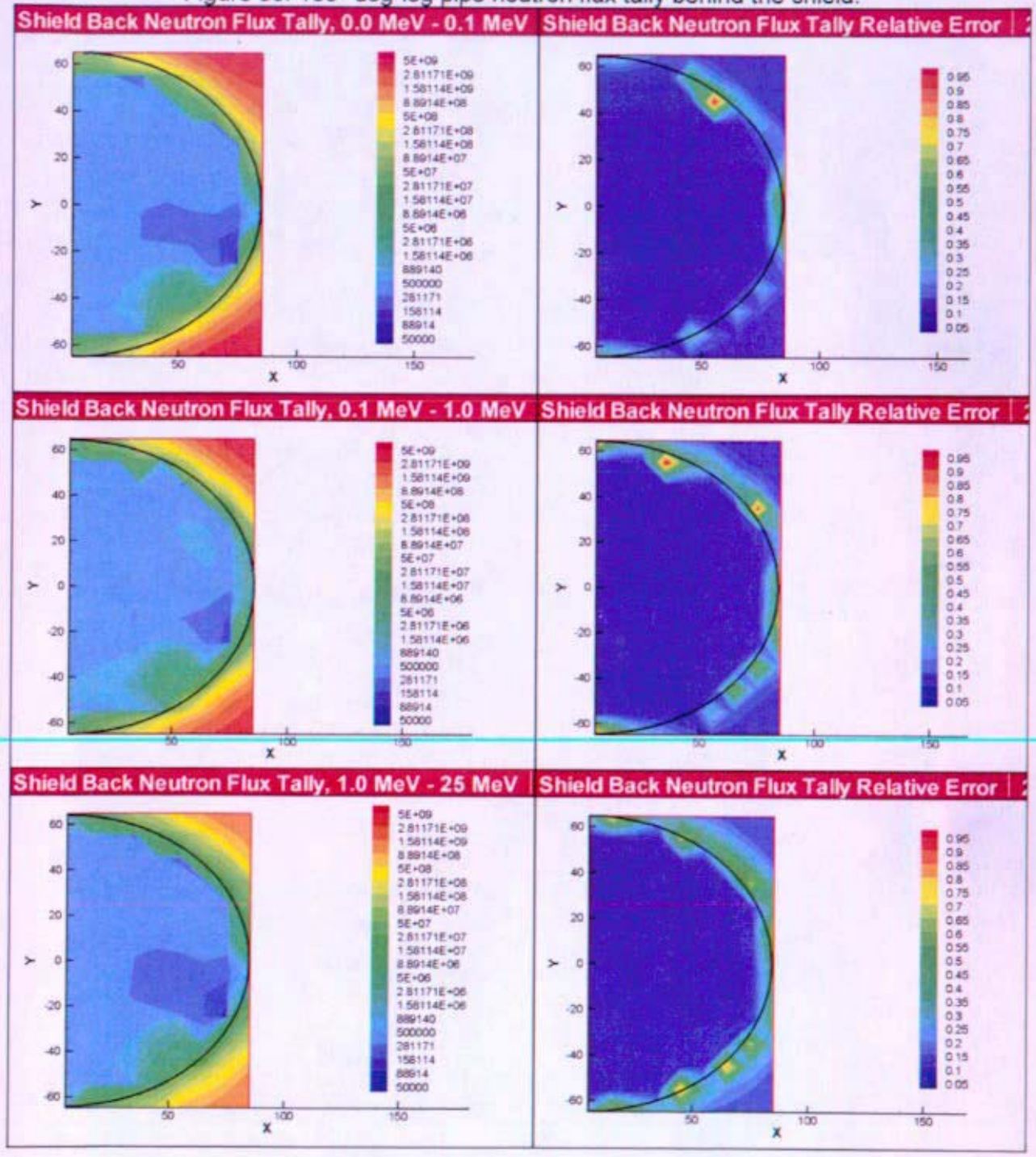

Figure 31: 180° spiral pipe neutron flux tally behind the shield.

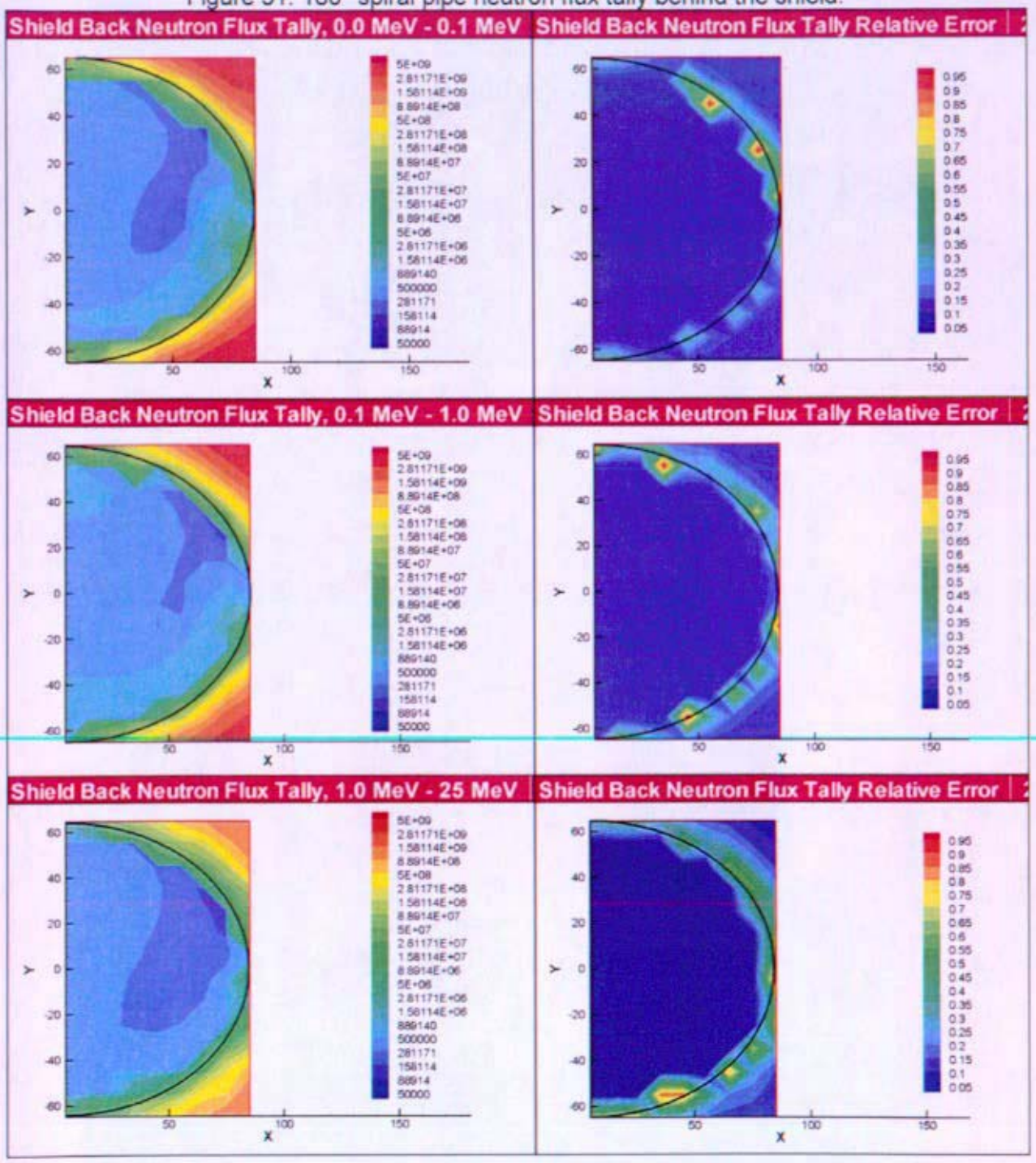

Figure 32: 180° dog-leg pipe neutron flux tally behind the shield.

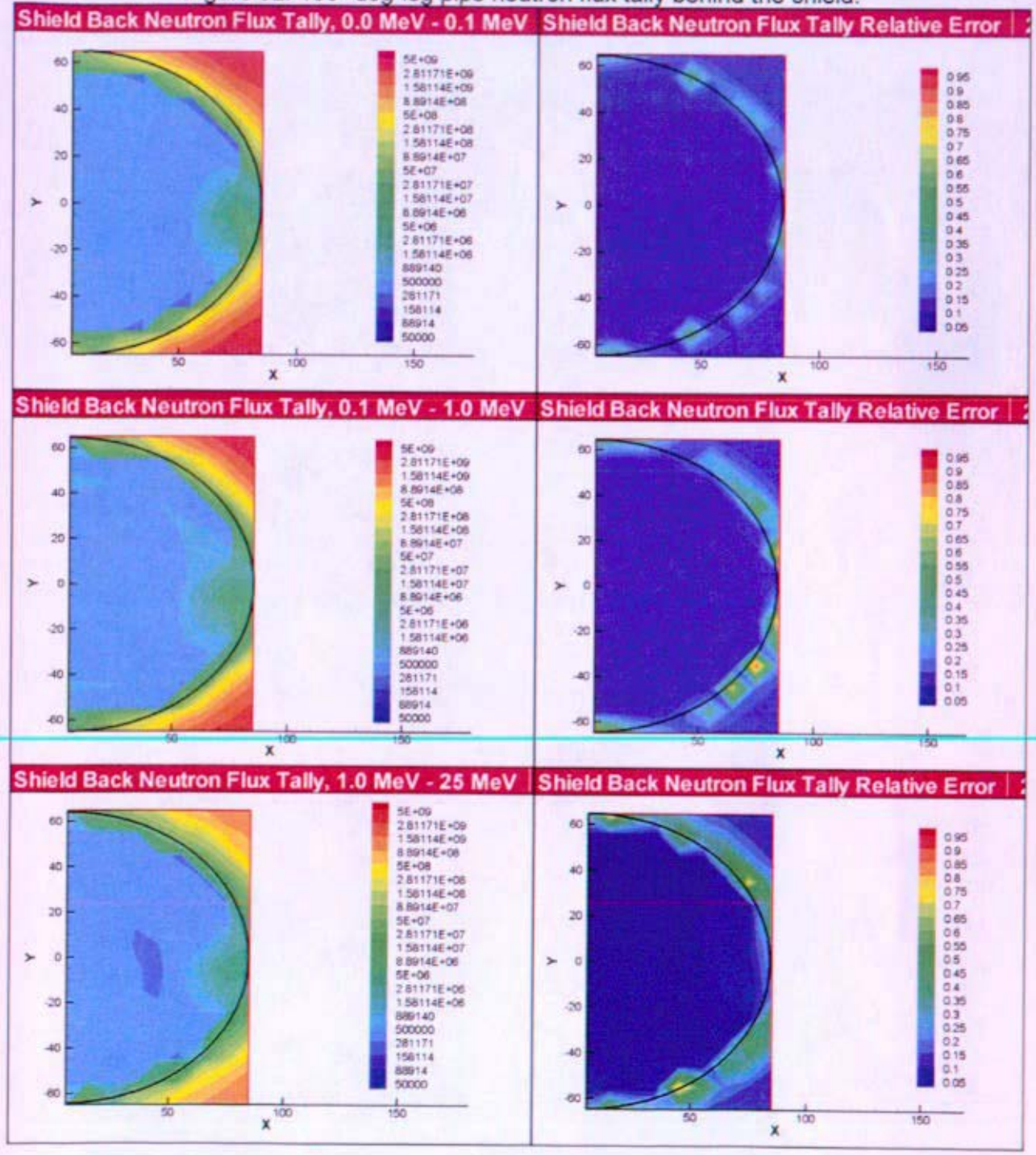

Figure 33: Pipes straight out from reactor head neutron flux tally behind the shield.

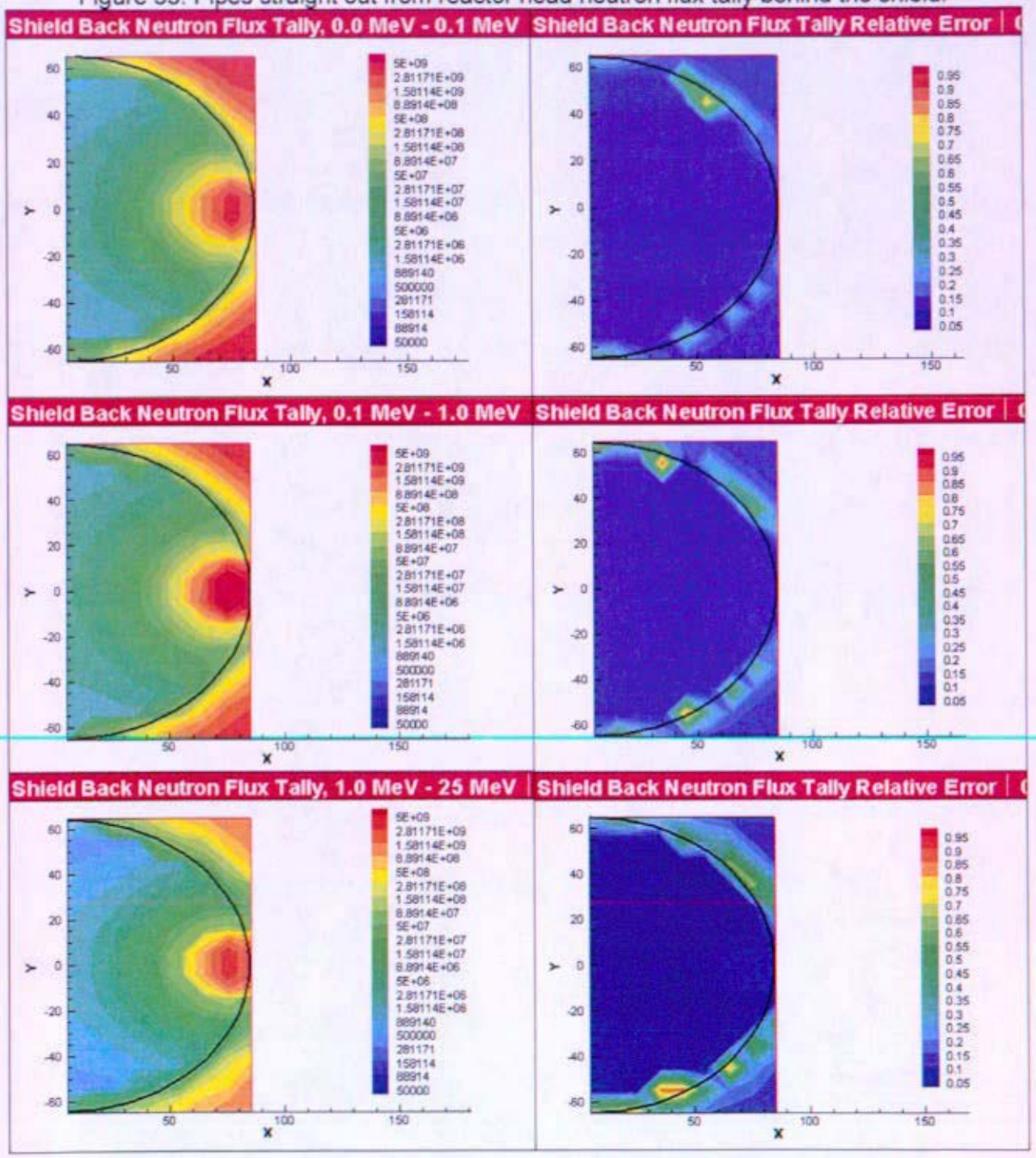

Figure 34: 180° spiral with thickened shield neutron flux tally behind the shield.

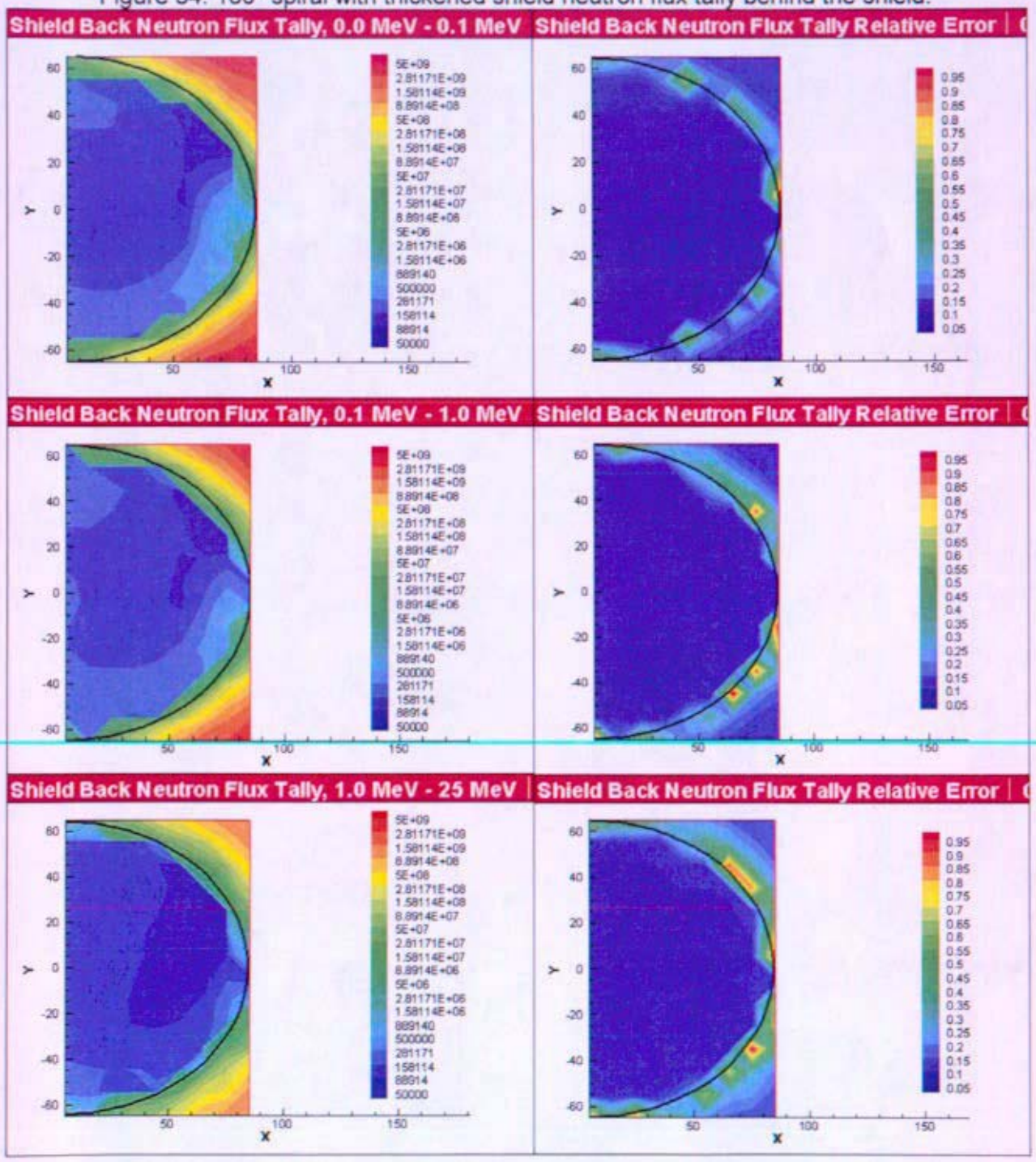

Ground Test Reactor Core Calculated Radiation Levels in M140 for Planning Purposes

R.S. Amato, Consultant
Shielding Design and Development
Ship Engineering Activity
Bechtel Bettis, Inc.

INTRODUCTION

A study was conducted to estimate the gamma radiation levels for end-of-life shipment of a representative Space Reactor Prototype Core (SRPC) in an M140-type shielded container. Since the SRPC is in the pre-conceptual design phase, the radiation level results are intended for planning and discussion purposes.

DISCUSSION

The SPAN5 computer code was applied to calculate the gamma radiation levels commencing 30 days after shutdown with the SRPC shielded by an equivalent M140 shielded container (14 inches of iron). The fission product gamma yield source data applied in the calculations were generated from SPENT3 for a fast reactor application with a 1.0 MeV core average neutron energy spectrum and 15 EFPY of operation. The SPAN5 thermal neutron fission product library (FSTAB) was not applied to define source data since calculations showed that dose rates would be about 30 percent under predicted relative to SPENT3.

The overall modeling parameters are presented in Table 1 and Figure 1.

Table 1: Core Modeling Parameters for UO2 Block Core, Annular Flow (DSO470 Model)

1. Operating History: 15 years at 100% Power (1 MW)
2. Core material / dimensions (Reference (a))
   - Core Diameter / Height = 57.50 cm / 66.4 cm
   - Hastelloy X Reactor Vessel Thickness = 0.635 cm
   - Core Fuel Area Fraction = 0.29
   - Core Void Area Fraction = 0.24
   - Core Safety Rod Area Fraction = 0.07
   - Core Block Area Fraction = 0.36 MoRe
   - Core Clad Area Fraction = 0.04 MoRe
   - UO2 Loading = 505.3 Kg , 93.2% U-235
   - Max Fissions per cc = 4.1E+20 ; Applied Peaking Factor = 1.45
3. SPAN5 Homogenized Core Model Volume Fractions
   (Excluding Center Control Rod Volume)
   - Center Rod = void
   - UO2 = 0.312
   - MoRe = 0.430
   - Core Void = 0.258
4. Core Neutron Spectrum from KAPL MCNP Core Model

Max Group Energy (MeV)	Group Flux
6.2500E-07	1.23363E+09
5.5300E-03	8.09826E+10
8.2100E-01	1.13120E+13
2.0000E+01	4.23609E+12

RESULTS AND CONCLUSIONS

The dose rate results are presented in Table 2, below.

Table 2: SPAN5 Calculated Peak Gamma Dose Rate (mrem/hr)

Time After Shutdown	P2	P1	P0
30 Days	4.09	44.9	9.58×10^7
90 Days	0.51	5.69	4.49×10^7
180 Days	0.31	3.35	3.00×10^7

Note: P0 is on contact with ¼" thick Hastelloy X Reactor Vessel
P1 is on contact with 14" Iron Shield, 200 mrem/hr Dose Rate Limit
P2 is 2 meters from surface of Iron Shield, 10 mrem/hr Dose Rate Limit

Table 2 shows that the gamma dose rates commencing 30 days after shutdown are 44.9 mrem/hr on contact with the shield surface and 4.09 mrem/hr at 2 meters from the shield surface. Therefore, the current conceptual SRPC satisfies the 10CFR71 normal shipment dose rate requirements for an M140 shipping container shield.

Figure 1: SPAN5 Shield Model

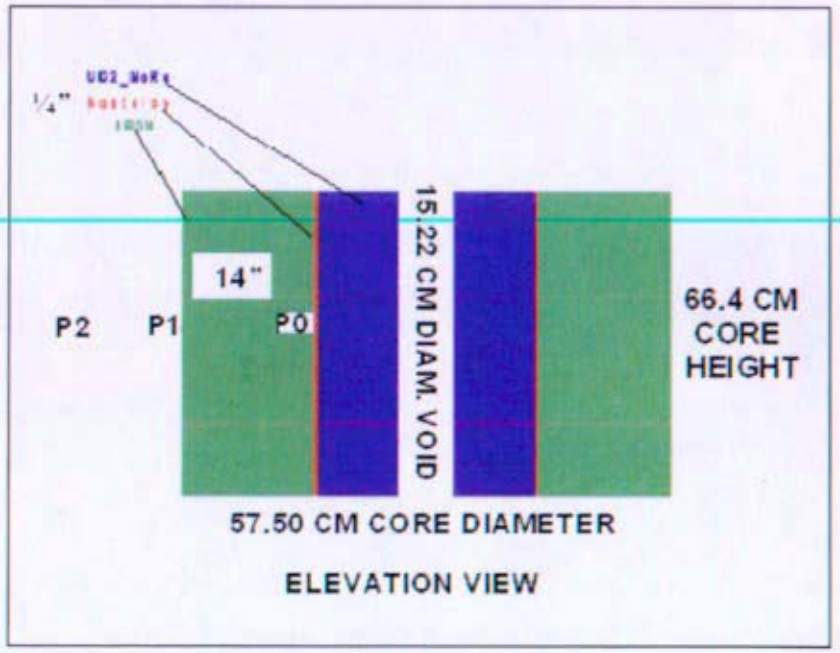

REFERENCE

(a) Attachment A to NRPCT Letter B-SE(RE)-0001, "Fuel Type Recommendation for the Project Prometheus Space Nuclear Reactor, For Naval Reactors Approval (U)," Table IV-13, CD Eshelman, DF McCoy, 28 July 2005.

Intentionally Left Blank

Projected Shutdown Radiation Levels Following Zero-Power Testing of a Space Reactor

Jonathan E. Stephens, Engineer
Space Reactor Shielding
Fleet Support Operation
KAPL, Inc.

INTRODUCTION

To assist in planning the Assembly Test and Launch Operations (ATLO) for a space reactor mission, it is important to know the expected radiation levels near the Prometheus reactor following zero-power testing. This type of testing, which may be performed on a prototype and/or flight unit, is typically done to verify core reactivity characteristics.

As the name implies, a "zero-power" test is done at a very low power level, but this level must be high enough to generate a reasonable response from the nuclear instrumentation. This study assumed a test power level of 0.01% of full power, since no test power level had yet been specified. For the 1-MWt Prometheus reactor, this was equivalent to 100 W. The SPAN point-kernel code, which has historically been used heavily by KAPL and Bettis shielding groups, was used for this analysis by utilizing the FSTAB option to simulate a given power history. Note that results in Enclosure (4) suggest that FSTAB may provide radiation level results 30% lower than SPENT3. Shutdown radiation levels were tracked for a range of activation and shutdown time intervals for a simple SPAN model.

DISCUSSION

The base case power history used in the analysis was 24 hours of operation at 0.01% power. Fission product decay gamma radiation levels were calculated at various times following shutdown. Other operation times were studied, ranging from an hour to many weeks. Alternate sources of radiation, such as activation of structural material, were assumed to be small and therefore were ignored. There were no specific radiation level criteria to be met, but it should be noted that the limits for shipping are 200 mrem/hr on the container surface and 10 mrem/hr at 2 meters from the container. Radiation levels above 100 mrem/hr constitute a "high radiation area."

The reactor model used in SPAN was a homogenization of the DSO470 design provided by the Space Reactor Engineering group. The model consisted of a 57.5-cm-diameter cylinder with a 66.4-cm height, which was a mixture of fuel (UO_2), safety rod (B_4C) and structural material (MoRe). This region was radially encompassed by a 0.635-cm Hastelloy-X reactor vessel. The maximum radiation levels outside the reactor were expected to be at the axial midplane of the core (on the outer surface of the vessel). Since the point-kernel method used by SPAN considers only materials in a direct line between fuel regions and dose points, it was not necessary to model regions axially above and below the fuel. To estimate radiation levels during shipping, an arbitrary 5-cm-thick iron container was added to the model, located about 5 cm outside the reactor vessel.

The core region contained several elements that were not available in the SPAN library because they are not commonly considered in terrestrial nuclear reactor design. Each such element was modeled using the library element with the nearest atomic number (to be conservative, a lower-Z element was always selected). The element substitution and the core homogenization were sufficient for the rough gamma calculations performed in the study.

RESULTS

Figure 1 shows radiation levels as a function of distance from the center of the core, following a 24-hour test at 0.01% power. Each curve is for a given decay interval following the test. The radial dimensions of the reactor and shipping container are displayed, as well as the radiation criteria for shipping. For the given power history it can be inferred from the plot that the radiation level limits for shipping are met after about 1 day following shutdown. A larger or thicker shipping container could reduce these levels dramatically.

In Figure 2, the decay time following shutdown is held constant at 24 hours, and the plots show maximum radiation level on the surface of the vessel (ignoring the shipping container) as a function of operating time at 0.01% power. The sensitivity study was repeated at 0.1% power and plotted to verify that radiation levels scaled linearly with operating power level, as expected. The plots show that shutdown radiation levels increase more slowly as operating time increases. This is because the buildup and decay of delayed gammas is approaching equilibrium. After a long time (greater than about 1 month) at constant power, the radiation levels do not continue to increase. On the other hand, for relatively short operation times, small uncertainties in operational time can result in significant uncertainties in shutdown radiation levels.

Figure 3 shows the maximum radiation level on the surface of the vessel as a function of the decay time following shutdown. Each plot is for a different operation time of the test, conducted at 0.01% power. For a 24-hour test, the maximum radiation level falls below 100 mrem/hr, the threshold for a high radiation area, after about 1 month. This is much more limiting than the results in Figure 1 for the shipping container, which showed that shipping was possible after just one day, even with such a conservative container model.

CONCLUSIONS

Zero-power testing of a space reactor for a power level and length of time similar to those assumed in this study will result in non-trivial radiation levels following shutdown. Shipping radiation criteria are not difficult to meet shortly following testing, but a more realistic container design is needed to calculate exactly how much decay time is needed. Much more limiting are dose rates on contact with the reactor vessel. Significant contact radiation levels could affect access to the vessel for activities such as final assembly of the spacecraft. Also of concern is the stowed configuration of the reactor in the launch vehicle; namely, its proximity to the payload. These issues can be mitigated by planning for a waiting period between testing and assembling the reactor to the spacecraft and/or appropriate sequencing of the assembly.

There are several potential ways to reduce the radiation levels following zero-power testing. The power level of the test could be reduced, though nuclear instrument cognizant engineers must be consulted to ensure the power level is high enough to obtain reasonable nuclear instrumentation response. Also, the length of the test could be reduced or the decay time following the test could be increased. For shipping, the container could be made thicker, or the distance from the reactor core to the nearest accessible location outside the container could be increased.

Figure 1: Radiation Levels Following Zero-Power Test (0.01% power for 24 hrs.)

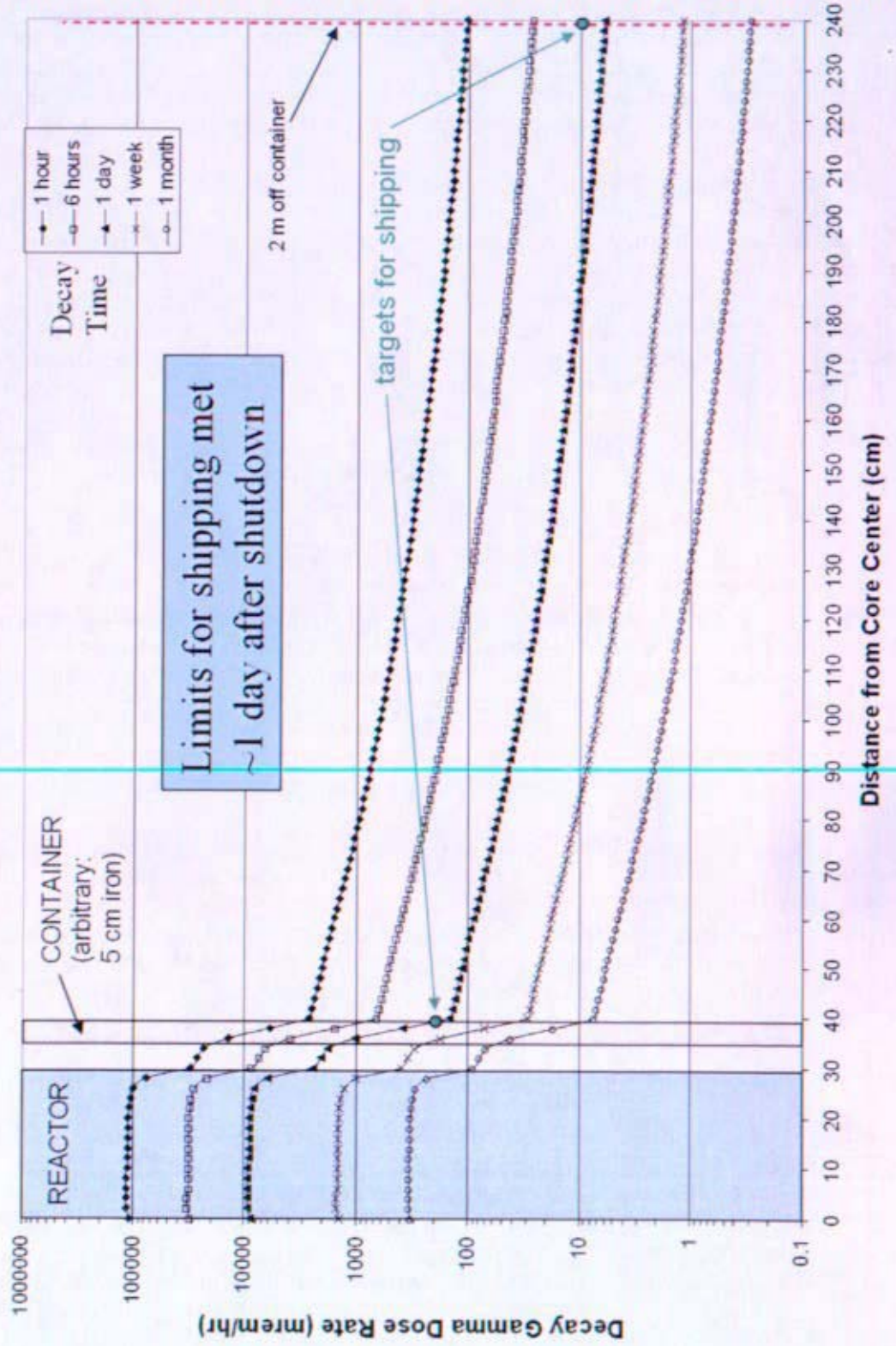

Figure 2: Radiation Levels Due to Zero-Power Testing (Following a 24-hr Decay Time)

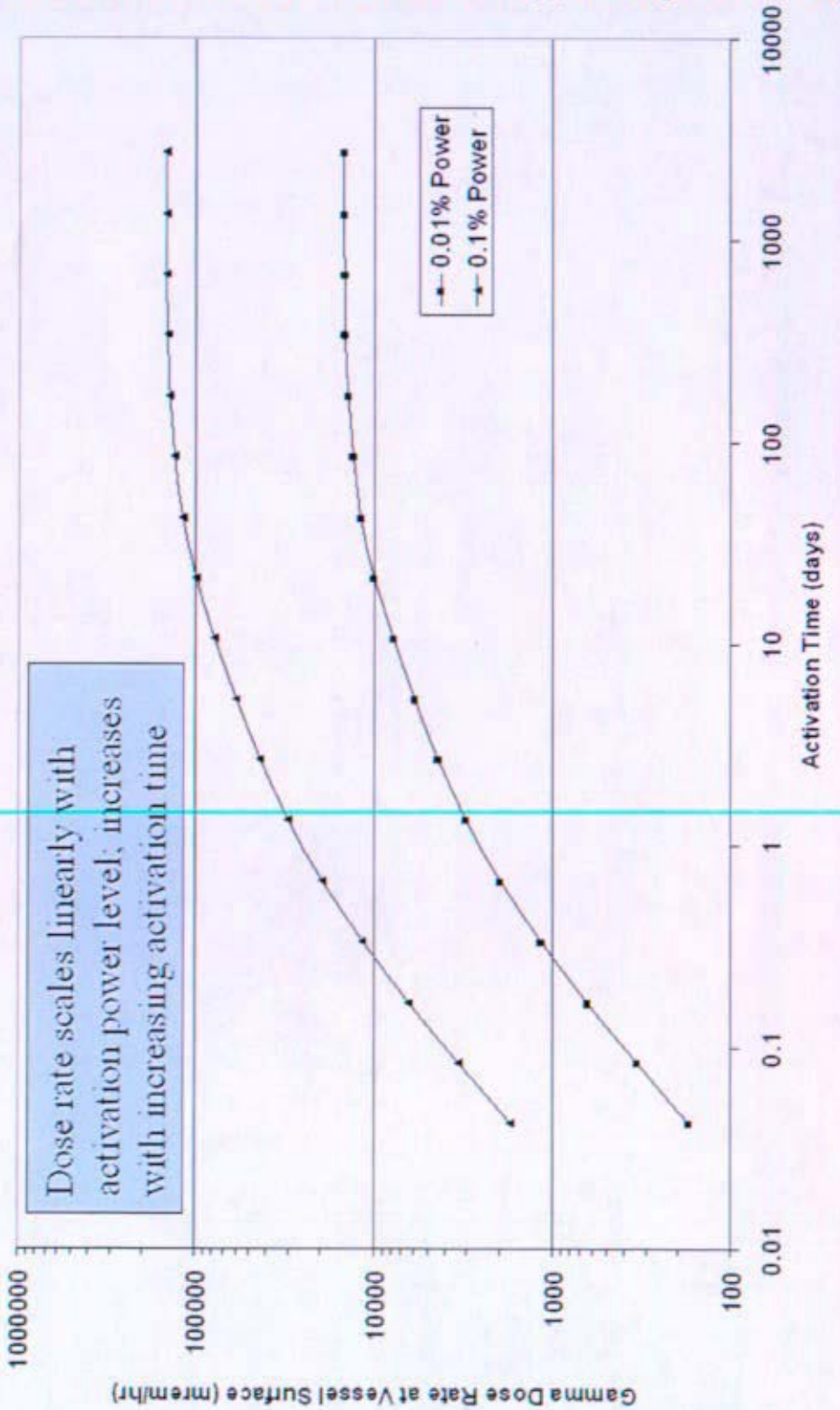

Figure 3: Radiation Levels Following Zero-Power Testing at 0.01% Power

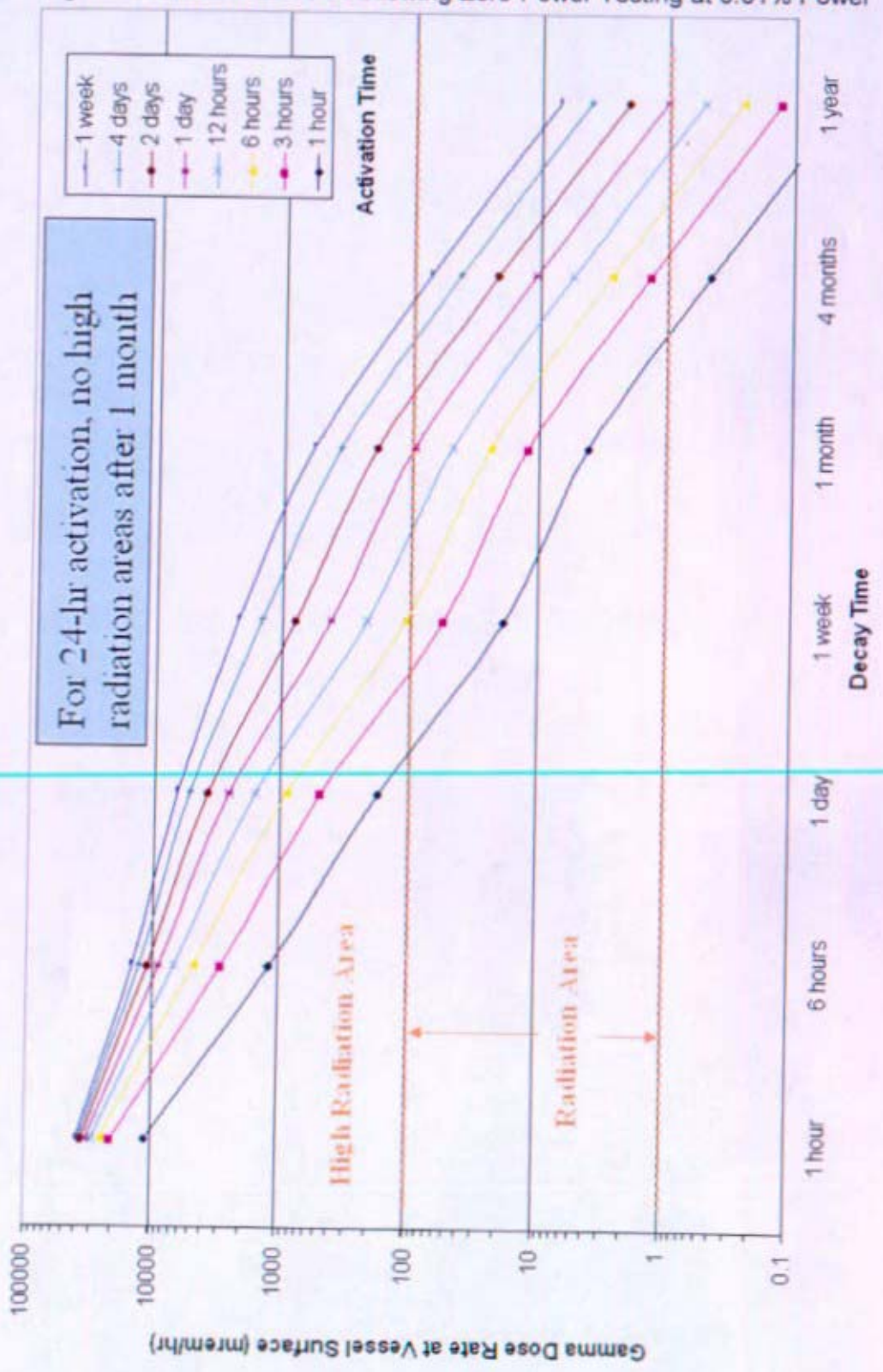

QUALIFICATION OF METHOD

All results presented herein were pre-decisional, and intended for planning and discussion purposes only. No method uncertainty or design assurance factors were applied to any of the results.

The SPAN code used in this analysis is production level on the supercomputer platform utilized, but it is not specifically qualified for space work.

This enclosure has been reviewed by and has the concurrence of the manager of KAPL FSO-Shielding. This enclosure is a summary of work documented in KAPL SWR-00073, which is Reference (a).

REFERENCES

(a) KAPL Shielding Work Record: SWR-00073, "SPP Space Shielding Analyses," J.E. Stephens, July 2005.

This page intentionally left blank.

Space Reactor Pressure Vessel Material Activation Analysis

Jonathan E. Stephens, Engineer
Space Reactor Shielding
Fleet Support Operation
KAPL, Inc.

INTRODUCTION

At the request of the Space Reactor Engineering group (W Gideon), a neutron activation analysis was performed on selected materials following extended full-power operation (e.g. ground test reactor operation). These materials were candidates for the reactor vessel, but the analysis is useful for any structural component consisting of one of the materials.

The NUGACS code, used extensively in NR program shielding work, was used to calculate the gamma source density (gammas/cc/sec) per unit neutron flux, given a relative power history and shutdown (decay) time.

DISCUSSION

There were 8 materials, which could be organized into 3 categories based on the dominant contributor to activation radiation:

- Tantalum-containing materials: Ta-10W, ASTAR 811C, FS-85
- Cobalt-containing materials: Hastelloy-X, PE-16, Haynes 230, Alloy 617
- Mo47Re (Molybdenum-Rhenium)

Table 1 lists the elements in each material that contribute significantly to activation gamma radiation in the short term (hours to days) and long term (months or more) following a year of operation. The magnitude of gamma radiation produced is dependent upon several factors:

Isotopic Number Density

A higher density of a given isotope will result in more activation.

Neutron Capture Cross Section

A higher capture cross section will result in more activation.

Activation Product Half-Life

An activation product with a very short half-life will result in a high gamma production rate, but only for the short term. An activation product with a very long half-life will result in a low gamma production rate, but for a very long time. The biggest radiation level concern is activation products with half-lives in the range of several months because they decay quickly enough to produce a high gamma rate, but not so quickly that the radiation levels decrease rapidly.

Furthermore, the half-life determines the time until the buildup and decay of the radioactive isotope reaches equilibrium. For example, consider a plant operating at constant power for 1 year, as in the power history used for this analysis. An activation product with a half-life notably shorter than 1 year, such as Ta-182 (114 days), should be approaching equilibrium after a year, such that the resulting gamma flux does not continue to increase greatly if the operational time is extended. On the other hand, an activation

product with a longer half-life, like Co-60 (5.27 years), would further increase in abundance with extended plant operation.

Table 1: Significant Contributors to Activation Gamma Radiation

	Co	Cr	La	Mo	Ni	Re	Ta	W
Ta-10W							L	s
ASTAR 811C						s	L	s
FS-85							L	s
Alloy 617	L	l		s	l			
Haynes 230	L	l	s	s	l			S
Hastelloy-X	L	l		s	l			s
PE-16	L	l		s	l			
Mo47Re				s		S		

S = major contributor in the short term (hours to days), s = minor contributor in the short term
L = major contributor in the long term (months or more), l = minor contributor in the long term

Material compositions were input into NUGACS based on data in the SPP Nuclear Design Basis, which is Reference (a). Cross section averaging parameters in NUGACS were based on an assumed temperature of 900K (value obtained from J Powers). The existing NUGACS library of reactions did not contain (n,gamma) reactions for several elements, including Ta, Nb, La, and Re. These were manually added to the library from data in References (b) and (c).

RESULTS

Figures 1 and 2 show the gamma source in each material of interest as a function of time after shutdown (having operated continuously for 1 year) due to thermal neutron activation and fast neutron activation, respectively. The gamma source is normalized per unit thermal flux (Figure 1) or fast flux (Figure 2), so the absolute gamma source would be obtained by multiplying this value by the maximum thermal/fast flux observed at the reactor vessel while at power.

From the figures and Table 1, it is clear that the highest amount of activation occurs in the tantalum-containing materials (Ta-10W, ASTAR 811C, and FS-85) and is due primarily to the activation of tantalum to Ta-182 (114-day half-life). The results are not surprising, since tantalum has a high activation cross section and Ta-182 has a half-life in the several-months range. Since the half-life is considerably shorter than the activation time, additional operating time would not likely result in significantly increased gamma levels. It should also be noted that in the near term following shutdown, there is a smaller contribution from activation of tungsten to W-187 (23.9-hr half-life).

The molybdenum-rhenium material, Mo47Re, has high activation gamma levels immediately following shutdown, but these levels decay rapidly, as suggested by the figures and Table 1. This is because the activation cross sections for the constituent elements are high, but the activation products have very short half-lives. The most significant contributors to gamma dose are the rhenium isotopes Re-186 and Re-188, which have half-lives of 3.7 days and 17 hours, respectively.

Figure 1

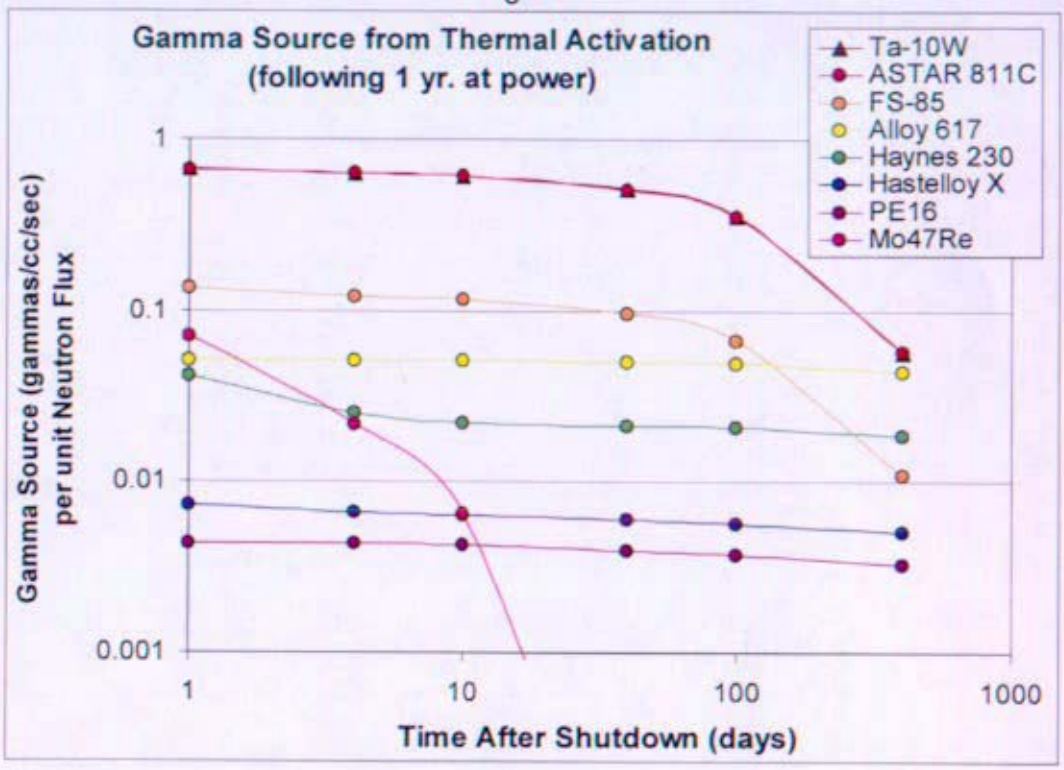

Figure 2

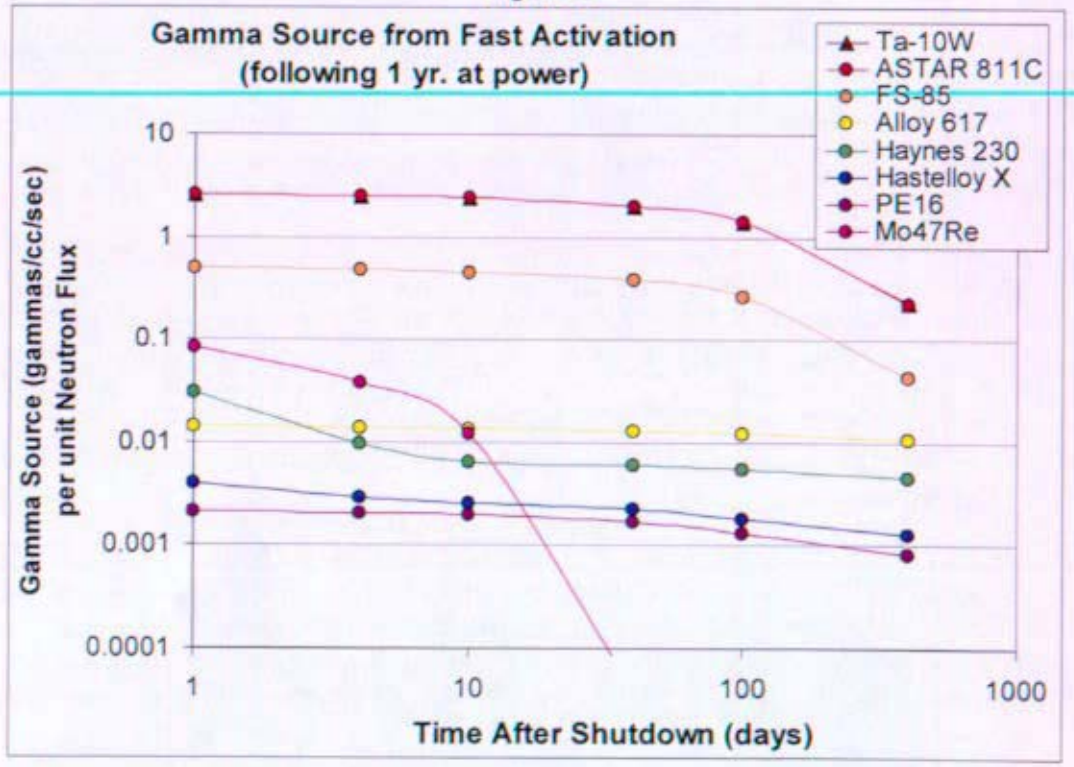

The remaining materials, PE-16, Haynes 230, Alloy 617 and Hastelloy X have activation gamma levels based mostly on Co-60 production. As seen in Table 1, there are smaller short term contributions from molybdenum and minor long term contributions from nickel and chromium. Co-60 has a 5.27-year half life, so the gamma radiation levels decay slowly. Also, since the half-life is much longer than the decay time, an equilibrium level of Co-60 has not been reached, so increased operational time would result in increased gamma levels.

CONCLUSIONS

From an activation radiation level standpoint within a few years after shutdown, tantalum-containing materials are not preferred. MoRe alloys perform well if sufficient time (> 1 month) is allowed for the activation products to decay. The cobalt-containing materials would be less problematic if the activation time (e.g. ground test reactor operation time) were reduced, or if the cobalt content could be reduced. Both tantalum and cobalt containing materials would have significant disposal concerns.

For any of the materials studied, the gamma radiation from fission product decay in the fuel would probably be greater than the contribution from activation gammas, reducing the significance of the material activation. Future work in this area should include a comparison of activation results to fission product decay gamma levels over a range of times following shutdown. The impact of using these different materials on irradiation testing and ground test reactor servicing and deactivation, especially in and behind the shield, would also be investigated in future studies.

QUALIFICATION OF METHOD

All results presented herein were pre-decisional, and intended for planning and discussion purposes only. No method uncertainty or design assurance factors were applied to any of the results.

The NUGACS code used in this analysis is production level on the supercomputer platform utilized, but it is not specifically qualified for space work.

This enclosure has been reviewed by and has the concurrence of the manager of KAPL FSO-Shielding. This enclosure is a summary of work documented in KAPL SWR-00073, which is Reference (d).

REFERENCES

(a) Enclosure to SPP-67410-0008, "Prometheus Reactor Nuclear Design Basis, Revision 0," Section 3.4, JK Witter, June 2005.

(b) "Chart of the Nuclides, 15th edition," Lockheed Martin, 1996.

(c) Browne & Firestone, "Table of Radioactive Isotopes," 1986.

(d) KAPL Shielding Work Record: SWR-00073, "SPP Space Shielding Analyses," J.E. Stephens, July 2005.

This page intentionally left blank.

Initial Ground Test Reactor Shield Sizing Study

Thomas M. Miller, Senior Engineer
Shielding Design and Development
Ship Engineering Activity
Bechtel Bettis, Inc.

INTRODUCTION

This is a discussion of some initial shielding calculations done for the space ground test reactor (GTR) facility. Calculations were performed with MCNP version 5 release 1.30 (Reference (a)) to determine the shield thickness required to meet certain contact dose rates on the surface of the shield.

DISCUSSION

The Bettis engineers designing the space GTR facility asked Bettis shielding to give an initial worst case estimate of the shield thickness for the space GTR. They requested that it be determined how much concrete would be needed in order to meet 3 different shield surface dose rates. The specified dose rates were:

125 mRem / 2800 hours ~ 0.0446 mRem/hr
500 mRem / 2800 hours ~ 0.179 mRem/hr
5000 mRem / 2800 hours ~ 1.786 mRem/hr

The time of 2800 hours represents the total time for a person working 8 hours a day, 7 days a week, for 50 weeks per year, which was thought to be a conservative assumption. It was also assumed that the reactor was always operating at full thermal power (1 MW), the energy release per fission was 201.2 MeV, and the average number of neutrons released per fission was 2.432.

The reactor used in the calculations, which was provided by the nuclear design team in July 2005, was designated dso470x. The shield included in this model contains layers of Be, B_4C, W, and LiH, but was not optimized to any specific configuration. Ordinary concrete (Reference (b) Appendix C) was assumed. The shielding calculations were performed via MCNP eigenvalue calculations (kcode), which provided the correct energy, spatial, and angular distribution of neutrons and photons in the reactor. Figure 1 shows a picture of the MCNP reactor and shield geometries. Only prompt fission neutrons and photons, delayed fission neutrons, capture photons, and photons due to neutron inelastic scattering were considered in this calculation. Other neutrons and photons due to the decay of radioactive fission products and photoneutrons were not considered.

The GTR design engineers also provided information about the configuration of the GTR facility, which was modeled around the reactor and shield. Figure 2 shows the reactor and shield as they were positioned inside of the GTR facility. In Figure 2, the position of the concrete shield, whose required thickness was estimated in this analysis, is shown.

RESULTS

For the concrete shield four MCNP calculations were performed. Each of these calculations had a different shield thickness, 1 cm, 30.48 cm, 60.96 cm, or 182.88 cm. The neutron and photon fluxes were calculated on the outside surface of the shield as a function of height above the concrete floor and as a function of energy. These fluxes were then multiplied by neutron or

photon flux to dose conversion factors, which are listed below in Table 1. The dose results for the four concrete thicknesses can be seen in Figures 3 through 6 with all of the results plotted together in Figure 7. In Figures 3 through 7 all the data points have error bars showing one standard deviation error in the result. In Figure 7 the location of the bottom of the vacuum vessel, bottom of the reactor, and bottom of the shield all above the concrete floor are marked.

At this point it was decided to look at the peak dose value on the surface of the shield for the different thicknesses and to plot those. The peak neutron dose was around 472.44 cm above the concrete floor while the peak gamma dose was at about 431.8 cm. These peak dose positions are not exactly true in all cases, but they serve as a good approximation. It should also be pointed out that these peak dose positions are all at an elevation level with the reactor. Figure 8 plots the neutron points for the concrete shield while Figure 9 plots the gamma points. No error bars are included in Figures 8 and 9. Instead the values that have been plotted are the calculated dose value plus two standard deviations. In other words, the values plotted in Figures 8 and 9 represent the maximum neutron or gamma dose above the concrete floor with a confidence level of 95 percent. Next, the data points in Figures 8 and 9 were each fit with an exponential function, so that the neutron and gamma dose at any shield thickness could be estimated. It is important to point out that the data point for the 1 cm thick shield was not included in the exponential fits. This was done because in the part of the shield closest to the reactor gammas are building up at a fast rate and neutrons are being attenuated at a fast rate. The exponential fit is intended to represent the exponential attenuation of the neutrons and gammas by the shield once the neutron and gamma spectra have reached equilibrium. Including this data point would add unwanted error to the fit by trying to fit a region where the gamma buildup is occurring at a rate greater than or equal to the gamma attenuation and neutron attenuation is occurring at a higher rate. The functions for the neutron and gamma dose in the concrete shield are shown in equations 1 and 2.

$$D_{cn}(r) = 2.518939E+12 * e^{-8.739077E-2*r} \qquad \text{Eqn. 1}$$

$$D_{cg}(r) = 2.508335E+11 * e^{-6.422341E-2*r} \qquad \text{Eqn. 2}$$

Equations 1 and 2, where r is the shield thickness, were then used to estimate the shield thicknesses required to meet the prescribed dose rates. These estimates are in Table 2.

CONCLUSIONS

The results in Table 2 state that a concrete-only shield will need to be around 2.75 to 3.25 m thick to meet the prescribed dose rates. A concrete shield 182.88 cm thick is worth about 7 orders of magnitude for neutron attenuation and about 4 orders of magnitude for gamma attenuation. On the outside of a 30.48 cm thick concrete shield the gamma dose will have built up about 20 percent.

In reality these numbers are estimates, and should only serve as an upper bound. This is true because the concrete thicknesses were calculated via the exponential fits. An actual calculation would need to be performed to verify this estimate.

Even though the all concrete shield is a reasonable possibility for the GTR shield it may not be the optimum configuration to conserve space. Future work from this point should investigate the use of layered shielding, and if water is included in these layers some sort of container should be modeled. Different high Z and low Z materials should be considered such as, water, borated water, polyethylene, borated polyethylene, stainless steel, tungsten, concrete, and high density concrete. These materials in general have their own pros and cons, which would also need to be taken into consideration. For example with a water shield one would have to be concerned with water chemistry, leaky containers, and possibly gammas from ^{16}N, ^{41}Ar, etc., which may suggest that even though manufacturing a water shield is relatively simple using concrete would be better.

QUALIFICATION OF METHOD

Dose rates were calculated with the radiation transport code MCNP version 5 release 1.30. This is a pre-production level computer code. The results are based on nominal geometry and do not include method uncertainty, design assurance, or design contingency factors.

REFERENCES

(a) X-5 Monte Carlo Team, "MCNP – A General Monte Carlo N-Particle Transport Code, Version 5," Los Alamos National Laboratory, LA-CP-03-0245, June 2004. (U)
(b) SDM-77, Revision 11, dated March 2005, "Shield Design Manual." (U)

Table 1: Neutron and Photon Flux to Dose Conversion Factors

Group Number	Upper Neutron Group Energy (MeV)	Neutron Flux to Dose (mRem/hr)/(n/cm^2 s)	Upper Photon Group Energy (MeV)	Photon Flux to Dose (mRem/hr)/(p/cm^2 s)
1	21.17	2.23E-01	10	1.071E-02
2	16.487	2.07E-01	9	9.801E-03
3	12.84	1.66E-01	8.5	9.350E-03
4	10	1.47E-01	8	8.912E-03
5	7.788	1.48E-01	7.5	8.482E-03
6	6.0653	1.54E-01	7	8.050E-03
7	4.7237	1.47E-01	6.5	7.612E-03
8	3.6788	1.36E-01	6	7.176E-03
9	2.865	1.27E-01	5.5	6.732E-03
10	2.2313	1.27E-01	5	6.265E-03
11	1.7377	1.28E-01	4.5	5.814E-03
12	1.3534	1.30E-01	4	5.332E-03
13	1.054	1.27E-01	3.5	4.854E-03
14	8.21E-01	1.12E-01	3	4.359E-03
15	6.39E-01	9.85E-02	2.75	4.103E-03
16	4.98E-01	8.26E-02	2.5	3.840E-03
17	3.88E-01	6.59E-02	2.2	3.500E-03
18	3.02E-01	5.26E-02	2	3.272E-03
19	2.35E-01	4.20E-02	1.75	2.971E-03
20	1.83E-01	3.35E-02	1.5	2.652E-03
21	1.43E-01	2.68E-02	1.25	2.294E-03
22	1.11E-01	2.15E-02	1	1.923E-03
23	8.65E-02	1.76E-02	0.8	1.593E-03
24	6.74E-02	1.32E-02	0.7	1.410E-03
25	4.09E-02	8.90E-03	0.6	1.222E-03
26	2.48E-02	6.02E-03	0.5	1.022E-03
27	1.50E-02	4.09E-03	0.4	8.150E-04
28	9.12E-03	3.59E-03	0.3	5.960E-04
29	5.53E-03	3.61E-03	0.2	3.710E-04
30	3.35E-03	3.63E-03	0.1	1.600E-04
31	2.03E-03	3.66E-03	0.08	1.300E-04
32	1.23E-03	3.70E-03	0.06	1.188E-04
33	7.49E-04	3.82E-03	0.05	1.295E-04
34	4.54E-04	3.95E-03	0.04	1.696E-04
35	2.75E-04	4.09E-03	0.03	2.865E-04
36	1.67E-04	4.20E-03	0.02	6.604E-04
37	1.30E-04	4.27E-03	0.015	1.227E-03
38	1.01E-04	4.32E-03	0.01	2.901E-03
39	7.89E-05	4.33E-03	Cut off Energy = 0.001	
40	6.14E-05	4.35E-03		
41	4.79E-05	4.37E-03		
42	3.73E-05	4.38E-03		
43	2.90E-05	4.40E-03		
44	2.26E-05	4.41E-03		
45	1.76E-05	4.43E-03		
46	1.37E-05	4.45E-03		
47	1.07E-05	4.46E-03		
48	8.32E-06	4.46E-03		
49	6.48E-06	4.46E-03		
50	5.04E-06	4.46E-03		
51	3.93E-06	4.46E-03		
52	3.06E-06	4.46E-03		
53	2.38E-06	4.46E-03		
54	1.86E-06	4.46E-03		
55	1.44E-06	4.46E-03		
56	1.13E-06	4.44E-03		
57	8.34E-07	4.34E-03		
58	6.25E-07	3.68E-03		
	Cut off Energy = 0.0			

Table 2: Estimates of Required Shield Thicknesses

Required Dose Rate (mRem/2800hr)	Required Concrete Shield Thickness (cm)
125	334
500	312
5000	276

Figure 1: DSO470X Reactor and Shield

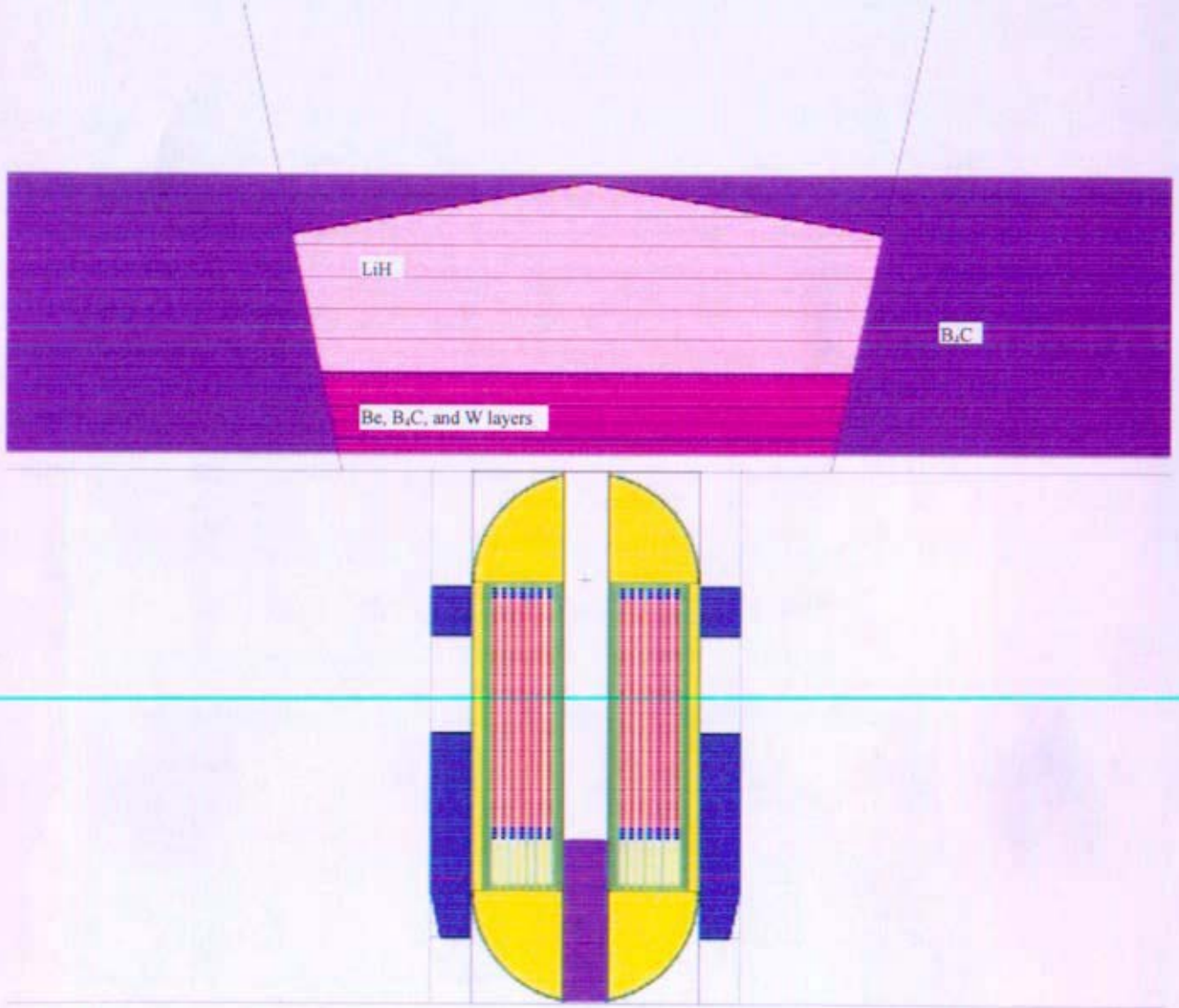

Figure 2: Ground Test Reactor Facility

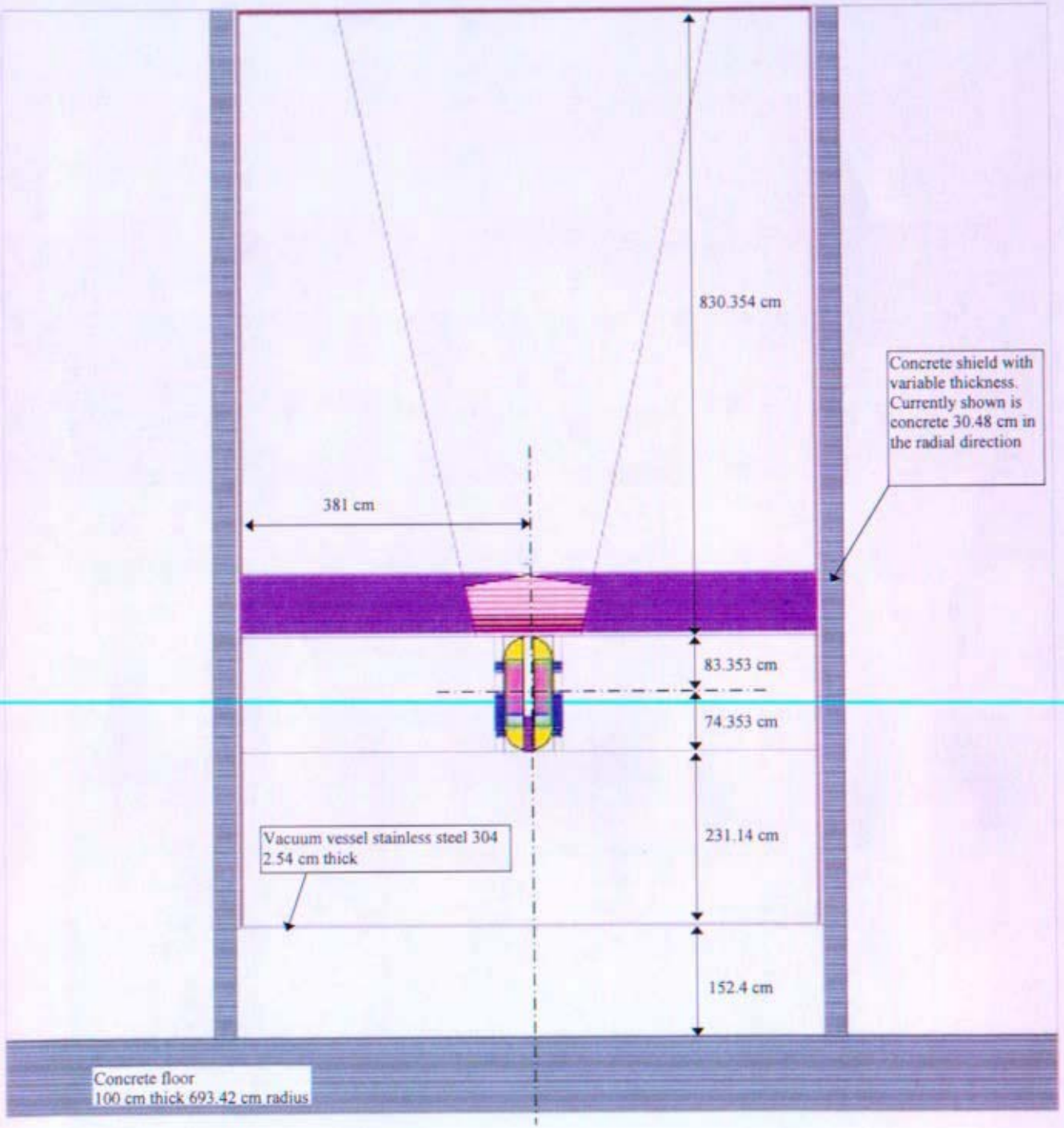

Figure 3: Surface Dose Profile with 1 cm of Concrete

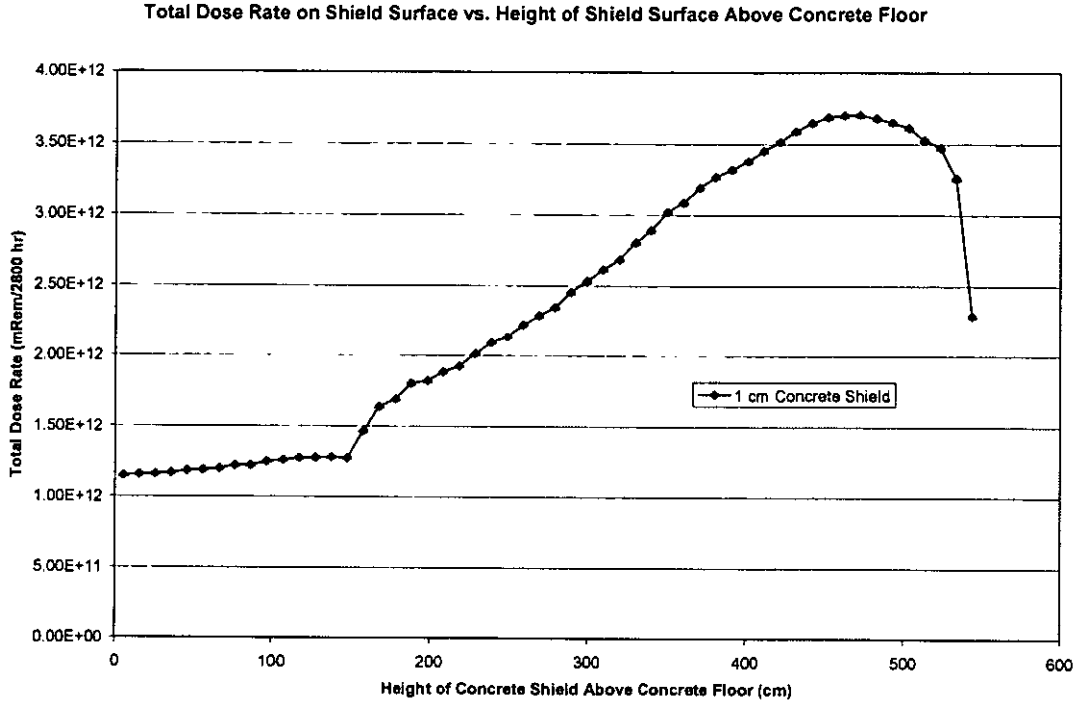

Figure 4: Surface Dose Profile with 30.48 cm of Concrete

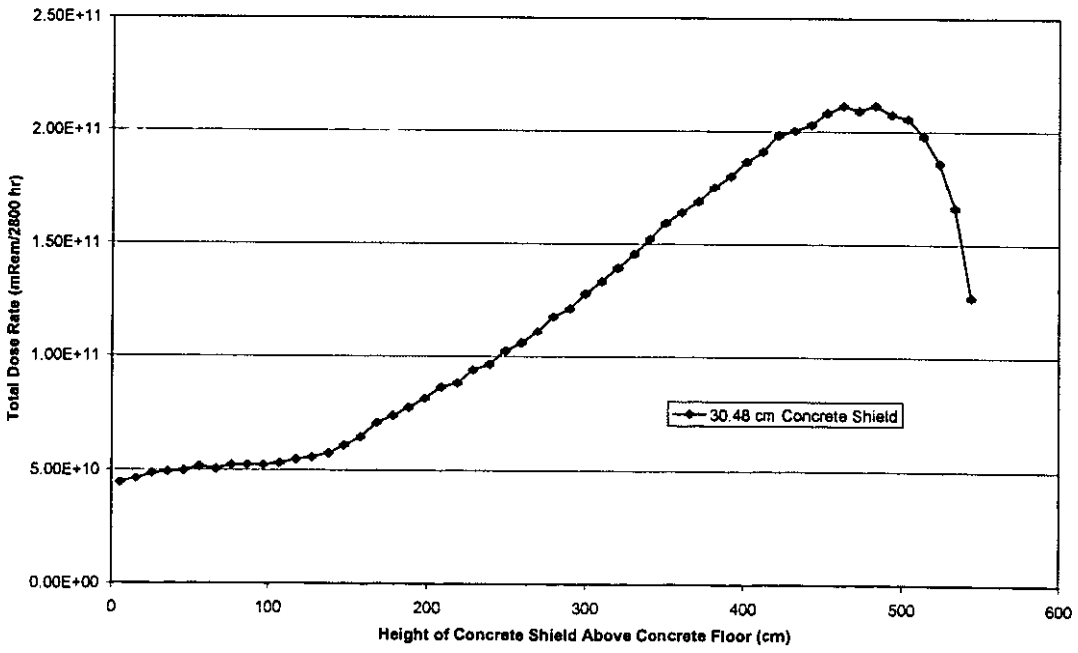

Figure 5: Surface Dose Profile with 60.96 cm of Concrete

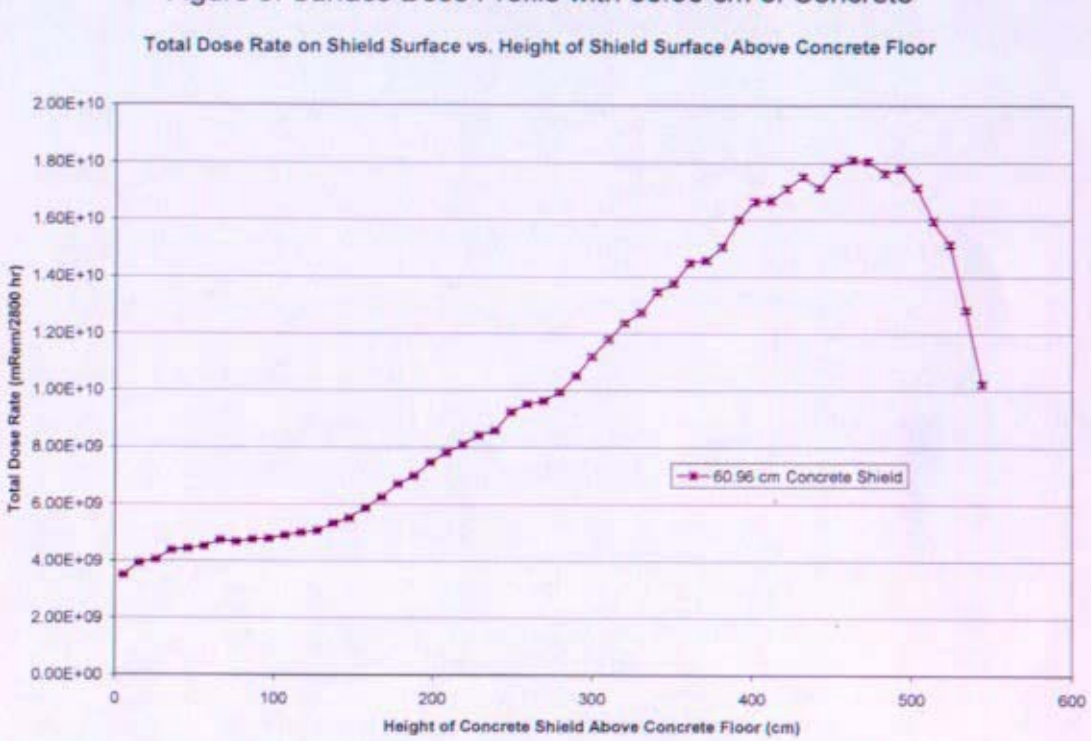

Figure 6: Surface Dose Profile with 182.88 cm of Concrete

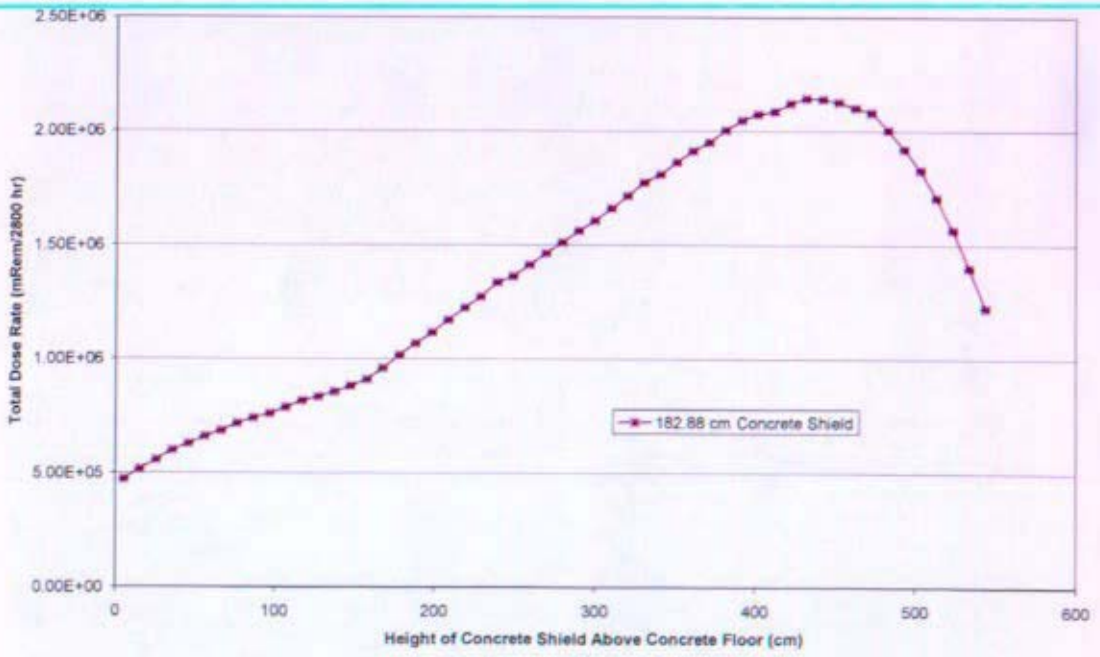

Figure 7: Surface Dose Profile for All Concrete Shield Thicknesses

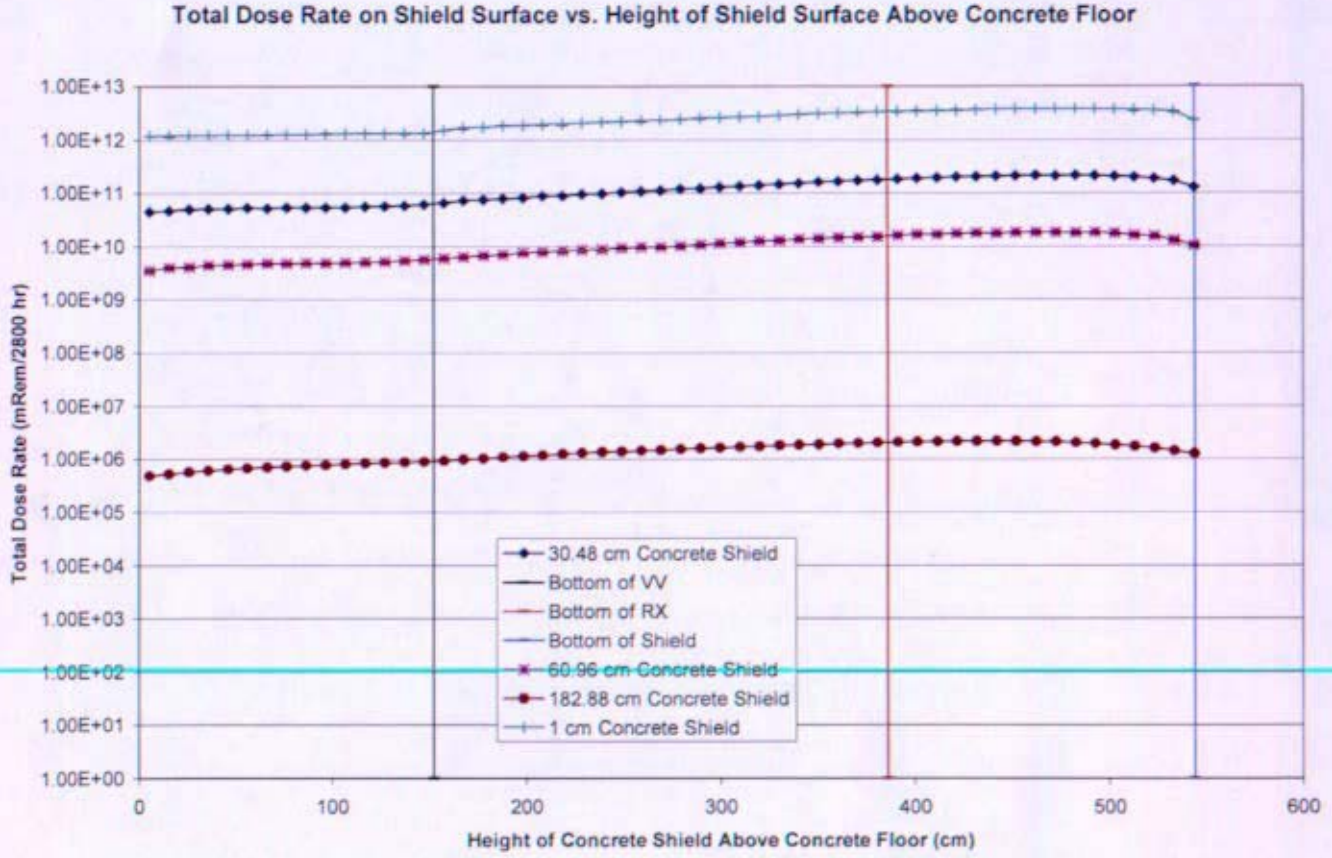

Figure 8: Peak Neutron Dose Profile for Concrete Shield, 95% Confidence

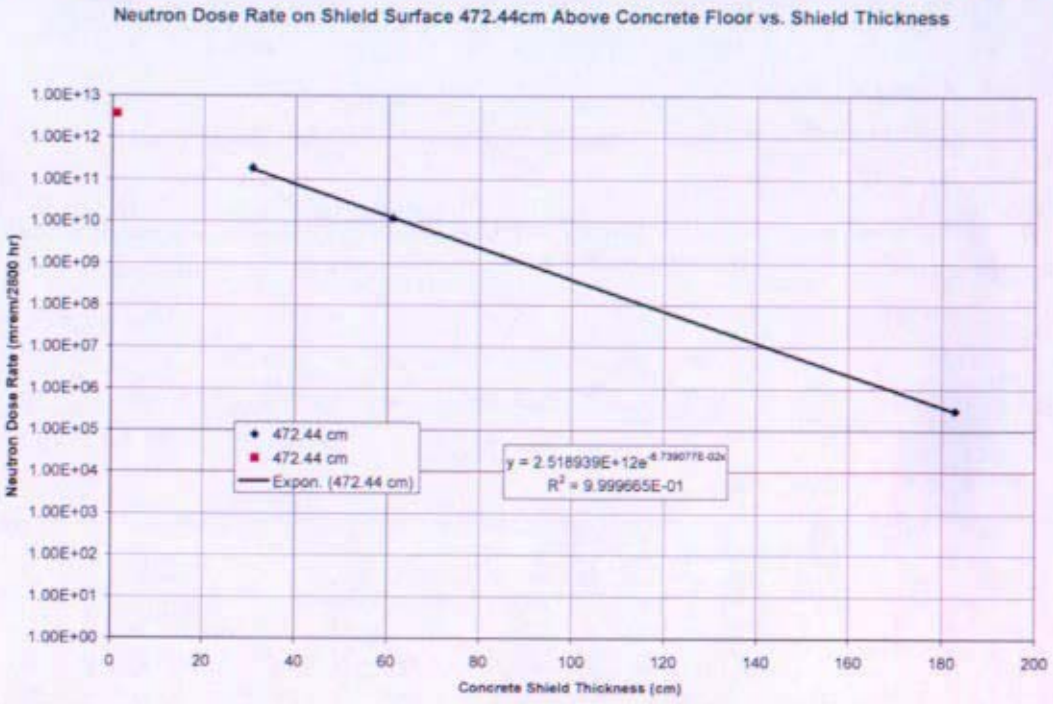

Figure 9: Peak Gamma Dose Profile for Concrete Shield, 95% Confidence

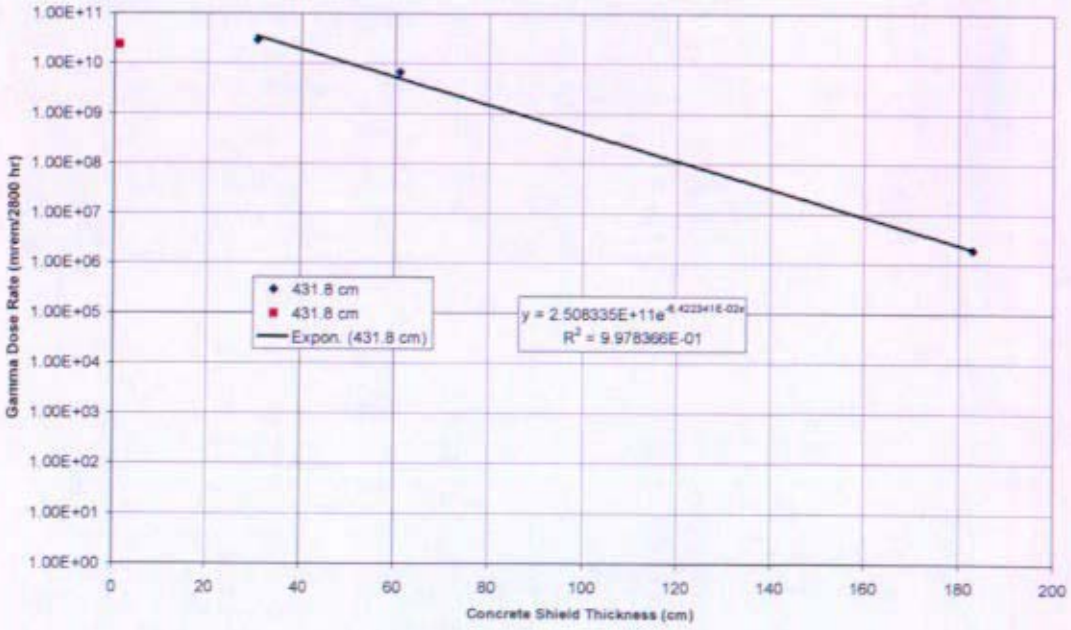

CONCURRENCE/DESIGN CHECK FORM FOR DOCUMENT NO. SPP-67210-0009 B-SE-0161 **Date:** 1/13/06

DOCUMENT TITLE: Summary of Prometheus Radiation Shielding Nuclear Design Analyses, for Information

REFERENCES (a) ENCLOSURES: 1-7

1. ADSARS: PERMANENT RECORD: Yes x No ___ Repository MFLIB Corporate Author: KAPL NR PROGRAM R

Key Words: SHIELD, MCNP, PARTISN, ATTILA, PIPES, CDM, PROMETHEUS, JIMO

Need to Know Categories REP

Available Sites:	BETT	KAPL	NRHQ	PNRO	SNRO				
Design File Location(s)	X	X							

2. DESIGN CHECK

Type of Check	Signature(s)	Comments: (Including Reference to Check Document If Appropriate)
A. No check considered necessary	C.E. Heyton	c,d,g,j,m for Enclosure (3)
B. Check vs. previous results/issues	C.C. Pfeil	ijg brief review to Encl. 1, 5, 6 & cover letter ensure no major descrepancies
C. Checked calculations made		
D. Checked computer input and/or output	ecp for D. Amato per telecon Enclosure 2 & 7	
E. Computer Programs approved/qualified		
F. Performed independent audit	ecp for T.M. Heller per telecon w/P. Amato 1/12/06	Encl. 4
G. Spot checked significant points		
H. Reviewed methods used		
I. Reviewed results for reasonableness		
J. Comparison with test data		
K. Reviewed vs. drawings		
L. Verified procedures		
M. Technical content reviewed		
N. Management verification of adequate review by others	M J Collins	i, m, n and NTK
O. Performed Lessons Learned Search		
P. Used Measurement Uncertainty Methods		
Q. Other Checks (Describe)		

3. CONCURRENCE REQUIREMENTS: Indicate signatures required by X:

	SPP MANAGER		ADVANCED CONCEPTS		FLUID DYNAM
	NUCLEAR ENGINEERING	X	SHIELDING		STRUC. ENGRG
	REACTOR TH/MECH DESIGN		REACTOR SAFETY		DRAFTING
	REACTOR EQUIPMENT		TO		QA
X	SPP MECHANICAL		RSO		OTHER
	SPP ELECTRICAL		FSO	per telecon 1/12/06	ECP for BETTIS
	FINANCE		MDO		BPMI
	PROJECT OFFICE		ARP	Sheila Heyward 1/13/06	ADMIN REVIEW
	ENERGY CONVERSION				

Cognizant Manager _____ (Must Be Subsection or Higher for External Letters)

4. AUTHORIZED CLASSIFIER: Reviewed By: M J Collins **CLASSIFICATION:** unclassified

5. RELATED SUBJECTS:

UTRS Implication (Y/N)	N	Commitment Made (Y/N)	N	Commitment Complete (Y/N)	N
Safety Council Review (Y/N)	N	Design Basis Info. (Y/N)	N	UTRS Doc. #	
		Design Review (Y/N)	N		

6. Distribution: see next page

NR
TJ Mueller, 08R/8033, For Information
S. Bell, 08I/8024
JM Crye, 08R
DE Dei, 08A/8011
JP Mosquera, 08C/8017
MD Natale, 08I/8024
TN Rodeheaver, 08I/8024
CH Oosterman, 08C/8017
JD Yoxtheimer, 08S/8034
W Evers, 08E

KAPL
JM Ashcroft, 132
PF Baldasaro, 111
CF Dempsey, 93
KC Loomis, 132
DF McCoy, 111
H. Schwartzman, 132
SA Simonson, 92
BC Campbell, 92
MJ Wollman, 111
EC Pheil, 132
J Stephens, 98
J Derboven, 98
G Zeigler, 98
MT Collins, 98
F Pineau, 98
LR Young, 23
B Gurau, 92
R Lewis, 92
D Poeth, 92

SNR
D. Clapper, 65
GM Millis, 65
DJ Potts, 65
MH Corson, 65

Bettis
CD Eshelman, 36E/SE
D. Hagerty, 38D/SE
DR Riley, 05P/MT
M. Zika, 01C/SE
J Wells
H Karnes
RS Amato
T Miller
V Simmons
W Ohlinger
DA McClaflin COB3/REO
WS Niznik 43T/SE
J Hack

PNR
J. Andes
JF Koury